UCLA
UCLA Electronic Theses and Dissertations

Title

Statistical Parametrization of the Cell Cytoskeleton (SPOCC): A non-invasive image quantification tool to identify and track sub-cellular processes

Permalink

https://escholarship.org/uc/item/8b61s02n

Author

Basu, Arkaprabha

Publication Date

2021

Peer reviewed|Thesis/dissertation

eScholarship.org Powered by the California Digital Library
University of California

UNIVERSITY OF CALIFORNIA
Los Angeles

Statistical Parametrization of the Cell Cytoskeleton (SPOCC): A non-invasive image quantification tool to identify and track sub-cellular processes

A dissertation submitted in partial satisfaction of the requirements for the degree Doctor of Philosophy in Chemistry

by

Arkaprabha Basu

2021

© Copyright by

Arkaprabha Basu

2021

ABSTRACT OF THE DISSERTATION

Statistical Parametrization of the Cell Cytoskeleton (SPOCC):

A non-invasive image quantification tool to identify

and track biological processes

by

Arkaprabha Basu

Doctor of Philosophy in Chemistry

University of California, Los Angeles, 2021

Professor Shimon Weiss, Chair

The actin cytoskeleton is an essential component of the cell aiding in a range of biological functions from movement and maintaining the shape of the cell to transporting sub-cellular cargo. In our work, we have investigated lung cancer and pre-cancer cells to understand the importance of actin cytoskeleton in identifying and tracking sub-cellular processes. In lung cancer cells, we have identified a novel intermediate phenotype during Epithelial Mesenchymal Transition (EMT) with a unique cytoskeletal architecture based on the relative orientation of stress fibers. From localization of actin binding proteins (APBs) we have demonstrated that the intermediate and final

state has predominantly different types of stress fibers. To quantify the cytoskeletal difference between these phenotypes, we have developed a method Statistical Parametrization of the Cell Cytoskeleton (SPOCC) that uses Orientational Order Parameter (OOP) as a figure of merit to track the progression of EMT. Our image quantification technique has improved throughput and is non-destructive compared to other existing techniques to track biological changes, such as mass-cytometry or RNA-sequencing. Due to the extensive inter-dependence of the cell cytoskeleton with its mechanical properties and in turn their invasiveness, we have correlated the OOP data with Young's modulus derived from AFM experiments to further validate the intermediate nature of the novel phenotype. In pre-cancer cells, it has been reported that cells derived from non-cancerous epithelial tissue samples also demonstrate enhanced invasiveness similar to mesenchymal cells. Here we have delved into the cytoskeletal architecture of this high migratory cells that demonstrated almost mesenchymal-like stress fiber structure. Using the cytoskeleton as a marker, we have identified that the MAPK/ERK pathway is active in these high migratory cells and is likely responsible for their modified morphological as well as biological characteristics.

The dissertation of Arkaprabha Basu is approved.

Steven M. Dubinett

Margot E. Quinlan

William M. Gelbart

Shimon Weiss, Committee Chair

University of California, Los Angeles

2021

To my teachers, all of them,

for everything they have taught me

Table of Contents

Table of Contents……..……..vi

Acknowledgements……viii

Vita……..x

Chapter 1: Introduction……1

1. Actin and Actin Dynamics……...3

1.1 Actin Cytoskeleton…….3

1.2 Actin Polymerization……..5

1.3 Stress Fibers and Actin Binding Proteins……...7

1.4 Roles in Cellular Processes……...….10

2. Cancer and Actin Dynamics…….11

2.1 Lung Cancer…….....11

2.2 Pre-cancer……...14

3. Analytical Methods……..15

References……16

Chapter 2: Statistical Parametrization of the Cell Cytoskeleton (SPOCC)……....…….....43

1. Existing Image Analysis Methods……....45

2. Orientational Order Parameter……..47

3. Statistical Parametrization of the Cell Cytoskeleton……49

References……52

Chapter 3: Quantitative Analysis of Actin Cytoskeleton's Morphological

Changes during EMT in Lung Cancer Cells…….60

Title and Abstract……62

Introduction…….63

Results……66

Discussion……...74

Conclusions…….77

Materials and Methods……..78
Acknowledgements……...…83
Authors' Contributions……..83
References…….83
Supplementary Information……..93
Chapter 4: Pre-malignancy and Cytoskeleton……..98
Title and Abstract…….100
Introduction……..101
Results……..104
Discussion…….112
Future Direction……115
Materials and Methods…… 115
References…… 119
Supplementary Information……..129

Acknowledgements

First are foremost I would like to express my thanks to my mentor Prof. Shimon Weiss, for without his active support and guidance this work would not be possible. His mentorship strategy of extending a level of independence that helps one mature as a scientist, has been an inspiration to me. I would like to thank all the members of the Weiss Lab who have helped me since I joined the lab in 2015. Yung Kuo and Xiyu Yi, my initial student mentors, taught me all the scientific protocols and computer algorithms. Xavier Michalet has been a wonderful colleague for scientific discussions and has always been available for help. Rinat Ankri and Xavier Michalet worked closely with me on a project involving life-time analysis of fluorescence proteins that resulted in a publication. Help from Jack Li, within and without the lab was a true gift, especially during the pandemic.

I would also like to thank my collaborators, Dr. Manash K. Paul, Dr. Mitchel Alioscha-Perez, Dr. Soma Ghosh, Prof. Yosef Yarden, Prof. Anna Grosberg, Prof. Hichem Sahli and Prof. Steven M. Dubinett. Throughout my work, Dr. Paul has taught me how to think about a biological problem and has been a great personal friend. He has helped in designing experiments and carrying out the more biological experiments required for the work. Dr. Alioscha-Perez generously sent me the fiber extraction software and Prof. Grosberg provided the OOP calculation algorithm. My committee members, Prof. Steven M. Dubinett, Prof. Margot E. Quinlan and Prof. William M. Gelbart have provided constructive feedback and suggestions on my work throughout, whom I thank for their guidance.

Prof. G. Naresh Patwari, my mentor in Indian Institute of Technology, Bombay, first introduced me to independent research and critical thinking, for which I thank him profusely. I

also owe a lot to the scientific conversations I had with Prof. Anindya Datta, Prof. Arindam Chowdhury and Prof. Sandip Kar of IIT Bombay.

In Maya Segal, a lab mate, I found a true friend who has helped me in more ways than I can mention, including scientific writings and presentations. Disari Deb, I thank for proof-reading my thesis and being a wonderful traveling companion. Friends such as Dr. Koushik Roy and Dr. Suman Dutta also deserve a big thanks. Lastly and most importantly, I express my gratitude to my parents, Dr. Tarakdas Basu and Dr. Ruma Basu, for being my first teachers and inculcating in me a passion for scientific pursuits.

Vita

Arkaprabha Basu

EDUCATION

Apr '17 – Present	Candidate in Philosophy, *University of California Los Angeles, USA*
Sep '15 – Apr '17	Master of Science, *University of California Los Angeles, USA*
Jul '13 – Apr '15	Master of Science, *Indian Institute of Technology Bombay, India*
Jul '10 – May '13	Bachelor of Science (with Honours in Chemistry), *Presidency College, Kolkata, University of Calcutta, India*

RESEARCH EXPERIENCE

Sep '15 - Present **Graduate Student Researcher**, *University of California Los Angeles, USA*
Thesis Title: Statistical Parametrization of the Cell Cytoskeleton (SPOCC): A non-invasive image quantification tool to identify and track sub-cellular processes in real time.

Jun '14 – Apr '15 **Masters Student Researcher**, *Indian Institute of Technology Bombay, India*
Thesis Title: Aggregation and Folding of Squaramides

May '14 – Jun '14 **Research Assistant**, *Jadavpur University, India*
· Developing **Solar Cells** with **Storage Capacity** by replacing the conventional nano-materials with novel materials with storage properties

Nov '13 – Dec '13 **Research Assistant**, *Central Glass and Ceramic Research Institute, India*
· Investigating effect of doping on multi-ferrous perovskite materials using **X-ray Photoelectron Spectroscopy (XPS)**

May '13 – Jun '13 **Indian Academy of Sciences Summer Research Fellow**, *National Institute for Interdisciplinary Science and Technology, India*
· Design, synthesis and photo-physical characterization of **Unsymmetrical Squaraine** molecules for **Dye Sensitized Solar Cell (DSSC)** Applications

ACHIEVEMENTS

Dec ’13	Ranked **24** out of 39,930 candidates in **National Eligibility Test (NET)** , India
Jan ’12	**UCO Bank Award** for research based undergraduate project, India
Jun ’11	Recipient of **DST-INSPIRE** scholarship by Department of Science and Technology, India

PUBLICATION

1. “Single Photon, Time-Gated, Phasor-Based Fluorescence Lifetime Imaging through Highly Scattering Medium” DOI: 10.1021

Ankri, R.; **Basu, A.**; Ulku, A. C.; Bruschini, C.; Charbon, E.; Weiss, S.; Michalet, X. **2020** *ACS Photonics* 7, 1, 68-79

2. “π-Stacking Driven Aggregation and Folding of Squaramides” DOI: 10.1021

Sen, S.; **Basu, A.**; Sen, T.; Patwari, G. N. **2020** *J. Phys. Chem. A*, 124, 28, 5832-5839

3. “PD-L1 recruits Phospholipase C and enhances EGFR signaling: relevance to resistance of EGFR+ lung tumor in immunotherapy” DOI: 10.2139

Ghosh, G.; Nataraj, N. B.; Noronha, A.; Patkar, S.; Sekar, A.; Mukherjee, A.; Winograd-Katz, S.; Lindzen, M.; Garcia, D. D.; Green, J.; Eisenberg, G.; Gil-Henn, H.; **Basu, A.**; Lender, Y.; Weiss, S.; Oren, M.; Motem, M.; Geiger, B.; Ruppin, E.; Yarden, Y. **2020** *Cell Reports*, 35(8):109181

CONFERENCE

Feb ‘21	Presented poster titled **“Quantitative Analysis of Actin Cytoskeleton’s Morphological Changes during EMT in Lung Cancer and Pre-Cancer Cell Lines”** in **Biophysical Society Annual Meeting 2021** DOI: 10.1016
Apr ‘19	Presented poster titled **“Regulation and Role of Actin Dynamics in Promoting Premalignant Cell Migration”** in **American Association for Cancer Research Annual Meeting 2019** DOI: 10.1158
Jan ’18	Presented poster in **NSF-STROBE Retreat**

Chapter 1

Introduction

This chapter is a literature review for the topics presented in this thesis. It includes a basic introduction to the actin cytoskeleton, its relevance in cancer (lung cancer specifically) and a broad description of standardized techniques used to study actin. It also includes a brief introduction to a new sub-population of airway epithelial cells that show partial mesenchymal properties.

1. Actin and Actin Dynamics:

1.1. Actin Cytoskeleton

The cell cytoskeleton is essential in basic functioning of the cell from movement and maintaining certain shapes to transport of subcellular moieties inside the cell. Actin, along with tubulin[1,2] and cytokeratin[3,4], forms the basis of the cell cytoskeleton. Actin has been evolutionarily conserved from primitive eukaryotes to modern Homo sapiens[5]. Though actin filaments show a greater divergence in bacteria compared to eukaryotes, the genes responsible demonstrates structural and functional relationship, which is suggestive of its importance in organisms[6]. There are as many as ten genes expressing different types of actin in plants, some of which are responsible for the maintenance of vegetative and reproductive tissues. Humans on other hand have six genes specifically for the expression of six different isoforms of actin[7] that can be broadly classified into three different types α-actin, β-actin and γ-actin[8,9]. These different isoforms are as much as 95% similar in their amino acid sequence but differ in the over-all charge of the molecules and hence their isoelectric points[10,11]. Though they show structural similarity, their functions are widely varied as well as their localization[12,13,14,15]. Throughout development, these isoforms are expressed in spatially as well as temporally varied patterns indicative of high levels of tissue as well as sub-cellular specificity[16,17,18,19,20].

α-actin is a tissue specific actin structure that is mostly expressed in vascular smooth muscles but also present in other tissues[21]. Cardiovascular and skeletal cells are the most common host for the expression of α-actin. The N-terminal section of α-actin differs from the other actin isoforms in the region that is responsible for actin polymerization[7,22]. Smooth muscle actin (SMA) is expressed in early embryonic development of the vascular tissue and eventually becomes the most abundant

protein in adult vascular smooth muscle tissues, such as aorta[23]. Cardiac α-actin is predominantly found in striated heart tissues[24,25] and skeletal α-actin is the primary actin isoform in skeletal muscles[26,27,28,29]. The CArG box, which is conserved across the promoters for smooth muscle actin is also believed to encode the spatially diverge expression. SMAs are also involved in wound healing process and tissue fibrosis[30,31,32,33,34]. Interestingly, mice generated without SMA were reported to have functioning cardiovascular systems indicating that skeletal α-actin can compensate for the lack of SMA to maintain normal functionality[35]. Based on enhanced presence of α-actin in the cytoskeleton of myofibroblasts, it can be inferred that α-actin is involved in the connection between the cortical actin filaments and the extra cellular matrix[36,37]. The role of α-actin in mechanotransduction is further established by the increase in expression of SMA upon application of mechanical forces on the cells[38,39,40,41,42].

β-actin is a type of cytoplasmic actin that is more ubiquitously present across different cell and tissue types[43]. β-actin is the major component of actin stress fibers, circular bundles and filopodias[15]. The importance of β-actin is evident from the non-viability of β-actin knockout embryos[44,45]. Its interaction with myosin II means that β-actin is responsible for cell adhesion and contraction in normal epithelial tissues which do not have α-actin. Inhibition of myosin II interaction with actin has been shown to drastically decrease the amount of stress fibers in cells. β-actin depleted cells were also known to be poly-nucleated which demonstrates that this type of cytoskeletal actin is involved in the formation of contractile rings, which is corroborated by other experiments that indicated that β-actin may be specifically required for cell division[15,45,46]. β-actin null cells showed decreased growth rate, higher rate of apoptosis and decreased motility[14]. Actin dynamics is known to affect the gene regulation through Serum Response Factor (SRF)[47,48] owing

to its association with all three RNA polymerases[49,50]. Cells without β-actin have a higher degree of change in gene expression than other actin isoforms and have decreased availability of G-actin[51].

γ-actin has two main types, the γ smooth muscle actin and γ cytoplasmic actin. γ smooth muscle actin is present of the walls of blood veins as well as gastrointestinal and genital tracts[52]. Cytoplasmic γ-actin is present in most epithelial cells. Cytoplasmic γ-actin forms the basis of cortical actin structures. In skeletal muscles, this actin isoform is localized in the costamere and this localization just under the membrane supports the involvement of γ-actin in the cortical mesh[53]. The most interesting expression of cytoplasmic γ-actin is in the mechanosensory stereocilia of hair cells that are necessary hearing. Involvement of γ-actin in the cortical network is demonstrated by its role in maintenance of asymmetry in the first division of meiosis[54]. Though γ-actin null mice were viable, they exhibited increased mortality and progressive hearing loss[55]. This indicates that though β-actin can compensate for γ-actin, it cannot maintain the integrity of the structures. Deletion of γ-actin in cells showed an upregulation of β-actin as much as 1.5 fold and enhanced neoplastic transformations such as epithelial-mesenchymal transition[15].

1.2. Actin Polymerization

The main reason for the conservation of actin across species is likely related to the polymerization ability of actin to form filaments and larger structures. Actin polymerization is the first of the formation of the cell cytoskeleton and generates the necessary force for cell movement. Actin monomers or globular actin (G-actin) are asymmetric in nature with a barbed end and a pointed end. These monomers are attached to actin depolymerization factor (ADF) and cofilin. The ADF/cofilin complex resists random formation of actin filaments in the cytoplasm. To initiate polymerization, the ADF/cofilin complex is replaced with another actin binding protein called

profilin before it can bind with an existing filament. This process is continued to elongate the polymer and the energy is provided by the hydrolysis of ATP molecules (Figure. 1).

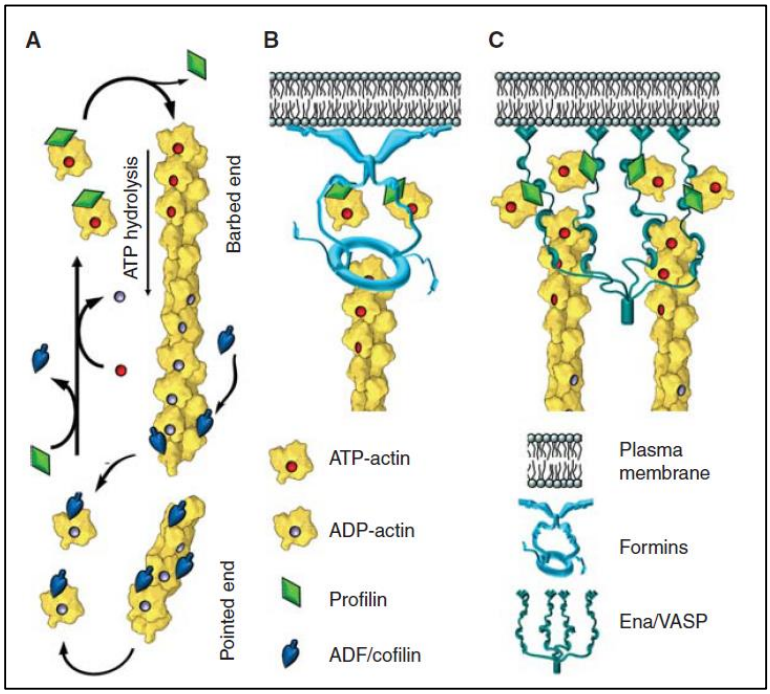


Fig. 1 | Actin filament formation[56]**.** (A) Actin monomers bound to ATP and profiling attach to the barbed end of the filament. The profiling is released and ATP hydrolysis takes place. (B) Formin-mediated actin polymerization, where formin increases the concentration of G-actin near the barbed end. (C) Ena/VASP complex mediated actin polymerization, where Ena/VASP complex aids in G-actin recruitment and prevents capping of the filament. Image courtesy Svitkina et. al. (ref. 56).

Actin filaments are asymmetric just like the monomers where all the monomers are oriented in the same direction. New monomers bind to the barbed end (plus end) of the filament thereby making the elongation process directional. This phenomenon is essential for directional cell movements such as cytokinesis. On the pointed end (minus end) of the filament, the ADF/cofilin complex aids in depolymerization of the filament, essentially generating a movement of the whole filament. The depolymerized G-actin replenishes the monomer pool and is recycled for polymerization on the barbed end[56,57,58]. Though nucleation events of actin polymerization are very frequent, dimers and trimers of actin are very unstable and so only a few nucleation event lead to a filament (Figure. 2).

Actin filaments can form more complex branched network structures from shorter filaments. Actin Related Protein 2/3 (Arp2/3), which is controlled by the WASP/Scar pathway[59] can bind to an actin monomer that binds to the barbed end of a filament. From the Arp2/3 site, another filament can start forming, generating a Y-type branching at an angle of approximately 70°[60,61]. This kind of branching is observed close to the cell membrane, where the actin fibers are thin and they interact with membrane proteins and receptor.

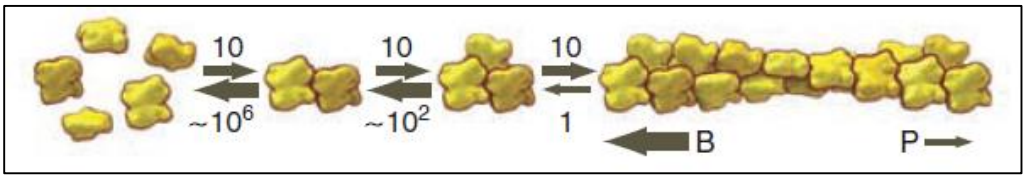


Fig. 2 | Relative rates of polymerization and depolymerization in oligomers vs. polymers.[62] Image courtesy Pollard et. al. (ref. 62).

Another mechanism for actin polarization is mediated via formin[63,64]. Formin has two domains that are relevant actin nucleation/elongation: formin homology 1 (FH1) and formin homology 2 (FH2). FH2 usually acts as a capping protein by forming a homodimer encircling the barbed end of actin filaments and restricting further elongation. FH1 also binds to the barbed end of an actin filament, but it binds multiple profilin-G-actin complexes like a lasso, while blocking capping proteins from attaching to the barbed end[65,66]. This process increases the local concentration of actin monomers near the polymerization site and enhancing the rate of elongation compared to normal diffusion-limited process.

1.3. Stress Fibers and Actin Binding Proteins

The actin polymer filaments serve as the building blocks to a larger and more diverse family of actin structures called stress fibers. These are essentially thick bundles of 10-30 actin filaments

held together by a family of proteins called actin binding proteins (ABP)[67,68,69]. Stress fibers are the primary contractile structure for most cell types[62,70,71]. The contractile force in stress fibers is generated with the assistance of myosin, and though the actomyosin contractile machinery is more ordered and efficient in skeletal muscles, they basically operate in the same mechanism in most cell types. Myosin has an actin binding site which constantly keep attaching and detaching with the actin filaments at the expense of ATPs. The motor domain of myosin is where the hydrolysis of ATP provides the energy for any kind of force generation and motion. The ATP hydrolysis brings about a conformational change in the motor domain which is amplified by the lever arm (called the power-stroke) and forms the basis of myosin motors[72,73,74]. The movement of the lever arm in concert with constant attachment and detachment of myosin with the actin filament is responsible for fiber contraction and movement. Some two headed myosin motors can bind to two actin filaments and processively "walk" along the filaments using the same basic mechanism resulting in sliding of one fiber with respect to the other[75,76,77].

Another actin binding protein that is very relevant for stress fiber formation is α-actinin. α-actinin is a cross-linking protein from the spectrin super-family that holds the single actin filaments together[78,79,80]. It forms a dimer with the actin binding heads on opposite sides enabling it to bind to two actin filaments at once. Isoform 2 and 3 of α-actinin are usually present in cardiac cells whereas isoform 1 and 4 are present is other types. In contractile stress fibers, α-actinin gets periodically displaced by myosin generating an alternating pattern[81,82]. Other cross-linking proteins such as fascin[83], filamin[84,85], zyxin[86,87] and epsin[88] are also involved in the formation of stress fibers.

Stress fibers are connected to the underlying matrix on certain locations called Focal Adhesions (FA) which are characterized by the presence of Focal Adhesion Kinase (FAK). It is hypothesized

that FAs can serve as a starting point for formation of stress fibers. FAs are also responsible for mechanotransduction and it has been shown that application of physical force can aid in development of FAs[89,90,91].

Based on the position of stress fibers and the ABPs involved, stress fibers are classified into three major types: dorsal stress fibers, transverse arcs and ventral stress fibers (Figure. 3). Dorsal stress fibers are non-contractile structures without myosin. They are capped on one end with FAK and can serve as precursors for elongation into other types of stress fibers. Transverse arcs are not connected to FAs but they can be connected to dorsal fibers and can convey contractile force through them. During cellular migration, the constant contractile activity of transverse arcs, drive them from the leading edge of the cell towards the center. This phenomenon is known as retrograde flow[92,93]. The most commonly seen form of stress fiber is the ventral stress fiber. These are usually formed by the joining of two dorsal fibers or a combination of dorsal fibers and transverse arcs. Ventral fibers are connected to FAs on both sides and act as the major actomyosin contractile machinery in cells. Another type of stress fiber has also been described which is known as the peri-nuclear actin cap. These have the same composition as ventral fibers, but they are formed over the nucleus. They control the shape and size of the nucleus as well as convey the force from the environment to the nucleus through mechanotransduction[70,94].

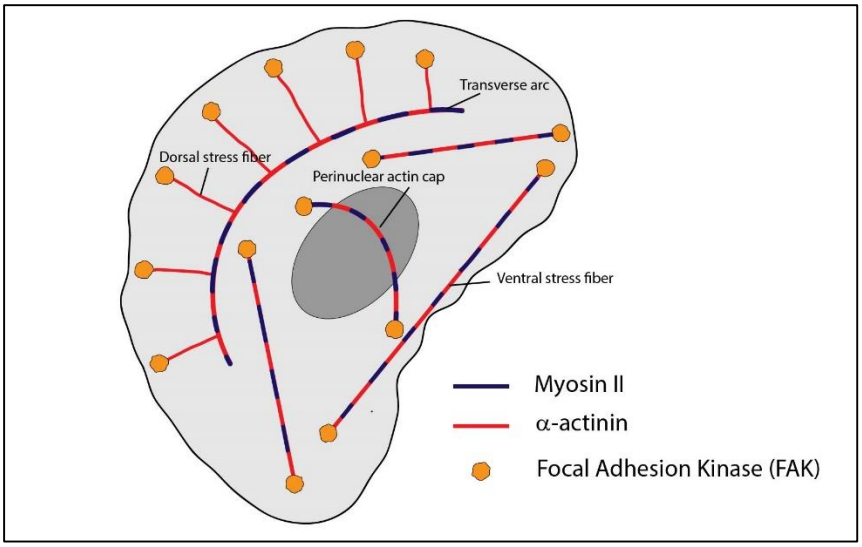


Fig. 3 | Different types of stress fibers and corresponding actin binding proteins.

A myriad of genetic pathways and control mechanism are responsible for the formation, recruitment, functioning and eventual disintegration of stress fibers. The most studied and validated pathway involves the small GTPases: RhoA, RhoB and RhoC[95]. RhoA has been demonstrated as the major controlling factor for stress fiber assembly[96], but RhoB and RhoC are also hypothesized to be relevant in certain cells. Rho controls the expression of multiple proteins required for the formation of stress fibers through myocardial related transcription factor. A downstream protein called Rho-associated protein kinase (ROCK) is more directly involved in stress fiber assembly[97,98]. ROCK directly phosphorylates the myosin light chain[99] thereby increasing the contractility of stress fibers[100]. Another Rho-related protein mDia1 serves as the nucleation site of new stress fibers near the cell membrane[101,102,103]. Rac1 and CDC42 indirectly affect the stress fiber formation by activating the actin nucleating complex Arp2/3.

1.4. Roles in cellular processes

Stress fibers are formed in response to mechanical stress in cells. This phenomenon demonstrates that stress fibers serve as a primary mechanotransduction machinery of cells[104,105]. Stress fibers, with the help of FAK conveys external stimuli as well as respond to it. The cytoskeletal response to external stimuli is evidenced by the drastically different organization and type of stress fibers between cells grown on soft and hard surfaces[106,107]. Cells on soft surfaces demonstrate thin disorganized stress fibers mostly transverse arcs and dorsal fibers; whereas cells grown on hard surfaces exhibit thick parallel ventral fibers[108]. Due to the contractile nature of the actomyosin bundles, they are the main component of any type of motion of the cell starting from shape change to migration[109]. Directed growth of stress fibers can control the shape of cells[110,111]. Cell migration can also be described as a series of protrusion and retraction events[112]. Cells achieve this by growing the stress fibers on the leading edge of the cell with concurrent disassembly on the lagging edge. This is especially prominent in keratinocytes. Cell migration is also observed in wound healing where cells are known to start forming stress fibers. In contractile tissues, stress fibers (Z-rings) essentially perform the entire purpose of the cell in concert with ABPs.

Though intra-cellular cargo transport is a feature of the tubulin network, the actin stress fiber network has also been demonstrated capable of transporting cargo[113]. The processive motion of some myosin proteins indicate that they can essentially slide along actin filaments without releasing and as such can easily be recruited as cargo transporters. Myosins have been reported to transport whole organelles such as lysosomes through the actin network[114]. The actin cytoskeleton is also involved in endocytosis[115] and exosytosis[116].

2. Cancer and Actin Dynamics:

2.1 Lung Cancer

Lung and bronchial cancer is one of the leading causes of death in the world, resulting in more than 135,000 deaths (22.4% of all cancer deaths) in United States just in the year 2020[117,118,119]. Cancer is usually identified by an uncontrolled growth of tumor cells that start starving the neighboring healthy tissue. They can form their own blood circulation system, known as angiogenesis[120]. Eventually, the tumor metastasizes and the tumor cells can travel through the blood stream to other regions of the body to form secondary tumors[121]. Tumors, like other healthy organs of the body, are mostly composed of epithelial cells, with apical to basal polarity[122,123], that adhere to one another[124] and are incapable of migrating. But during metastasis, the epithelial cells undergo a drastic transformation known as epithelial to mesenchymal transition (EMT)[125,126,127,128,129]. Mesenchymal cells, on the other hand, do not adhere to one another, demonstrate enhanced motility and are more resistant to apoptosis. EMT is a phenomenological protocol that is also activated during wound healing fibrosis in healthy tissues as well as during embryo development neural streak formation[130]. Though the transition is same, the genetic signaling responsible in each case is not entirely conserved.

E-cadherin, is a Ca^{2+} mediated adhesion protein, that helps in forming the epithelial sheet and maintaining contact inhibition, thus acting as a tumor suppressor[131]. Proteins such as Zeb1[132], Snail and Slug[133] inhibit E-cadherin expression and upregulate the expression of N-cadherin[134]. N-cadherin, on the other hand activates the MAPK/ERK pathway and initiates EMT. Along with expression of proteins like N-cadherin[135,136], Snail, Slug and Zeb1, formation of stress fibers is also a phenomenon that accompanies EMT[137,138]. Mesenchymal cells need higher migration capabilities[139,140] along with modified elasticity[141,142,143,144,145,146] to navigate through the dense tissue environment and enter blood streams. As discussed above, stress fibers are essential for these movements. Cells enter the blood vessel through very small pores that require nuclear

blebbing[147,148]. Nuclear blebbing is the deformation of the nucleus that accommodates the passage through small pores but can also cause cell death if the nucleus cannot regain its shape[149]. Perinuclear actin caps play an important role in maintaining the size and shape of the nucleus and can also aid in shape recovery of the nucleus after blebbing.

The exact process of cytoskeletal rearrangement during EMT is not well understood. But based on the model of stress fiber formation it is known that the existence of focal adhesions is essential for the cell to develop stress fibers[71]. Another EMT marker protein vimentin[150] is known to increase the formation and maturation of focal adhesion sites[151,152], which then serve as nucleation sites for stress fibers. Vimentin is an intermediate filament that is expressed during the early phases of EMT before the actin cytoskeleton takes over.

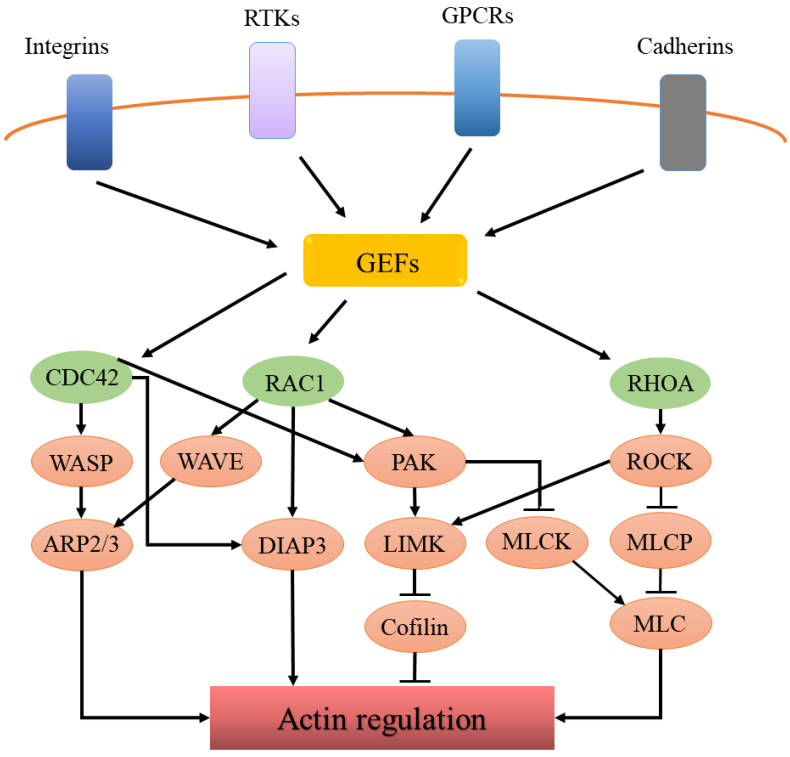


Fig. 4 | Representative pathways of actin cytoskeletal reorganization during EMT. Image adapted from Fife et. al. (ref. 153).

There is an extensive amount of overlap between the genetic signaling for EMT and the formation of stress fibers. The Rho family of proteins play an integral role in EMT as well as stress fiber formation[126,153]. Though stress fiber formation is considered a downstream response to EMT, there is a growing recognition that formation of stress fiber might facilitate EMT as well. The MAPK/ERK pathway is another signaling pathway active during EMT. TGFβ1 is a known inducer of EMT in mammalian cells and its activation of EMT through both the Rho-GTPase pathway and the MAPK/ERK pathway have been demonstrated[154]. Another signaling pathway has recently emerged as relevant for EMT known as the Wnt pathway[155]. Though there is evidence of cross-talk between the Wnt and MAPK pathways through Jun-N-terminal Kinase (JNK), both of these pathways can independently affect EMT[156].

2.2 Pre-cancer

The existing idea for cancer progression cites that first a tumor is formed which upon metastasis can start secondary tumors. Essentially, only cells in pre-existing tumors can undergo EMT and migrate to secondary locations. This theory has clinical application in identifying primary tumors and developing therapeutic strategies. But there has been evidence of metastasis without any identifiable primary tumor[157] and circulating tumor cells in as early as stage I non-small cell lung cancer (NSLC)[158,159,160]. But recently it has been demonstrated that certain non-tumor cells also demonstrate high motility and apoptotic resistance like mesenchymal cells[161,162]. They can migrate to secondary locations and start tumors before the primary tumor has formed making treatment difficult. This phenomenon is called field cancerization[163]. Though these high migratory cells exhibit stress fibers, they are not entirely mesenchymal. Their stress fiber structures are also different from normal mesenchymal cells and their cytoskeletal structure can be the key to uncovering their inherent semi-mesenchymal properties.

3. Analytical Methods

Over the years, there have been multiple approaches to study the actin cytoskeleton of cells. Simple western blot analyses can provide information about up and down-regulation of actin in general and has been used extensively[164,165]. But most cellular processes involve reorganization of existing actin in the cell from monomer to polymer and then between different types of stress fiber structures. Also, certain processes can involve localized actin concentration changes within the cell. These events cannot be estimated by western blot analysis. Quantitative fluorescence microscopy solves some of these issues, but the high concentration of actin monomers creates high background signal thereby limiting the quality of images. With the development of probes like Lifeact[166] that specifically bind to actin filaments rather than monomers, the problem of high background has been mitigated. Coupled with multi-color super-resolution imaging methods, fluorescence imaging has become an indispensable tool for studying actin and its dynamics[167,168,169]. TIRF microscopy with polarized light sources was used to demonstrate the myosin walking on actin filament phenomenon[170]. Fluorescence microscopy has also been used to study the polymerization/depolymerization dynamics of actin in real time[171,172]. Electron Microscopy provided further details regarding the structure of actin monomers as well as their dynamics[58,72.173]. Another approach to employ pull down method followed by mass cytometry to analyze real time interaction between actin and ABPs[174]. In the pull down assays, the ABPs bound to actin are also isolated and can provide quantitative information regarding which specific ABPs were attached spatially and temporally. Quantitative RNA-sequencing techniques have also generated vast amounts of information regarding the expression levels of genes responsible for actin regulation during dynamic cellular processes[175,176].

Recently, there have been efforts to extract further information from fluorescent images. There is a high degree of correlation between different types of stress fibers, their relative orientations and the localization of ABPs. Image analysis techniques have been employed to extract statistical information regarding the stress fibers thereby quantifying the cytoskeleton[177,178,179].

References:

(1) Cuenca-Zamora, E. J.; Ferrer-Marín, F.; Rivera, J.; Teruel-Montoya, R. Tubulin in Platelets: When the Shape Matters. *Int. J. Mol. Sci.* **2019**, *20* (14), 1–13. https://doi.org/10.3390/ijms20143484.

(2) Coleman, A. K.; Joca, H. C.; Shi, G.; Lederer, W. J.; Ward, C. W. Tubulin Acetylation Increases Cytoskeletal Stiffness to Regulate Mechanotransduction in Striated Muscle. *J. Gen. Physiol.* **2021**, *153* (7), 1–8. https://doi.org/10.1085/jgp.202012743.

(3) Kumar, A.; Jagannathan, N. Cytokeratin: A Review on Current Concepts. *Int. J. Orofac. Biol.* **2018**, *2* (1), 6. https://doi.org/10.4103/ijofb.ijofb_3_18.

(4) Guo, D.; Xu, Q.; Pabla, S.; Koomen, J.; Biddinger, P.; Sharma, A.; Pabla, S.; Pacholczyk, R.; Chang, C. C.; Friedrich, K.; Mohammed, K.; Smallridge, R. C.; Copland, J. A.; She, J. X.; Weinberger, P. M. Cytokeratin-8 in Anaplastic Thyroid Carcinoma: More than a Simple Structural Cytoskeletal Protein. *Int. J. Mol. Sci.* **2018**, *19* (2). https://doi.org/10.3390/ijms19020577.

(5) Gunning, P. W.; Ghoshdastider, U.; Whitaker, S.; Popp, D.; Robinson, R. C. The Evolution of Compositionally and Functionally Distinct Actin Filaments. *J. Cell Sci.* **2015**, *128* (11), 2009–2019. https://doi.org/10.1242/jcs.165563.

(6) Hightower, R. C.; Meagher, R. B. The Molecular Evolution of Actin. *Genetics* **1986**, *114* (1), 315–332. https://doi.org/10.1093/genetics/114.1.315.

(7) Vandekerckhove, J.; Weber, K. At Least Six Different Actins Are Expressed in a Higher Mammal: An Analysis Based on the Amino Acid Sequence of the Amino-Terminal Tryptic Peptide. *J. Mol. Biol.* **1978**, *126* (4), 783–802. https://doi.org/10.1016/0022-2836(78)90020-7.

(8) Herman, I. M. Actin Isoforms. *Curr. Opin. Cell Biol.* **1993**, *5* (1), 48–55. https://doi.org/10.1016/S0955-0674(05)80007-9.

(9) Dugina, V. B.; Shagieva, G. S.; Kopnin, P. B. Biological Role of Actin Isoforms in Mammalian Cells. *Biochem.* **2019**, *84* (6), 583–592. https://doi.org/10.1134/S0006297919060014.

(10) Garrels, J. I.; Gibson, W. Identification and Characterization of Multiple Forms of Actin. *Cell* **1976**, *9* (4 PART 2), 793–805. https://doi.org/10.1016/0092-8674(76)90142-2.

(11) Rubenstein, P. A. The Functional Imortance of Multiple Actin Isoforms. *BioEssays* **1990**, *12* (7), 309–315.

(12) Chen, A.; Arora, P. D.; McCulloch, C. A.; Wilde, A. Cytokinesis Requires Localized β-Actin Filament Production by an Actin Isoform Specific Nucleator. *Nat. Commun.* **2017**, *8* (1). https://doi.org/10.1038/s41467-017-01231-x.

(13) Cervero, P.; Wiesner, C.; Bouissou, A.; Poincloux, R.; Linder, S. Lymphocyte-Specific Protein 1 Regulates Mechanosensory Oscillation of Podosomes and Actin Isoform-Based Actomyosin Symmetry Breaking. *Nat. Commun.* **2018**, *9* (1).

https://doi.org/10.1038/s41467-018-02904-x.

(14) Patrinostro, X.; O'Rourke, A. R.; Chamberlain, C. M.; Moriarity, B. S.; Perrin, B. J.; Ervasti, J. M. Relative Importance of Bcyto-and Γcyto-Actin in Primary Mouse Embryonic Fibroblasts. *Mol. Biol. Cell* **2017**, *28* (6), 771–782. https://doi.org/10.1091/mbc.E16-07-0503.

(15) Dugina, V.; Zwaenepoel, I.; Gabbiani, G.; Clément, S.; Chaponnier, C. B- and Γ-Cytoplasmic Actins Display Distinct Distribution and Functional Diversity. *J. Cell Sci.* **2009**, *122* (16), 2980–2988. https://doi.org/10.1242/jcs.041970.

(16) Westhoff, C. C.; Schoner, K.; Hartmann, S.; Sesterhenn, A. M.; Moll, R. Actin Isoform Expression Patterns in Adult Extracardiac and Cardiac Rhabdomyomas Indicate a Different Cell of Origin. *Virchows Arch.* **2017**, *470* (3), 285–290. https://doi.org/10.1007/s00428-017-2069-3.

(17) Hill, M. A.; Gunning, P. Beta and Gamma Actin MRNAs Are Differentially Located within Myoblasts. *J. Cell Biol.* **1993**, *122* (4), 825–832. https://doi.org/10.1083/jcb.122.4.825.

(18) Watanabe, H.; Kislauskis, E. H.; Mackay, C. A.; Mason-Savas, A.; Marks, S. C. Actin MRNA Isoforms Are Differentially Sorted in Normal Osteoblasts and Sorting Is Altered in Osteoblasts from a Skeletal Mutation in the Rat. *J. Cell Sci.* **1998**, *111* (9), 1287–1292.

(19) Bassell, G. J.; Zhang, H.; Byrd, A. L.; Femino, A. M.; Singer, R. H.; Taneja, K. L.; Lifshitz, L. M.; Herman, I. M.; Kosik, K. S. Sorting of β-Actin MRNA and Protein to Neurites and Growth Cones in Culture. *J. Neurosci.* **1998**, *18* (1), 251–265. https://doi.org/10.1523/jneurosci.18-01-00251.1998.

(20) McHugh, K. M.; Crawford, K.; Lessard, J. L. A Comprehensive Analysis of the Developmental and Tissue-Specific Expression of the Isoactin Multigene Family in the Rat. *Dev. Biol.* **1991**, *148* (2), 442–458. https://doi.org/10.1016/0012-1606(91)90263-3.

(21) Gabbiani, G.; Kocher, O.; Vandekerckhove, J.; Gent, B.-; Weber, K. Actin Expression in Smooth Muscle Cells of Rat Aortic Intimal Thickening, Human Atheromatous Plaque, and Cultured Rat Aortic Media. *J. Clin. Invest.* **1984**, *73* (1), 148–152. https://doi.org/10.1172/JCI111185.

(22) Chaponnier, C.; Goethals, M.; Janmey, P. A.; Gabbiani, F.; Gabbiani, G.; Vandekerckhove, J. The Specific NH2-Terminal Sequence Ac-EEED of α-Smooth Muscle Actin Plays a Role in Polymerization in Vitro and in Vivo. *J. Cell Biol.* **1995**, *130* (4), 887–895. https://doi.org/10.1083/jcb.130.4.887.

(23) Wang, J.; Zohar, R.; McCulloch, C. A. Multiple Roles of α-Smooth Muscle Actin in Mechanotransduction. *Exp. Cell Res.* **2006**, *312* (3), 205–214. https://doi.org/10.1016/j.yexcr.2005.11.004.

(24) Matsson, H.; Eason, J.; Bookwalter, C. S.; Klar, J.; Gustavsson, P.; Sunnegårdh, J.; Enell, H.; Jonzon, A.; Vikkula, M.; Gutierrez, I.; Granados-Riveron, J.; Pope, M.; Bu'lock, F.; Cox, J.; Robinson, T. E.; Song, F.; Brook, D. J.; Marston, S.; Trybus, K. M.; Dahl, N. Alpha-Cardiac Actin Mutations Produce Atrial Septal Defects. *Hum. Mol. Genet.* **2008**, *17* (2), 256–265. https://doi.org/10.1093/hmg/ddm302.

(25) Frank, D.; Rangrez, A. Y.; Friedrich, C.; Dittmann, S.; Stallmeyer, B.; Yadav, P.; Bernt, A.; Schulze-Bahr, E.; Borlepawar, A.; Zimmermann, W. H.; Peischard, S.; Seebohm, G.; Linke, W. A.; Baba, H. A.; Krüger, M.; Unger, A.; Usinger, P.; Frey, N.; Schulze-Bahr, E.

Cardiac α-Actin (ACTC1) Gene Mutation Causes Atrial-Septal Defects Associated with Late-Onset Dilated Cardiomyopathy. *Circ. Genomic Precis. Med.* **2019**, *12* (8), 345–356. https://doi.org/10.1161/CIRCGEN.119.002491.

(26) Swynghedauw, B. Developmental and Functional Adaptation of Contractile Proteins in Cardiac and Skeletal Muscles. *Physiol. Rev.* **1986**, *66* (3), 710–771. https://doi.org/10.1152/physrev.1986.66.3.710.

(27) Hewett, T. E.; Grupp, I. L.; Grupp, G.; Robbins, J. α-Skeletal Actin Is Associated with Increased Contractility in the Mouse Heart. *Circ. Res.* **1994**, *74* (4), 740–746. https://doi.org/10.1161/01.RES.74.4.740.

(28) Bertola, L. D.; Ott, E. B.; Griepsma, S.; Vonk, F. J.; Bagowski, C. P. Developmental Expression of the Alpha-Skeletal Actin Gene. *BMC Evol. Biol.* **2008**, *8* (1). https://doi.org/10.1186/1471-2148-8-166.

(29) Brennan, K. J.; Hardeman, E. C. Quantitative Analaysis of the Human A-Skeletal Actin Gene in Transgenic Mice. *J. Biol. Chem.* **1993**, *268* (1), 719–725.

(30) Shinde, A. V.; Humeres, C.; Frangogiannis, N. G. The Role of α-Smooth Muscle Actin in Fibroblast-Mediated Matrix Contraction and Remodeling. *Biochim. Biophys. Acta - Mol. Basis Dis.* **2017**, *1863* (1), 298–309. https://doi.org/10.1016/j.bbadis.2016.11.006.

(31) Grinnell, F. Mini-Review on the Cellular Mechanisms of Disease Fibroblasts, Myofibroblasts, and Wound Contraction. *J. Cell Biol.* **1994**, *124* (4), 401–404.

(32) Jester, J. V.; Petroll, W. M.; Barry, P. A.; Cavanagh, H. D. Expression of α-Smooth Muscle (α-SM) Actin during Corneal Stromal Wound Healing. *Investig. Ophthalmol. Vis.*

Sci. **1995**, *36* (5), 809–819.

(33) Rockey, D. C.; Du, Q.; Shi, Z. Smooth Muscle α-Actin Deficiency Leads to Decreased Liver Fibrosis via Impaired Cytoskeletal Signaling in Hepatic Stellate Cells. *Am. J. Pathol.* **2019**, *189* (11), 2209–2220. https://doi.org/10.1016/j.ajpath.2019.07.019.

(34) Jimi, S.; Kimura, M.; De Francesco, F.; Riccio, M.; Hara, S.; Ohjimi, H. Acceleration Mechanisms of Skin Wound Healing by Autologous Micrograft in Mice. *Int. J. Mol. Sci.* **2017**, *18*.

(35) Schildmeyer, L. A.; Braun, R.; Taffet, G.; Debiasi, M.; Burns, A. E.; Bradley, A.; Schwartz, R. J. Impaired Vascular Contractility and Blood Pressure Homeostasis in the Smooth Muscle A-actin Null Mouse. *FASEB J.* **2000**, *14* (14), 2213–2220. https://doi.org/10.1096/fj.99-0927com.

(36) Arora, P. D.; Narani, N.; McCulloch, C. A. G. The Compliance of Collagen Gels Regulates Transforming Growth Factor-β Induction of α-Smooth Muscle Actin in Fibroblasts. *Am. J. Pathol.* **1999**, *154* (3), 871–882. https://doi.org/10.1016/S0002-9440(10)65334-5.

(37) Tomasek, J. J.; Gabbiani, G.; Hinz, B.; Chaponnier, C.; Brown, R. A. Myofibroblasts and Mechano: Regulation of Connective Tissue Remodelling. *Nat. Rev. Mol. Cell Biol.* **2002**, *3* (5), 349–363. https://doi.org/10.1038/nrm809.

(38) Hinz, B.; Dugina, V.; Ballestrem, C.; Wehrle-Haller, B.; Christine, C. A-Smooth Muscle Actin Is Crucial for Focal Adhesion Maturation in Myofibroblasts. *Mol. Biol. Cell* **2003**, *14* (June), 2508–2519. https://doi.org/10.1091/mbc.E02.

(39) Wang, J.; Fan, J.; Laschinger, C.; Arora, P. D.; Kapus, A.; Seth, A.; McCulloch, C. A. Smooth Muscle Actin Determines Mechanical Force-Induced P38 Activation. *J. Biol. Chem.* **2005**, *280* (8), 7273–7284. https://doi.org/10.1074/jbc.M410819200.

(40) Wang, J.; Seth, A.; Mcculloch, A. G. Force Regulates Smooth Muscle Actin in Cardiac Fibroblasts. *Am. J. Physiol. - Hear. Circ. Physiol.* **2000**, *279* (6 48-6), 2776–2785. https://doi.org/10.1152/ajpheart.2000.279.6.h2776.

(41) Wang, J.; Chen, H.; Seth, A.; McCulloch, C. A. Mechanical Force Regulation of Myofibroblast Differentiation in Cardiac Fibroblasts. *Am. J. Physiol. - Hear. Circ. Physiol.* **2003**, *285* (5 54-5), 1871–1881. https://doi.org/10.1152/ajpheart.00387.2003.

(42) Kuehlmann, B.; Bonham, C. A.; Zucal, I.; Prantl, L.; Gurtner, G. C. Mechanotransduction in Wound Healing and Fibrosis. *J. Clin. Med.* **2020**, *9* (5), 1423. https://doi.org/10.3390/jcm9051423.

(43) Cytoskeleton, A.; Motility, C.; Karakozova, M.; Kozak, M.; Wong, C. C. L.; Bailey, A. O.; Iii, J. R. Y.; Mogilner, A.; Zebroski, H.; Kashina, A. Arginylation of B-Actin Regulates. *Science (80-.).* **2006**, No. July, 192–196.

(44) Shawlot, W.; Deng, J. M.; Fohn, L. E.; Behringer, R. R. Restricted B-Galactosidase Expression of a Hygromycin-LacZ Targeted to the B-Actin Locus and Embryonic Lethality of B-Actin Mutant Mice. *Transgenic Res.* **1998**, *7*, 95–103.

(45) Bunnell, T. M.; Ervasti, J. M. Delayed Embryonic Development and Impaired Cell Growth and Survival in Actg1 Null Mice. *Cytoskeleton* **2010**, *67* (9), 564–572. https://doi.org/10.1002/cm.20467.

(46) Dugina, V.; Shagieva, G.; Khromova, N.; Kopnin, P. Divergent Impact of Actin Isoforms on Cell Cycle Regulation. *Cell Cycle* **2018**, *17* (23), 2610–2621. https://doi.org/10.1080/15384101.2018.1553337.

(47) Small, E. M. The Actin-MRTF-SRF Gene Regulatory Axis and Myofibroblast Differentiation. *J. Cardiovasc. Transl. Res.* **2012**, *5* (6), 794–804. https://doi.org/10.1007/s12265-012-9397-0.

(48) Yao, J.; Sasaki, Y.; Wen, Z.; Bassell, G. J.; Zheng, J. Q. An Essential Role for β-Actin MRNA Localization and Translation in Ca2+-Dependent Growth Cone Guidance. *Nat. Neurosci.* **2006**, *9* (10), 1265–1273. https://doi.org/10.1038/nn1773.

(49) Hofmann, W. A.; Stojiljkovic, L.; Fuchsova, B.; Vargas, G. M.; Mavrommatis, E.; Philimonenko, V.; Kysela, K.; Goodrich, J. A.; Lessard, J. L.; Hope, T. J.; Hozak, P.; de Lanerolle, P. Actin Is Part of Pre-Initiation Complexes and Is Necessary for Transcription by RNA Polymerase II. *Nat. Cell Biol.* **2004**, *6* (11), 1094–1101. https://doi.org/10.1038/ncb1182.

(50) Hu, P.; Wu, S.; Hernandez, N. A Role for B -Actin in RNA Polymerase III Transcription. *Genes Dev.* **2004**, 3010–3015. https://doi.org/10.1101/gad.1250804.an.

(51) Bunnell, T. M.; Burbach, B. J.; Shimizu, Y.; Ervasti, J. M. β-Actin Specifically Controls Cell Growth, Migration, and the G-Actin Pool. *Mol. Biol. Cell* **2011**, *22* (21), 4047–4058. https://doi.org/10.1091/mbc.E11-06-0582.

(52) VANDEKERCKHOVE, J.; WEBER, K. The Complete Amino Acid Sequence of Actins from Bovine Aorta, Bovine Heart, Bovine Fast Skeletal Muscle, and Rabbit, Slow Skeletal Muscle: A Protein-Chemical Analysis of Muscle Actin Differentiation. *Differentiation*

1979, *14* (1–3), 123–133. https://doi.org/10.1111/j.1432-0436.1979.tb01021.x.

(53) Hanft, L. M.; Rybakova, I. N.; Patel, J. R.; Rafael-Fortney, J. A.; Ervasti, J. M. Cytoplasmic γ-Actin Contributes to a Compensatory Remodeling Response in Dystrophin-Deficient Muscle. *Proc. Natl. Acad. Sci. U. S. A.* **2006**, *103* (14), 5385–5390. https://doi.org/10.1073/pnas.0600980103.

(54) Brockmann, C.; Huarte, J.; Dugina, V.; Challet, L.; Rey, E.; Conne, B.; Swetloff, A.; Nef, S.; Chaponnier, C.; Vassalli, J. D. Beta-and Gamma-Cytoplasmic Actins Are Required for Meiosis in Mouse Oocytes. *Biol. Reprod.* **2011**, *85* (5), 1025–1039. https://doi.org/10.1095/biolreprod.111.091736.

(55) Belyantseva, I. A.; Perrin, B. J.; Sonnemann, K. J.; Zhu, M.; Stepanyan, R.; McGee, J.; Frolenkov, G. I.; Walsh, E. J.; Friderici, K. H.; Friedman, T. B.; Ervasti, J. M. γ-Actin Is Required for Cytoskeletal Maintenance but Not Development. *Proc. Natl. Acad. Sci. U. S. A.* **2009**, *106* (24), 9703–9708. https://doi.org/10.1073/pnas.0900221106.

(56) Svitkina, T. The Actin Cytoskeleton and Actin-Based Motility. *Cold Spring Harb. Perspect. Biol.* **2018**, *10* (1), 1–22. https://doi.org/10.1101/cshperspect.a018267.

(57) Pollard, T. D.; Borisy, G. G. Cellular Motility Driven by Assemblyand Disassembly of Actin Filaments. *Cell* **2003**, *112*, 453–465.

(58) Chou, S. Z.; Pollard, T. D. Mechanism of Actin Polymerization Revealed by Cryo-EM Structures of Actin Filaments with Three Different Bound Nucleotides. *Proc. Natl. Acad. Sci. U. S. A.* **2019**, *116* (10), 4265–4274. https://doi.org/10.1073/pnas.1807028115.

(59) Machesky, L. M.; Mullins, R. D.; Higgs, H. N.; Kaiser, D. A.; Blanchoin, L.; May, R. C.;

Hall, M. E.; Pollard, T. D. Scar, a WASp-Related Protein, Activates Nucleation of Actin Filaments by the Arp2/3 Complex. *Proc. Natl. Acad. Sci. U. S. A.* **1999**, *96* (7), 3739–3744. https://doi.org/10.1073/pnas.96.7.3739.

(60) Rouiller, I.; Xu, X. P.; Amann, K. J.; Egile, C.; Nickell, S.; Nicastro, D.; Li, R.; Pollard, T. D.; Volkmann, N.; Hanein, D. The Structural Basis of Actin Filament Branching by the Arp2/3 Complex. *J. Cell Biol.* **2008**, *180* (5), 887–895. https://doi.org/10.1083/jcb.200709092.

(61) Liman, J.; Bueno, C.; Eliaz, Y.; Schafer, N. P.; Waxham, M. N.; Wolynes, P. G.; Levine, H.; Cheung, M. S. The Role of the Arp2/3 Complex in Shaping the Dynamics and Structures of Branched Actomyosin Networks. *Proc. Natl. Acad. Sci.* **2020**, *117* (20), 10825–10831. https://doi.org/10.1073/pnas.1922494117.

(62) Pollard, T. D.; Cooper, J. A. Actin, a Central Player in Cell Shape and Movement. *Science (80-.).* **2009**, *326* (5957), 1208–1212. https://doi.org/10.1126/science.1175862.

(63) Paul, A. S.; Pollard, T. D. Review of the Mechanism of Processive Actin Filament Elongation by Formins. *Cell Motil. Cytoskeleton* **2009**, *66* (8), 606–617. https://doi.org/10.1002/cm.20379.

(64) Zigmond, S. H. Formin-Induced Nucleation of Actin Filaments. *Curr. Opin. Cell Biol.* **2004**, *16* (1), 99–105. https://doi.org/10.1016/j.ceb.2003.10.019.

(65) Zigmond, S. H.; Evangelists, M.; Boone, C.; Yang, C.; Dar, A. C.; Sicheri, F.; Forkey, J.; Pring, M. Formin Leaky Cap Allows Elongation in the Presence of Tight Capping Proteins. *Curr. Biol.* **2003**, *13* (20), 1820–1823. https://doi.org/10.1016/j.cub.2003.09.057.

(66) Kovar, D. R.; Wu, J.-Q.; Pollard, T. D. Profilin-Mediated Competition Betwee Capping Protein and Formin Cdc12p during Cytokinesis in Fission Yeast. *Mol Biol Cell* **2005**, *16* (May), 2313–2324. https://doi.org/10.1091/mbc.E04.

(67) Pollard, T. D. Actin and Actin-Binding Proteins. A Critical Evaluation of Mechanisms and Functions. *Ann. Rev. Biochem.* **1986**, *55*, 987–1035.

(68) Pollard, T. D. Actin and Actin-Binding Proteins. *Cold Spring Harb Perspect Biol* **2016**, *8*, 1–18.

(69) Gross, S. R. Actin Binding Proteins: Their Ups and Downs in Metastatic Life. *Cell Adhes. Migr.* **2013**, *7* (2), 199–213. https://doi.org/10.4161/cam.23176.

(70) Tojkander, S.; Gateva, G.; Lappalainen, P. Actin Stress Fibers - Assembly, Dynamics and Biological Roles. *J. Cell Sci.* **2012**, *125* (8), 1855–1864. https://doi.org/10.1242/jcs.098087.

(71) Pellegrin, S.; Mellor, H. Actin Stress Fibers. *J. Cell Sci.* **2007**, *120* (20), 3491–3499. https://doi.org/10.1242/jcs.018473.

(72) Mentes, A.; Huehn, A.; Liu, X.; Zwolak, A.; Dominguez, R.; Shuman, H.; Ostap, E. M.; Sindelar, C. V. High-Resolution Cryo-EM Structures of Actin-Bound Myosin States Reveal the Mechanism of Myosin Force Sensing. *Proc. Natl. Acad. Sci. U. S. A.* **2018**, *115* (6), 1292–1297. https://doi.org/10.1073/pnas.1718316115.

(73) Gunther, L. K.; Rohde, J. A.; Tang, W.; Cirilo, J. A.; Marang, C. P.; Scott, B. D.; Thomas, D. D.; Debold, E. P.; Yengo, C. M. FRET and Optical Trapping Reveal Mechanisms of Actin Activation of the Power Stroke and Phosphate Release in Myosin V. *J. Biol. Chem.*

2020, *295* (51), 17383–17397. https://doi.org/10.1074/jbc.RA120.015632.

(74) Matusovsky, O. S.; Kodera, N.; Maceachen, C.; Ando, T.; Cheng, Y. S.; Rassier, D. E. Millisecond Conformational Dynamics of Skeletal Myosin II Power Stroke Studied by High-Speed Atomic Force Microscopy. *ACS Nano* **2021**, *15* (2), 2229–2239. https://doi.org/10.1021/acsnano.0c06820.

(75) Lee Sweeney, H.; Holzbaur, E. L. F. Motor Proteins. *Cold Spring Harb. Perspect. Biol.* **2018**, *10* (5), 1–18. https://doi.org/10.1101/cshperspect.a021931.

(76) Robert-Paganin, J.; Pylypenko, O.; Kikuti, C.; Sweeney, H. L.; Houdusse, A. Force Generation by Myosin Motors: A Structural Perspective. *Chem. Rev.* **2020**, *120* (1), 5–35. https://doi.org/10.1021/acs.chemrev.9b00264.

(77) Ryan, J. M.; Nebenführ, A. Update on Myosin Motors: Molecular Mechanisms and Physiological Functions. *Plant Physiol.* **2018**, *176* (1), 119–127. https://doi.org/10.1104/pp.17.01429.

(78) Sjoblom, B.; Salmazo, A.; Djinovic-Carugo, K. A-Actinin Structure and Regulation. *Cell. Mol. Life Sci.* **2008**, *65*, 2688–2701.

(79) Otey, C. A.; Carpen, O. α-Actinin Revisited: A Fresh Look at an Old Player. *Cell Motil. Cytoskeleton* **2004**, *58* (2), 104–111. https://doi.org/10.1002/cm.20007.

(80) Blanchard, A.; Ohanian, V.; Critchley, D. The Structure and Function of α-Actinin. *J. Muscle Res. Cell Motil.* **1989**, *10* (4), 280–289. https://doi.org/10.1007/BF01758424.

(81) Pavalko, F. M.; Burridge, K. Disruption of the Actin Cytoskeleton after Microinjection of Proteolytic Fragments of α-Actinin. *J. Cell Biol.* **1991**, *114* (3), 481–491.

https://doi.org/10.1083/jcb.114.3.481.

(82) Edlund, M.; Lotano, M. A.; Otey, C. A. Dynamics of α-Actinin in Focal Adhesions and Stress Fibers Visualized with α-Actinin-Green Fluorescent Protein. *Cell Motil. Cytoskeleton* **2001**, *48* (3), 190–200. https://doi.org/10.1002/1097-0169(200103)48:3<190::AID-CM1008>3.0.CO;2-C.

(83) Lin, S.; Taylor, M. D.; Singh, P. K.; Yang, S. How Does Fascin Promote Cancer Metastasis? *FEBS J.* **2021**, *288* (5), 1434–1446. https://doi.org/10.1111/febs.15484.

(84) Kumar, A.; Shutova, M. S.; Tanaka, K.; Iwamoto, D. V.; Calderwood, D. A.; Svitkina, T. M.; Schwartz, M. A. Filamin A Mediates Isotropic Distribution of Applied Force across the Actin Network. *J. Cell Biol.* **2019**, *218* (8), 2481–2491. https://doi.org/10.1083/JCB.201901086.

(85) Donada, A.; Balayn, N.; Sliwa, D.; Lordier, L.; Ceglia, V.; Baschieri, F.; Goizet, C.; Favier, R.; Tosca, L.; Tachdjian, G.; Denis, C. V.; Plo, I.; Vainchenker, W.; Debili, N.; Rosa, J. P.; Bryckaert, M.; Raslova, H. Disrupted Filamin A/AIIbb3 Interaction Induces Macrothrombocytopenia by Increasing RhoA Activity. *Blood* **2019**, *133* (16), 1778–1788. https://doi.org/10.1182/blood-2018-07-861427.

(86) Oakes, P. W.; Wagner, E.; Brand, C. A.; Probst, D.; Linke, M.; Schwarz, U. S.; Glotzer, M.; Gardel, M. L. Optogenetic Control of RhoA Reveals Zyxin-Mediated Elasticity of Stress Fibres. *Nat. Commun.* **2017**, *8*. https://doi.org/10.1038/ncomms15817.

(87) Wang, Y. X.; Wang, D. Y.; Guo, Y. C.; Guo, J. Zyxin: A Mechanotransductor to Regulate Gene Expression. *Eur. Rev. Med. Pharmacol. Sci.* **2019**, *23* (1), 413–425. https://doi.org/10.26355/eurrev_201901_16790.

(88) Messa, M.; Fernández-Busnadiego, R.; Sun, E. W.; Chen, H.; Czapla, H.; Wrasman, K.; Wu, Y.; Ko, G.; Ross, T.; Wendland, B.; De Camilli, P. Epsin Deficiency Impairs Endocytosis by Stalling the Actin-Dependent Invagination of Endocytic Clathrin-Coated Pits. *Elife* **2014**, *3* (August2014), 1–25. https://doi.org/10.7554/eLife.03311.

(89) Burridge, K.; Guilluy, C. Focal Adhesions, Stress Fibers and Mechanical Tension. *Exp. Cell Res.* **2016**, *343* (1), 14–20. https://doi.org/10.1016/j.yexcr.2015.10.029.

(90) Bauer, M. S.; Baumann, F.; Daday, C.; Redondo, P.; Durner, E.; Jobst, M. A.; Milles, L. F.; Mercadante, D.; Pippig, D. A.; Gaub, H. E.; Gräter, F.; Lietha, D. Structural and Mechanistic Insights into Mechanoactivation of Focal Adhesion Kinase. *Proc. Natl. Acad. Sci. U. S. A.* **2019**, *116* (14), 6766–6774. https://doi.org/10.1073/pnas.1820567116.

(91) Katoh, K. Activation of Rho-Kinase and Focal Adhesion Kinase Regulates the Organization of Stress Fibers and Focal Adhesions in the Central Part of Fibroblasts. *PeerJ* **2017**, *2017* (11). https://doi.org/10.7717/peerj.4063.

(92) Rutkowski, D. M.; Vavylonis, D. Discrete Mechanical Model of Lamellipodial Actin Network Implements Molecular Clutch Mechanism and Generates Arcs and Microspikes . *bioRxiv* **2021**, 1–30.

(93) Lee, S.; Kassianidou, E.; Kumar, S. Actomyosin Stress Fiber Subtypes Have Unique Viscoelastic Properties and Roles in Tension Generation. *Mol. Biol. Cell* **2018**, *29* (16), 1992–2004. https://doi.org/10.1091/mbc.E18-02-0106.

(94) Maninová, M.; Vomastek, T. Dorsal Stress Fibers, Transverse Actin Arcs, and Perinuclear Actin Fibers Form an Interconnected Network That Induces Nuclear Movement in Polarizing Fibroblasts. *FEBS J.* **2016**, *283* (20), 3676–3693.

https://doi.org/10.1111/febs.13836.

(95) Chardin, P.; Boquet, P.; Madaule, P.; Popoff, M. R.; Rubin, E. J.; Gill, D. M. The Mammalian G Protein RhoC Is ADP-Ribosylated by Clostridium Botulinum Exoenzyme C3 and Affects Actin Microfilaments in Vero Cells. *EMBO J.* **1989**, *8* (4), 1087–1092. https://doi.org/10.1002/j.1460-2075.1989.tb03477.x.

(96) Paterson, H. F.; Self, A. J.; Garrett, M. D.; Just, I.; Aktories, K.; Hall, A. Microinjection of Recombinant P21(Rho) Induces Rapid Changes in Cell Morphology. *J. Cell Biol.* **1990**, *111* (3), 1001–1007. https://doi.org/10.1083/jcb.111.3.1001.

(97) Leung, T.; Chen, X. Q.; Manser, E.; Lim, L. The P160 RhoA-Binding Kinase ROK Alpha Is a Member of a Kinase Family and Is Involved in the Reorganization of the Cytoskeleton. *Mol. Cell. Biol.* **1996**, *16* (10), 5313–5327. https://doi.org/10.1128/mcb.16.10.5313.

(98) Ward, Y.; Yap, S. F.; Ravichandran, V.; Matsumura, F.; Ito, M.; Spinelli, B.; Kelly, K. The GTP Binding Proteins Gem and Rad Are Negative Regulators of the Rho-Rho Kinase Pathway. *J. Cell Biol.* **2002**, *157* (2), 291–302. https://doi.org/10.1083/jcb.200111026.

(99) Amano, M.; Ito, M.; Kimura, K.; Fukata, Y.; Chihara, K.; Nakano, T.; Matsuura, Y.; Kaibuchi, K. Phosphorylation and Activation of Myosin by Rho-Associated Kinase (Rho-Kinase). *J. Biol. Chem.* **1996**, *271* (34), 20246–20249. https://doi.org/10.1074/jbc.271.34.20246.

(100) Katoh, K.; Kano, Y.; Amano, M.; Onishi, H.; Kaibuchi, K.; Fujiwara, K. Rho-Kinase-Mediated Contraction of Isolated Stress Fibers. *J. Cell Biol.* **2001**, *152* (3), 569–583. https://doi.org/10.1083/jcb.153.3.569.

(101) Higashida et al. Actin Polymerization – Driven Molecular Movement of MDia1 In. **2007**, *303* (March 2004), 2007–2011.

(102) Watanabe, N.; Madaule, P.; Reid, T.; Ishizaki, T.; Watanabe, G.; Kakizuka, A.; Saito, Y.; Nakao, K.; Jockusch, B. M.; Narumiya, S. P140mDia, a Mammalian Homolog of Drosophila Diaphanous, Is a Target Protein for Rho Small GTPase and Is a Ligand for Profilin. *EMBO J.* **1997**, *16* (11), 3044–3056. https://doi.org/10.1093/emboj/16.11.3044.

(103) Watanabe, N.; Kato, T.; Fujita, A.; Ishizaki, T.; Narumiya, S. Cooperation between MDia1 and ROCK in Rho-Induced Actin Reorganization. *Nat. Cell Biol.* **1999**, *1* (3), 136–143. https://doi.org/10.1038/11056.

(104) Colombelli, J.; Besser, A.; Kress, H.; Reynaud, E. G.; Girard, P.; Caussinus, E.; Haselmann, U.; Small, J. V.; Schwarz, U. S.; Stelzer, E. H. K. Mechanosensing in Actin Stress Fibers Revealed by a Close Correlation between Force and Protein Localization. *J. Cell Sci.* **2009**, *122* (10), 1665–1679. https://doi.org/10.1242/jcs.054577.

(105) Hayakawa, K.; Tatsumi, H.; Sokabe, M. Actin Stress Fibers Transmit and Focus Force to Activate Mechanosensitive Channels. *J. Cell Sci.* **2008**, *121* (4), 496–503. https://doi.org/10.1242/jcs.022053.

(106) Discher, D. E.; Janmey, P.; Wang, Y. L. Tissue Cells Feel and Respond to the Stiffness of Their Substrate. *Science (80-.).* **2005**, *310* (5751), 1139–1143. https://doi.org/10.1126/science.1116995.

(107) Engler, A. J.; Sen, S.; Sweeney, H. L.; Discher, D. E. Matrix Elasticity Directs Stem Cell Lineage Specification. *Cell* **2006**, *126*, 677–689.

(108) Prager-Khoutorsky, M.; Lichtenstein, A.; Krishnan, R.; Rajendran, K.; Mayo, A.; Kam, Z.; Geiger, B.; Bershadsky, A. D. Fibroblast Polarization Is a Matrix-Rigidity-Dependent Process Controlled by Focal Adhesion Mechanosensing. *Nat. Cell Biol.* **2011**, *13* (12), 1457–1465. https://doi.org/10.1038/ncb2370.

(109) Sun, J.; Zhang, D.; Zheng, Y.; Zhao, Q.; Zheng, M.; Kovacevic, Z.; Richardson, D. R. Targeting the Metastasis Suppressor, NDRG1, Using Novel Iro Chelators: Regulation of Stress Fiber-Mediated Tumor Cell Migration via Modulation of the ROCK1/PMLC2 Signaling Pathway. *Mol. Pharmacol.* **2013**, *83* (2), 454–469. https://doi.org/10.1124/mol.112.083097.

(110) Malek, A. M.; Izumo, S. Mechanism of Endothelial Cell Shape Change and Cytoskeletal Remodeling in Response to Fluid Shear Stress. *J. Cell Sci.* **1996**, *109* (4), 713–726.

(111) Szymanski, D.; Staiger, C. J. The Actin Cytoskeleton: Functional Arrays for Cytoplasmic Organization and Cell Shape Control. *Plant Physiol.* **2018**, *176* (1), 106–118. https://doi.org/10.1104/pp.17.01519.

(112) Ponti, A.; Machacek, M.; Gupton, S. L.; Waterman-Storer, C. M.; Danuser, G. Two Distinct Actin Networks Drive the Protrusion of Migrating Cells. *Science (80-.).* **2004**, *305* (5691), 1782–1786. https://doi.org/10.1126/science.1100533.

(113) Gross, S. P.; Vershinin, M.; Shubeita, G. T. Cargo Transport: Two Motors Are Sometimes Better Than One. *Curr. Biol.* **2007**, *17* (June), R478–R486.

(114) Cramer, L. Organelle Transport: Dynamic Actin Tracks for Myosin Motors. *Curr. Biol.* **2008**, *18* (22), 1066–1068. https://doi.org/10.1016/j.cub.2008.09.048.

(115) Joseph, J. G.; Liu, A. P. Mechanical Regulation of Endocytosis: New Insights and Recent Advances. *Adv. Biosyst.* **2020**, *4* (5), 1–15. https://doi.org/10.1002/adbi.201900278.

(116) Caster, D. J.; Korte, E. A.; Tan, M.; Barati, M. T.; Tandon, S.; Creed, T. M.; Salant, D. J.; Hata, J. L.; Epstein, P. N.; Huang, H.; Powell, D. W.; McLeish, K. R. Neutrophil Exocytosis Induces Podocyte Cytoskeletal Reorganization and Proteinuria in Experimental Glomerulonephritis. *Am. J. Physiol. - Ren. Physiol.* **2018**, *315* (3), F595–F606. https://doi.org/10.1152/ajprenal.00039.2018.

(117) Jemal, A.; Siegel, R.; Ward, E.; Hao, Y.; Xu, J.; Murray, T.; Thun, M. J. Cancer Statistics, 2008. *CA. Cancer J. Clin.* **2008**, *58* (2), 71–96. https://doi.org/10.3322/ca.2007.0010.

(118) Siegel, R. L.; Miller, K. D.; Jemal, A. Cancer Statistics, 2020. *CA. Cancer J. Clin.* **2020**, *70* (1), 7–30. https://doi.org/10.3322/caac.21590.

(119) Kochanek, K. D.; Xu, J.; Arias, E. Mortality in the United States, 2019. *NCHS Data Brief* **2020**, No. 395, 1–8.

(120) Lugano, R.; Ramachandran, M.; Dimberg, A. Tumor Angiogenesis: Causes, Consequences, Challenges and Opportunities. *Cell. Mol. Life Sci.* **2020**, *77* (9), 1745–1770. https://doi.org/10.1007/s00018-019-03351-7.

(121) Hanahan, D.; Weinberg, R. A. Hallmarks of Cancer: The next Generation. *Cell* **2011**, *144* (5), 646–674. https://doi.org/10.1016/j.cell.2011.02.013.

(122) Martin-Belmonte, F.; Perez-Moreno, M. Epithelial Cell Polarity, Stem Cells and Cancer. *Nat. Rev. Cancer* **2012**, *12* (1), 23–38. https://doi.org/10.1038/nrc3169.

(123) Tepass, U.; Tanentzapf, G.; Ward, R.; Fehon, R. Epithelial Cell Polarity and Cell Junction

in Drosophila. *Annu. Rev. Genet.* **2001**, *35*, 747–784.

(124) Vasioukhin, V.; Bauer, C.; Yin, M.; Fuchs, E. Directed Actin Polymerization Is the Driving Force for Epithelial Cell-Cell Adhesion-Catenin Associates with Several Other Actin-Binding. *Cell* **2000**, *100*, 209–219.

(125) Kalluri, R.; Weinberg, R. A. The Basics of Epithelial-Mesenchymal Transition. *J. Clin. Invest.* **2009**, *119* (6), 1420–1428. https://doi.org/10.1172/JCI39104.1420.

(126) Lamouille, S.; Xu, J.; Derynck, R. Molecular Mechanisms of Epithelial-Mesenchymal Transition. *Nat. Rev. Mol. Cell Biol.* **2014**, *15* (3), 178–196. https://doi.org/10.1038/nrm3758.

(127) Roche, J. The Epithelial-to-Mesenchymal Transition in Canc. *Cancers (Basel).* **2018**, *10* (52).

(128) Nurwidya, F.; Takahashi, F.; Murakami, A.; Takahashi, K. Epithelial Mesenchymal Transition in Drug Resistance and Metastasis of Lung Cancer. *Cancer Res. Treat.* **2012**, *44* (3), 151–156. https://doi.org/10.4143/crt.2012.44.3.151.

(129) Xiao, D.; He, J. Epithelial Mesenchymal Transition and Lung Cancer. *J. Thorac. Dis.* **2010**, *2* (3), 154–159. https://doi.org/10.3978/j.issn.2072-1439.2010.02.03.7.

(130) Nieto, M. A. Epithelial Plasticity: A Common Theme in Embryonic and Cancer Cells. *Science (80-.).* **2013**, *342* (6159). https://doi.org/10.1126/science.1234850.

(131) Na, T. Y.; Schecterson, L.; Mendonsa, A. M.; Gumbiner, B. M. The Functional Activity of E-Cadherin Controls Tumor Cell Metastasis at Multiple Steps. *Proc. Natl. Acad. Sci. U. S. A.* **2020**, *117* (11), 5931–5937. https://doi.org/10.1073/pnas.1918167117.

(132) Zhang, P.; Sun, Y.; Ma, L. ZEB1: At the Crossroads of Epithelial-Mesenchymal Transition, Metastasis and Therapy Resistance. *Cell Cycle* **2015**, *14* (4), 481–487. https://doi.org/10.1080/15384101.2015.1006048.

(133) Grzegrzolka, J.; Biala, M.; Wojtyra, P.; Kobierzycki, C.; Olbromski, M.; Gomulkiewicz, A.; Piotrowska, A.; Rys, J.; Podhorska-Okolow, M.; Dziegiel, P. Expression of EMT Markers SLUG and TWIST in Breast Cancer. *Anticancer Res.* **2015**, *35* (7), 3961–3968.

(134) Loh, C.-Y.; Chai, J. Y.; Tang, T. F.; Wong, W. F.; Sethi, G.; Shanmugam, M. K.; Chong, P. P.; Loo, C. Y. The E-Cadherin and N-Cadherin Switch in Epithelial-to-Mesenchymal Transition: Signaling, Therapeutic Implications, and Challenges. *Cells* **2019**, *8* (10), 1118.

(135) Zhang, X.; Liu, G.; Kang, Y.; Dong, Z.; Qian, Q.; Ma, X. N-Cadherin Expression Is Associated with Acqusition of EMT Phenotype and with Enhanced Invasion in Erlotinib-Resistant Lung Cancer Cell Lines. *PLoS One* **2013**, *8* (3).

(136) Nakajima, S.; Doi, R.; Toyoda, E.; Tsuji, S.; Wada, M.; Koizumi, M.; Tulachan, S. S.; Ito, D.; Kami, K.; Mori, T.; Kawaguchi, Y.; Fujimoto, K.; Hosotani, R.; Imamura, M. N-Cadherin Expression and Epithelial-Mesenchymal Transition in Pancreatic Carcinoma. *Clin. Cancer Res.* **2004**, *10* (12 I), 4125–4133. https://doi.org/10.1158/1078-0432.CCR-0578-03.

(137) Haynes, J.; Srivastava, J.; Madson, N.; Wittmann, T.; Barber, D. L. Dynamic Actin Remodeling during Epithelial-Mesenchymal Transition Depends on Increased Moesin Expression. *Mol. Biol. Cell* **2011**, *22* (24), 4750–4764. https://doi.org/10.1091/mbc.E11-02-0119.

(138) Aseervatham, J. Cytoskeletal Remodeling in Cancer. *Biology (Basel).* **2020**, *9* (11), 1–40.

https://doi.org/10.3390/biology9110385.

(139) Dolati, S.; Kage, F.; Mueller, J.; Müsken, M.; Kirchner, M.; Dittmar, G.; Sixt, M.; Rottner, K.; Falckea, M. On the Relation between Filament Density, Force Generation, and Protrusion Rate in Mesenchymal Cell Motility. *Mol. Biol. Cell* **2018**, *29* (22), 2674–2886. https://doi.org/10.1091/mbc.E18-02-0082.

(140) Bertolo, A.; Gemperli, A.; Gruber, M.; Gantenbein, B.; Baur, M.; Potzel, T.; Stoyanov, J. In Vitro Cell Motility as a Potential Stem Cell Marker for Multipotency. *Stem Cells Transl. Med.* **2015**, *4*, 84–90.

(141) Osborne, L. D.; Li, G. Z.; How, T.; O'Brien, E. T.; Blobe, G. C.; Superfine, R.; Mythreye, K. TGF-β Regulates LARG and GEF-H1 during EMT to Affect Stiffening Response to Force and Cell Invasion. *Mol. Biol. Cell* **2014**, *25* (22), 3528–3540. https://doi.org/10.1091/mbc.E14-05-1015.

(142) Lin, H. H.; Lin, H. K.; Lin, I. H.; Chiou, Y. W.; Chen, H. W.; Liu, C. Y.; Harn, H. I. C.; Chiu, W. T.; Wang, Y. K.; Shen, M. R.; Tang, M. J. Mechanical Phenotype of Cancer Cells: Cell Softening and Loss of Stiffness Sensing. *Oncotarget* **2015**, *6* (25), 20946–20958. https://doi.org/10.18632/oncotarget.4173.

(143) Guck, J.; Schinkinger, S.; Lincoln, B.; Wottawah, F.; Ebert, S.; Romeyke, M.; Lenz, D.; M., E. H.; Ananthakrishnan, R.; Mitchell, D.; Kas, J.; Ulvick, S.; Bilby, C. Optical Deformability as an Inherent Cell Marker for Testing Malignant Transformation and Metastatic Competence. *Biophys. J.* **2005**, *88*, 3689–3698.

(144) Fritsch, A.; Höckel, M.; Kiessling, T.; Nnetu, K. D.; Wetzel, F.; Zink, M.; Käs, J. A. Are Biomechanical Changes Necessary for Tumour Progression? *Nat. Phys.* **2010**, *6* (10),

730–732. https://doi.org/10.1038/nphys1800.

(145) Tavares, S.; Vieira, A. F.; Taubenberger, A. V.; Araújo, M.; Martins, N. P.; Brás-Pereira, C.; Polónia, A.; Herbig, M.; Barreto, C.; Otto, O.; Cardoso, J.; Pereira-Leal, J. B.; Guck, J.; Paredes, J.; Janody, F. Actin Stress Fiber Organization Promotes Cell Stiffening and Proliferation of Pre-Invasive Breast Cancer Cells. *Nat. Commun.* **2017**, *8* (May). https://doi.org/10.1038/ncomms15237.

(146) Gladilin, E.; Ohse, S.; Boerries, M.; Busch, H.; Xu, C.; Schneider, M.; Meister, M.; Eils, R. TGFβ-Induced Cytoskeletal Remodeling Mediates Elevation of Cell Stiffness and Invasiveness in NSCLC. *Sci. Rep.* **2019**, *9* (1), 1–12. https://doi.org/10.1038/s41598-019-43409-x.

(147) Chikina, A. S.; Rubtsova, S. N.; Lomakina, M. E.; Potashnikova, D. M.; Vorobjev, I. A.; Alexandrova, A. Y. Transition from Mesenchymal to Bleb-Based Motility Is Predominantly Exhibited by CD133-Positive Subpopulation of Fibrosarcoma Cells. *Biol. Cell* **2019**, *111* (10), 245–261. https://doi.org/10.1111/boc.201800078.

(148) Sharma, S.; Bhonde, R. Influence of Nuclear Blebs and Micronuclei Status on the Growth Kinetics of Human Mesenchymal Stem Cells. *J. Cell. Physiol.* **2015**, *230* (3), 657–666. https://doi.org/10.1002/jcp.24789.

(149) Ndozangue-Touriguine, O.; Hamelin, J.; Bréard, J. Cytoskeleton and Apoptosis. *Biochem. Pharmacol.* **2008**, *76* (1), 11–18. https://doi.org/10.1016/j.bcp.2008.03.016.

(150) Kidd, M. E.; Shumaker, D. K.; Ridge, K. M. The Role of Vimentin Intermediate Filaments in the Progression of Lung Cancer. *Am. J. Respir. Cell Mol. Biol.* **2014**, *50* (1), 1–6. https://doi.org/10.1165/rcmb.2013-0314TR.

(151) Strouhalova, K.; Přechová, M.; Gandalovičová, A.; Brábek, J.; Gregor, M.; Rosel, D. Vimentin Intermediate Filaments as Potential Target for Cancer Treatment. *Cancers (Basel).* **2020**, *12* (1), 1–20. https://doi.org/10.3390/cancers12010184.

(152) Ostrowska-Podhorodecka, Z.; McCulloch, C. A. Vimentin Regulates the Assembly and Function of Matrix Adhesions. *Wound Repair Regen.* **2021**, No. March, 1–11. https://doi.org/10.1111/wrr.12920.

(153) Fife, C. M.; McCarroll, J. A.; Kavallaris, M. Movers and Shakers: Cell Cytoskeleton in Cancer Metastasis. *Br. J. Pharmacol.* **2014**, *171* (24), 5507–5523. https://doi.org/10.1111/bph.12704.

(154) Xie, L.; Law, B. K.; Chytil, A. M.; Brown, K. A.; Aakre, M. E.; Moses, H. L. Activation of the Erk Pathway Is Required for TGF-B1-Induced EMT in Vitro. *Neoplasia* **2004**, *6* (5), 603–610. https://doi.org/10.1593/neo.04241.

(155) Esposito, M.; Fang, C.; Cook, K. C.; Park, N.; Wei, Y.; Spadazzi, C.; Bracha, D.; Gunaratna, R. T.; Laevsky, G.; DeCoste, C. J.; Slabodkin, H.; Brangwynne, C. P.; Cristea, I. M.; Kang, Y. TGF-β-Induced DACT1 Biomolecular Condensates Repress Wnt Signalling to Promote Bone Metastasis. *Nat. Cell Biol.* **2021**, *23* (3), 257–267. https://doi.org/10.1038/s41556-021-00641-w.

(156) Yamanaka, H.; Moriguchi, T.; Masuyama, N.; Kusakabe, M.; Hanafusa, H.; Takada, R.; Takada, S.; Nishida, E. JNK Functions in the Non-Canonical Wnt Pathway to Regulate Convergent Extension Movements in Vertebrates. *EMBO Rep.* **2002**, *3* (1), 69–75. https://doi.org/10.1093/embo-reports/kvf008.

(157) Greco, F. A.; Hainsworth, J. D. Introduction: Unknown Primary Cancer. *Semin. Oncol.*

2009, *36* (1), 6–7. https://doi.org/10.1053/j.seminoncol.2008.10.007.

(158) Tanaka, F.; Yoneda, K.; Kondo, N.; Hashimoto, M.; Takuwa, T.; Matsumoto, S.; Okumura, Y.; Rahman, S.; Tsubota, N.; Tsujimura, T.; Kuribayashi, K.; Fukuoka, K.; Nakano, T.; Hasegawa, S. Circulating Tumor Cell as a Diagnostic Marker in Primary Lung Cancer. *Clin. Cancer Res.* **2009**, *15* (22), 6980–6986. https://doi.org/10.1158/1078-0432.CCR-09-1095.

(159) Okumura, Y.; Tanaka, F.; Yoneda, K.; Hashimoto, M.; Takuwa, T.; Kondo, N.; Hasegawa, S. Circulating Tumor Cells in Pulmonary Venous Blood of Primary Lung Cancer Patients. *Ann. Thorac. Surg.* **2009**, *87* (6), 1669–1675. https://doi.org/10.1016/j.athoracsur.2009.03.073.

(160) Ignatiadis, M.; Rothé, F.; Chaboteaux, C.; Durbecq, V.; Rouas, G.; Criscitiello, C.; Metallo, J.; Kheddoumi, N.; Singhal, S. K.; Michiels, S.; Veys, I.; Rossari, J.; Larsimont, D.; Carly, B.; Pestrin, M.; Bessi, S.; Buxant, F.; Liebens, F.; Piccart, M.; Sotiriou, C. HER2-Positive Circulating Tumor Cells in Breast Cancer. *PLoS One* **2011**, *6* (1), 6–11. https://doi.org/10.1371/journal.pone.0015624.

(161) Pagano, P. C.; Tran, L. M.; Bendris, N.; O'Byrne, S.; Tse, H. T.; Sharma, S.; Hoech, J. W.; Park, S. J.; Liclican, E. L.; Jing, Z.; Li, R.; Krysan, K.; Paul, M. K.; Fontebasso, Y.; Larsen, J. E.; Hakimi, S.; Seki, A.; Fishbein, M. C.; Gimzewski, J. K.; Di Carlo, D.; Minna, J. D.; Walser, T. C.; Dubinett, S. M. Identification of a Human Airway Epithelial Cell Subpopulation with Altered Biophysical, Molecular, and Metastatic Properties. *Cancer Prev. Res.* **2017**, *10* (9), 514–524. https://doi.org/10.1158/1940-6207.CAPR-16-0335.

(162) Friedman, E.; Lipkin, M.; Verderame, M.; Pollack, R. Altered Actin Cytoskeletal Patterns in Two Premalignant Stages in Human Colon Carcinoma Development. *Cancer Res.* **1985**, *45* (7), 3236–3242.

(163) Sanchez-Garcia, I. The Crossroads of Oncogenesis and Metastasis. *N. Engl. J. Med.* **2009**, 297–299.

(164) Gown, A. M.; Vogel, A. M.; Gordon, D.; Lu, P. L. A Smooth Muscle-Specific Monoclonal Antibody Recognizes Smooth Muscle Actin Isozymes. *J. Cell Biol.* **1985**, *100* (3), 807–813. https://doi.org/10.1083/jcb.100.3.807.

(165) Kinner, B.; Spector, M. Expression of Smooth Muscle Actin in Osteoblasts in Human Bone. *J. Orthop. Res.* **2002**, *20* (3), 622–632. https://doi.org/10.1016/S0736-0266(01)00145-0.

(166) Riedl, J.; Crevenna, A. H.; Kessenbrock, K.; Yu, J. H.; Neukirchen, D.; Bista, M.; Bradke, F.; Jenne, D.; Holak, T. A.; Werb, Z.; Sixt, M.; Wedlich-Soldner, R. Lifeact: A Versatile Marker to Visualize F-Actin. *Nat. Methods* **2008**, *5* (7), 605–607. https://doi.org/10.1038/nmeth.1220.

(167) Pan, L.; Yan, R.; Li, W.; Xu, K. Super-Resolution Microscopy Reveals the Native Ultrastructure of the Erythrocyte Cytoskeleton. *Cell Rep.* **2018**, *22* (5), 1151–1158. https://doi.org/10.1016/j.celrep.2017.12.107.

(168) Qi, J.; Liu, Y.; Chu, C.; Chen, X.; Zhu, W.; Shu, Y.; He, S.; Chai, R.; Zhong, G. A Cytoskeleton Structure Revealed by Super-Resolution Fluorescence Imaging in Inner Ear Hair Cells. *Cell Discov.* **2019**, *5* (1), 10–12. https://doi.org/10.1038/s41421-018-0076-4.

(169) Suleiman, H. Y.; Roth, R.; Jain, S.; Heuser, J. E.; Shaw, A. S. Injury-Induced Actin Cytoskeleton Reorganization in Podocytes Revealed by Super-Resolution Microscopy. *JCI Insight* **2017**, *2* (16).

(170) Sun, Y.; Schroeder, H. W.; Beausang, J. F.; Homma, K.; Ikebe, M.; Goldman, Y. E. Myosin VI Walks "Wiggly" on Actin with Large and Variable Tilting. *Mol. Cell* **2007**, *28* (6), 954–964. https://doi.org/10.1016/j.molcel.2007.10.029.

(171) Kuhn, J. R.; Pollard, T. D. Real-Time Measurements of Actin Filament Polymerization by Total Internal Reflection Fluorescence Microscopy. *Biophys. J.* **2005**, *88* (2), 1387–1402. https://doi.org/10.1529/biophysj.104.047399.

(172) Pavlov, D.; Muhlrad, A.; Cooper, J.; Wear, M.; Reisler, E. Actin Filament Severing by Cofilin. *J. Mol. Biol.* **2007**, *365* (5), 1350–1358. https://doi.org/10.1016/j.jmb.2006.10.102.

(173) Merino, F.; Pospich, S.; Funk, J.; Wagner, T.; Küllmer, F.; Arndt, H. D.; Bieling, P.; Raunser, S. Structural Transitions of F-Actin upon ATP Hydrolysis at near-Atomic Resolution Revealed by Cryo-EM. *Nat. Struct. Mol. Biol.* **2018**, *25* (6), 528–537. https://doi.org/10.1038/s41594-018-0074-0.

(174) Krishnaswamy, S.; Zivanovic, N.; Sharma, R.; Pe'Er, D.; Bodenmiller, B. *Learning Time-Varying Information Flow from Single-Cell Epithelial to Mesenchymal Transition Data*; 2018; Vol. 13. https://doi.org/10.1371/journal.pone.0203389.

(175) Karacosta, L. G.; Anchang, B.; Ignatiadis, N.; Kimmey, S. C.; Benson, J. A.; Shrager, J. B.; Tibshirani, R.; Bendall, S. C.; Plevritis, S. K. Mapping Lung Cancer Epithelial-Mesenchymal Transition States and Trajectories with Single-Cell Resolution. *Nat.*

Commun. **2019**, *10* (1), 1–15. https://doi.org/10.1038/s41467-019-13441-6.

(176) van Dijk, D.; Sharma, R.; Nainys, J.; Yim, K.; Kathail, P.; Carr, A. J.; Burdziak, C.; Moon, K. R.; Chaffer, C. L.; Pattabiraman, D.; Bierie, B.; Mazutis, L.; Wolf, G.; Krishnaswamy, S.; Pe'er, D. Recovering Gene Interactions from Single-Cell Data Using Data Diffusion. *Cell* **2018**, *174* (3), 716-729.e27. https://doi.org/10.1016/j.cell.2018.05.061.

(177) Alioscha-Perez, M.; Benadiba, C.; Goossens, K.; Kasas, S.; Dietler, G.; Willaert, R.; Sahli, H. A Robust Actin Filaments Image Analysis Framework. *PLoS Comput. Biol.* **2016**, *12* (8), 1–23. https://doi.org/10.1371/journal.pcbi.1005063.

(178) Hauke, L.; Narasimhan, S.; Primeßnig, A.; Kaverina, I. A Focal Adhesion Filament Cross-Correlation Kit for Fast , Automated Segmentation and Correlation of Focal Adhesions and Actin Stress Fibers in Cells . Author Summary. **2021**.

(179) Rimoli, C. V.; Augusto, C.; Cruz, V.; Curcio, V.; Mavrakis, M. 4polar-STORM Polarized Super-Resolution Imaging of Actin Filament Organization in Cells. **2021**.

Chapter 2

Statistical Parametrization of the Cell Cytoskeleton

SPOCC

This chapter is a detailed description of **Statistical Parametrization of the Cell Cytoskeleton** or **SPOCC**. This technique has been used for studying lung cancer and pre-cancer cells in the following chapters. This chapter contains a brief summary of the different existing image analysis platforms as well as detailed description of the image analysis and statistical calculations required for SPOCC.

1. Existing Image Analysis Methods

The actin cytoskeleton is a dynamic network that responds to external and internal stimuli. Such stimulations can induce polymerization and depolymerization of actin to balance the external force. Multiple studies have been carried out to understand the cytoskeletal response to a variety of external forces such as fluid shear stress[1,2,3,4,5], simulated micro-gravity[6,7,8,9,10], cyclic stretching[11,12,13] etc. and observed through fluorescence microscopy. Cellular processes ranging from a few seconds to a few days can be accurately observed by imaging them and with the advent of super-resolution techniques[14,15,16], information can be obtained with a higher degree of spatial and temporal resolution. But a fluorescence image (or video) requires interpretation, no matter how drastic the change is, which makes the analysis subjective. Hence, there has been a great deal of interest in developing quantification techniques to extract more information from cytoskeletal images without compromising its reliability.

The basic extraction strategies in existing analysis methods can be broadly classified into three categories: filament directionality, filament network and single-filament extraction[17,18,19] (Figure. 1). In the directionality based analysis, earlier approaches were based on Fourier transforms and then filtering the Fourier transform coefficients[20]. Recent works have used more sophisticated transforms such as wavelets[21,22], curvelets[23,24], contourlets[25,26] and shearlets[27,28] based on various requirements. The basis function for these transforms provide a very useful tool for orientational analysis. These processes do not consider separate foreground/background segmentation which reduces the corresponding errors but limits the application to directionality related analysis.

For network based analysis, the image is filtered to extract the filament network as a whole[29]. In some cases, the filtering is done with respect to some template matching[30] that incorporates known

information regarding the targets already. The limitation of these algorithms is that they do not perform well in detecting network junctions where two filaments overlap. This is solved in part by incorporating linear models for filaments in contour based methods[31]. In some work, the orientational information is replaced by velocity and density information. This kind of analysis is especially relevant in trying to understand active polymerization/depolymerization processes[32].

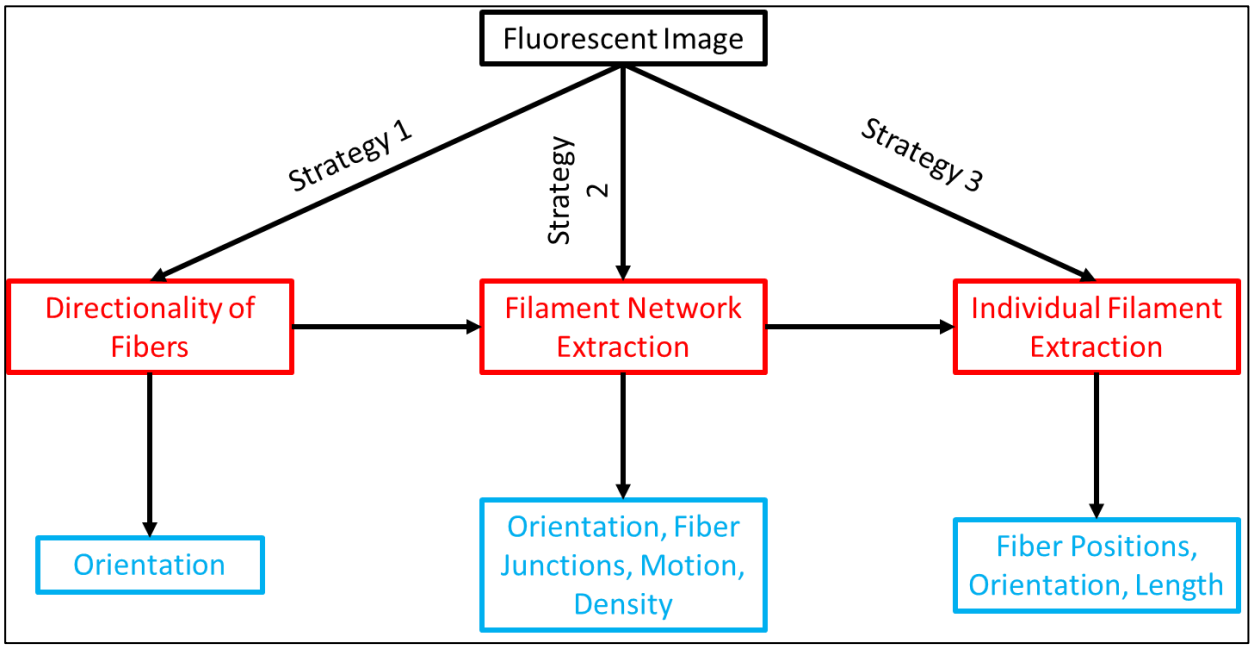


Fig. 1 | Summary of existing strategies for extracting fibers and related information from fluorescent images. The second row (in red) shows the basis for fiber extraction in each of the strategies. The third row (in blue) shows the information that can be extracted from each of these strategies. This image is inspired from Alioscha–Perez et. al.[33].

Segmentation of an image into multiple relevant parts is of particular interest for filament extraction. An image consists of background noise as well as the features of interest, so it is important to separate the noise part from the feature part. Simple or directional Gaussian[34] and Laplace[35] filters are used in general for denoising as background noise has a different frequency compared to the signal. But in an actual cell, there are non-noise artefact elements such as aggregate structures or non-specific fluorescent tagging which cannot be corrected using this

process. Coherent enhancement filters can distinguish flowing patterns from artefact but they cannot handle out of focus blurring due to the three dimensional nature of cells. Some works have also used Radon transformation[36] as a denoising step.

Once the filaments are detected and separated from noise and non-noise artefacts, the filament image needs to be binarized. Network binarization separates the pixels that are part of the filament image from the ones that are not. This enables further line detection to extract the fibers individually. Standard binarization protocols include global thresholding, Otsu's brightness thresholding[37] and local thresholding based on neighboring regions. A combination of global and local thresholding is also used for better efficiency and accuracy[18,38]. From the binarized image, individual fibers are detected using line segment detectors. There are multiple models of line detection and there is always a trade-off between accurate detection of fibers and the computational load[19]. Though the line detection algorithm detects lines of a certain small length, such extracted segments are iteratively merged to generate the final image which also provides information regarding the location, length and orientation of the extracted fibers.

2. Orientational Order Parameter (OOP)

Multiple parameters have been used to assign characteristics to cells such as size, aspect ratio and flatness. Similar approaches have been made to analyze the cytoskeleton of the cell. Comparing length of fibers is a useful tool, but can be limited by the fact that the length of fibers would depend on the overall size of the cell. Relative orientation of fibers, on the other hand, can provide detailed insight into the nature of the cytoskeleton. Transverse arcs and dorsal stress fiber are likely to form disorganized patterns based on their structures. But ventral fibers are usually parallel to one another, though they can lose their parallel nature under certain conditions. Based on the nature,

the distribution of angles can be broad or narrow. A statistical metric is essential to quantify the organization of stress fibers in cells. Simple methods such as fitting the distribution of a Gaussian or normal distribution and calculating the standard deviation[39]. More complicated models can also be used for the fitting, such as the von Mises circular distribution[40,41,42], which is a wrapped normal distribution. But the angular distribution of stress fibers does not often follow either Gaussian or normal distribution. Also, fitting the angular distribution to any particular function presupposes the knowledge of a biological model, which can be erroneous.

An alternate metric for analyzing the angular distribution of stress fibers is the Orientational Order Parameter (OOP). OOP does not require the data to follow any particular model and objectively calculates the relative order between the fibers. OOP has been extensively used in biology[43] to quantify order of bacteria[44], fibroblasts[45] and cardiac muscles[46].

For the calculation of OOP, first the angles are treated as vectors and then the corresponding order tensor for every vector is generated.

$$Angle \xrightarrow{yields} \begin{bmatrix} p_{i,x} \\ p_{i,y} \end{bmatrix}$$

$$Order\ Tensor = \begin{bmatrix} p_{i,x}p_{i,x} & p_{i,x}p_{i,y} \\ p_{i,x}p_{i,y} & p_{i,y}p_{i,y} \end{bmatrix}$$

Then the mean order tensor is calculated for the distribution.

$$Mean\ order\ tensor\ =\ T\ =\ \langle 2\begin{bmatrix} p_{i,x}p_{i,x} & p_{i,x}p_{i,y} \\ p_{i,x}p_{i,y} & p_{i,y}p_{i,y} \end{bmatrix} - \begin{bmatrix} 1 & 0 \\ 0 & 1 \end{bmatrix}\rangle$$

Orientational Order Parameter is defined as the maximum possible eigenvalue of the mean order tensor.

$$OOP = max[eigenvalue(T)]$$

If the p_x and p_y components of the angle vectors are replaced with cos(α) and sin(α) respectively, then the equation can be simplified further.

$$OOP = \langle cos\big(2(\alpha - \alpha_0)\big)\rangle$$

where α_0 is the mean angle of the distribution.

For completely ordered systems, the OOP value is 1 and for completely disorganized systems the OOP value is 0. In real cases, we can expect the OOP value to be somewhere between 0 and 1, with higher values corresponding to a higher degree of order (Figure 2). OOP calculation of simulated Gaussian and normal distribution of angles can corroborate the validity of OOP as a measure of order.

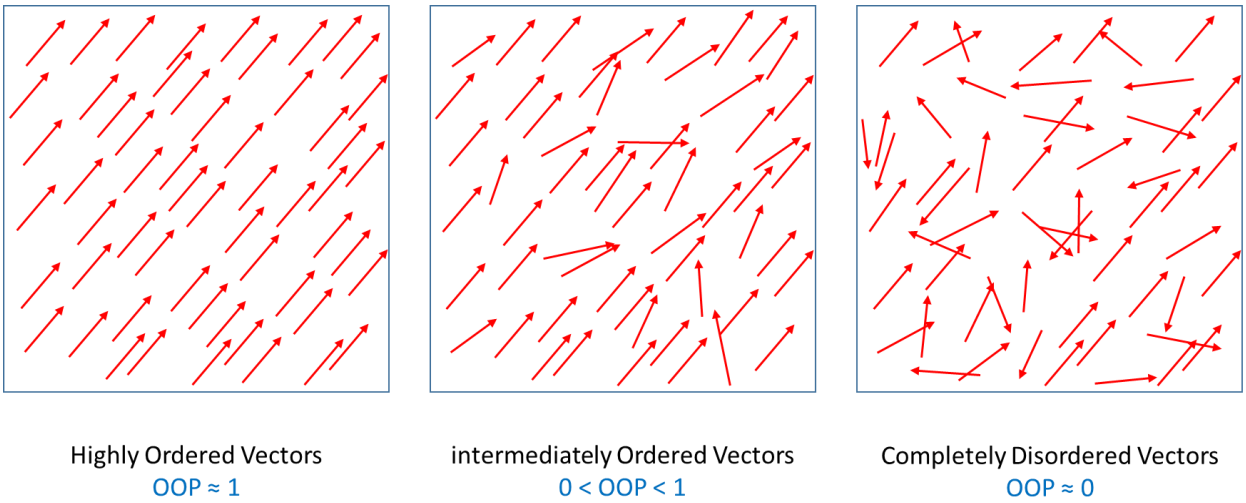


Fig. 2 | Vector with different orders and their corresponding OOP values. Each arrow corresponds to the direction of that vector (angle). The order of the vectors is decreasing from left to right. The highly ordered system will have an OOP close to one whereas the completely disordered system will have an OOP close to zero.

3. Statistical Parametrization of the Cell Cytoskeleton (SPOCC)

In this work, we have combined filament extraction with OOP calculation to develop a new method of quantifying the organization of stress fibers called the **Statistical Parametrization of the Cell**

Cytoskeleton (SPOCC) (Figure. 3). This method is capable of evaluating a figure of merit for any biological process that involves cytoskeletal rearrangement.

The fluorescent image can be thought of as a sum of multiple components, such as filament image, artefact image and noise. The filament and the artefact images are calculated using a sparse source separation approach. As the filaments and artefacts have completely different geometric patterns, two separate models were used for their evaluations[47]. The artefact image was modelled based on undecimated wavelet transform, whereas due to the curvilinear nature of the filaments, the filament image was modelled based on curvelets transform. This image decomposition was performed based on the Morphological Component Analysis Lab (MCALab) libraries, using 100 iterations.

Once the filament image is separated the filaments are enhanced using a sequence of filters. The first filter used is a Gaussian filter which is defined as a convolution operator with a Gaussian Kernel. Then a Laplace filter is applied with the following Kernel:

$$L = \beta \times \begin{bmatrix} 0 & -1 & 0 \\ -1 & -4 & -1 \\ 0 & -1 & 0 \end{bmatrix}$$

where β is set to a value between 0 and 10. A third directional Gaussian filter is also used. These processes are carried out to sharpen the image and enhance the edges.

The next step is a filament network segmentation, which is done with a multi-scale line detection algorithm[48]. Here, every pixel around a chosen pixel is analyzed for the likelihood of that pixel being part of a line with a certain width. This step is repeated for every pixel iteratively. Next, the likelihood is calculated for a pixel to be at the center of a line (of a particular width) passing through it at a particular direction by analyzing the neighboring pixel. The output image is also binarized using Wellner's adaptive thresholding[49].

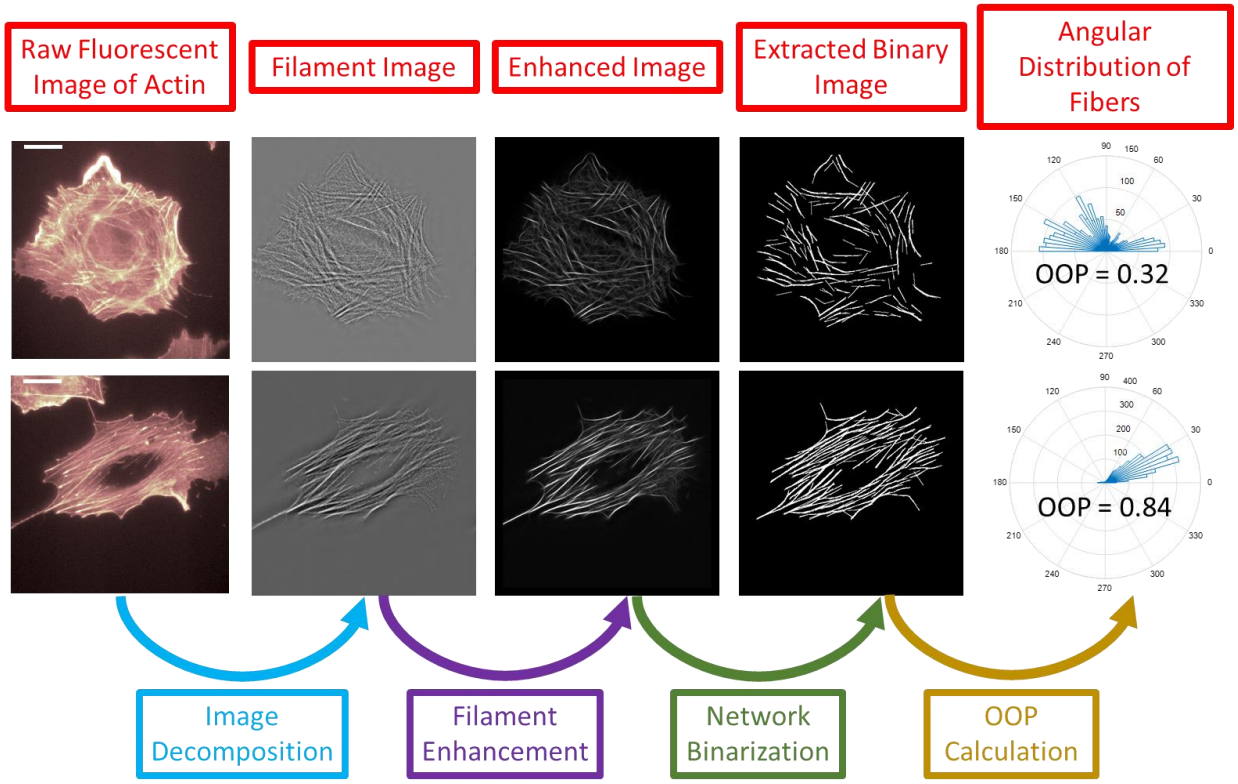


Fig. 3 | Flowchart of SPOCC. Two cells with disoriented and oriented fiber patters being processed using SPOCC. Top row (red) shows the output of the different steps (bottom row, color-coded). Scale bar: 16μm.

A line segmentation of this binarized image generates a list of line segments with a fixed minimum length. Basically, a fixed length line segment is fitted to the non-zero pixels using least square fitting. If the fitting error is larger than one pixel then a new line segment is started. This step is repeated until no further line segments can be fitted to the non-zero pixels. All overlapping line segments with the same direction are then stitched together to form long single filaments. Further a curvature threshold can be set to stitch up segments that have very close angles (but not exactly the same). From the list of angles, the OOP was calculated using the protocol descried previously[44,46,43].

We have specifically applied SPOCC to study the dynamic actin remodeling in lung cancer cells during Epithelial Mesenchymal Transition and validated OOP as a figure of merit for EMT

progression. We have demonstrated that this figure of merit can efficiently quantify drug response of cytoskeletal reorganization. We have also employed SPOCC to distinguish between different cytoskeletal phenotypes in lung cancer as well as pre-cancer cells.

References:

(1) Jackson, W. M.; Jaasma, M. J.; Tang, R. Y.; Keaveny, T. M. Mechanical Loading by Fluid Shear Is Sufficient to Alter the Cytoskeletal Composition of Osteoblastic Cells. *Am. J. Physiol. - Cell Physiol.* **2008**, *295* (4), 1007–1015. https://doi.org/10.1152/ajpcell.00509.2007.

(2) Gardinier, J. D.; Majumdar, S.; Duncan, R. L.; Wang, L. Cyclic Hydraulic Pressure and Fluid Flow Differentially Modulate Cytoskeleton Re-Organization in MC3T3 Osteoblasts. *Cell. Mol. Bioeng.* **2009**, *2* (1), 133–143. https://doi.org/10.1007/s12195-008-0038-2.

(3) Son, K.; Small, M.; Sehmi, R.; Janssen, L. The Eosinophil Actin Cytoskeleton Undergoes Rapid Rearrangement in Response to Fluid Shear Stress. *J. Leukoc. Biol.* **2020**, *108*, 129–137.

(4) Loufrani, L.; Henrion, D. Role of the Cytoskeleton in Flow (Shear Stress)-Induced Dilation and Remodeling in Resistance Arteries. *Med Biol Eng Comput* **2008**, *46*, 451–460.

(5) Osborn, E. A.; Rabodzey, A.; Dewey Jr., C. F.; Hartwig, J. H. Endothelial Actin Cytoskeleton Remodeling during Mechanostimulation with Fluid Shear Stress. *Am. J. Physiol. - Cell Physiol.* **2006**, *290*, C444–C452.

(6) Nabavi, N.; Khandani, A.; Camirand, A.; Harrison, R. E. Effects of Microgravity on

Osteoclast Bone Resorption and Osteoblast Cytoskeletal Organization and Adhesion. *Bone* **2011**, *49* (5), 965–974. https://doi.org/10.1016/j.bone.2011.07.036.

(7) Dai, Z.; Wu, F.; Chen, J.; Xu, H.; Wang, H.; Guo, F.; Yingjun, T.; Ding, B.; Wang, J.; Wan, Y.; Li, Y. Actin Microfilaments Mediates Osteoblast Cbfa1 Responsiveness to BMP2 under Simulated Microgravity. *PLoS One* **2013**, *8* (5).

(8) Nassef, M. Z.; Kopp, S.; Wehland, M.; Melnik, D.; Sahana, J.; Krüger, M.; Corydon, T. J.; Oltmann, H.; Schmitz, B.; Schütte, A.; Bauer, T. J.; Infanger, M.; Grimm, D. Real Microgravity Influences the Cytoskeleton and Focal Adhesions in Human Breast Cancer Cells. *Int. J. Mol. Sci.* **2019**, *20* (13), 1–25. https://doi.org/10.3390/ijms20133156.

(9) Janmaleki, M.; Pachenari, M.; Seyedpour, S. M.; Shahghadami, R.; Sanati-Nezhad, A. Impact of Simulated Microgravity on Cytoskeleton and Viscoelastic Properties of Endothelial Cell. *Sci. Rep.* **2016**, *6* (August), 1–11. https://doi.org/10.1038/srep32418.

(10) Crawford-Young, S. J. Effects of Microgravity on Cell Cytoskeleton and Embryogenesis. *Int. J. Dev. Biol.* **2006**, *50*, 183–191.

(11) Kaunas, R.; Usami, S.; Chien, S. Regulation of Stretch-Induced JNK Activation by Stress Fiber Orientation. *Cell. Signal.* **2006**, *18*, 1924–1931.

(12) Zhao, L.; Sang, C.; Yang, C.; Zhuang, F. Effects of Stress Fiber Contractility on Uniaxial Stretch Guiding Mitosis Orientation and Stress Fiber Alignment. *J. Biomech.* **2011**, *44* (13), 2388–2394. https://doi.org/10.1016/j.jbiomech.2011.06.033.

(13) Gögele, C.; Hoffmann, C.; Konrad, J.; Merkel, R.; Schwarz, S.; Tohidnezhad, M.; Hoffmann, B.; Schulze-Tanzil, G. G. Cyclically Stretched ACL Fibroblasts Emigrating

from Spheroids Adapt Their Cytoskeleton and Ligament-Related Expression Profile. *Cell Tissue Res.* **2021**. https://doi.org/10.1007/s00441-021-03416-9.

(14) Pan, L.; Yan, R.; Li, W.; Xu, K. Super-Resolution Microscopy Reveals the Native Ultrastructure of the Erythrocyte Cytoskeleton. *Cell Rep.* **2018**, *22* (5), 1151–1158. https://doi.org/10.1016/j.celrep.2017.12.107.

(15) Qi, J.; Liu, Y.; Chu, C.; Chen, X.; Zhu, W.; Shu, Y.; He, S.; Chai, R.; Zhong, G. A Cytoskeleton Structure Revealed by Super-Resolution Fluorescence Imaging in Inner Ear Hair Cells. *Cell Discov.* **2019**, *5* (1), 10–12. https://doi.org/10.1038/s41421-018-0076-4.

(16) Suleiman, H. Y.; Roth, R.; Jain, S.; Heuser, J. E.; Shaw, A. S. Injury-Induced Actin Cytoskeleton Reorganization in Podocytes Revealed by Super-Resolution Microscopy. *JCI Insight* **2017**, *2* (16).

(17) Elosegui-Artola, A.; Jorge-Penas, A.; Moreno-Arortzena, O.; Oregi, A.; Lasa, M.; Garcia-Anzar, J. M.; De Juan-Pardo, E. M.; Aldabe, R. Image Analysis for the Quantitative Comparison of Stress Fibers and Focal Adhesions. *PLoS One* **2014**, *9* (9).

(18) Eltzner, B.; Wollnik, C.; Gottschlich, C.; Huckemann, S.; Rehfeldt, F. The Filament Sensor for near Real-Time Detection of Cytoskeletal Fiber Structures. *PLoS One* **2015**, *10* (5), 1–28. https://doi.org/10.1371/journal.pone.0126346.

(19) Grompone von Gioi, R.; Jakubowicz, J.; Morel, J.-M.; Randall, G. LSD: A Line Segment Detector. *Image Process. Line* **2012**, *2*, 35–55. https://doi.org/10.5201/ipol.2012.gjmr-lsd.

(20) Marquez, J. P. Fourier Analysis and Automated Measurement of Cell and Fiber Angular Orientation Distributions. *Int. J. Solids Struct.* **2006**, *43* (21), 6413–6423.

https://doi.org/10.1016/j.ijsolstr.2005.11.003.

(21) Malvar, S.; Carmo, B. S. Wavelet Analysis of a Flexible Filament Kinematics: Emulating C. Elegans Swimming Behavior. *J. Brazilian Soc. Mech. Sci. Eng.* **2021**, *43* (4), 1–13. https://doi.org/10.1007/s40430-021-02915-8.

(22) Clarke, A.; McQueen, P. G.; Fang, H. Y.; Kannan, R.; Wang, V.; McCreedy, E.; Wincovitch, S.; Giniger, E. Abl Signaling Directs Growth of a Pioneer Axon in Drosophila by Shaping the Intrinsic Fluctuations of Actin. *Mol. Biol. Cell* **2020**, *31* (6), 466–477. https://doi.org/10.1091/mbc.E19-10-0564.

(23) Sampo, J.; Takalo, J.; Siltanen, S.; Miettinen, A.; Lassas, M.; Timonen, J. Curvelet-Based Method for Orientation Estimation of Particles from Optical Images. *Opt. Eng.* **2014**, *53* (3), 033109. https://doi.org/10.1117/1.oe.53.3.033109.

(24) Candès, E.; Demanet, L.; Donoho, D.; Ying, L. Fast Discrete Curvelet Transforms. *Multiscale Model. Simul.* **2006**, *5* (3), 861–899. https://doi.org/10.1137/05064182X.

(25) Huang, Y.; Hu, X.; Hao, L.; Gao, Y.; Liu, Z.; Wang, P. Quantitative Analysis of Cell Morphology Based on Contourlet Transform. *IET Image Process.* **2020**, *14* (12), 2826–2832.

(26) Zhou, Y.; Zhang, W.; Li, H.; Ji, B. Automatic Directional Analysis of Cell Microscopy Images. *Proc. 2017 12th IEEE Conf. Ind. Electron. Appl. ICIEA 2017* **2018**, *2018-February*, 70–74. https://doi.org/10.1109/ICIEA.2017.8282816.

(27) Sayadi, M.; Ghassemian, H.; Naimi, R.; Imani, M. A New Composite Multimodality Image Fusion Method Based on Shearlet Transform and Retina Inspired Model. *Iran.*

Conf. Mach. Vis. Image Process. MVIP **2020**, *2020-February*, 1–5. https://doi.org/10.1109/MVIP49855.2020.9116919.

(28) Arunachalam, M.; Savarimuthu, S. R. An Efiicient and Automatic Glioblastoma Brain Tumor Detection Using Shift Invariant Shearlet Transform and Neural Network. *Int. J. Imaging Syst. Technol.* **2017**, *27*, 216–226.

(29) Herberich, G.; Würflinger, T.; Sechi, A.; Windoffer, R.; Leube, R.; Aach, T. Fluorescence Microscopic Imaging and Image Analysis of the Cytoskeleton. *Conf. Rec. - Asilomar Conf. Signals, Syst. Comput.* **2010**, 1359–1363. https://doi.org/10.1109/ACSSC.2010.5757755.

(30) Rigort, A.; Günther, D.; Hegerl, R.; Baum, D.; Weber, B.; Prohaska, S.; Medalia, O.; Baumeister, W.; Hege, H. C. Automated Segmentation of Electron Tomograms for a Quantitative Description of Actin Filament Networks. *J. Struct. Biol.* **2012**, *177* (1), 135–144. https://doi.org/10.1016/j.jsb.2011.08.012.

(31) Xu, T.; Vavylonis, D.; Tsai, F.-C.; Koenderink, G. H.; Nie, W.; Yusuf, E.; Lee, I.-J.; Wu, J.-Q.; Huang, X. SOAX: A Software for Quantification of 3D Biopolymer Networks. *Sci. Rep.* **2015**, *5* (9081).

(32) Moch, M.; Herberich, G.; Aach, T.; Leube, R. E.; Windoffer, R. Measuring the Regulation of Keratin Filament Network Dynamics. *Proc. Natl. Acad. Sci. U. S. A.* **2013**, *110* (26), 10664–10669. https://doi.org/10.1073/pnas.1306020110.

(33) Alioscha-Perez, M.; Benadiba, C.; Goossens, K.; Kasas, S.; Dietler, G.; Willaert, R.; Sahli, H. A Robust Actin Filaments Image Analysis Framework. *PLoS Comput. Biol.* **2016**, *12* (8), 1–23. https://doi.org/10.1371/journal.pcbi.1005063.

(34) Freeman, W. T.; Adelson, E. H. The Design and Use of Steerable Filters. *IEEE Trans. Pattern Anal. Mach. Intell.* **1991**, *13* (9), 891–906.

(35) van Vliet, L. J.; Young, I. T.; Beckers, G. L. A Nonlinear Laplace Operator as Edge Detector in Noisy Images. *Comput. Vision, Graph. Image Process.* **1989**, *45* (2), 167–195. https://doi.org/10.1016/0734-189X(89)90131-X.

(36) Winkler, C.; Vinzenz, M.; Small, J. V.; Schmeiser, C. Actin Filament Tracking in Electron Tomograms of Negatively Stained Lamellipodia Using the Localized Radon Transform. *J. Struct. Biol.* **2012**, *178* (1), 19–28. https://doi.org/10.1016/j.jsb.2012.02.011.

(37) Otsu, N. A Threshold Selection Method from Gray-Level Histograms. *IEEE Trans. Syst. Man Cybern.* **1979**, *20* (1), 62–66.

(38) Zemel, A.; Rehfeldt, F.; Brown, A. E. X.; Discher, D. E.; Safran, S. A. Optimal Matrix Rigidity for Stress-Fibre Polarization in Stem Cells. *Nat. Phys.* **2010**, *6* (6), 468–473. https://doi.org/10.1038/nphys1613.

(39) Davidson, P.; Bigerelle, M.; Bounichane, B.; Giazzon, M.; Anselme, K. Definition of a Simple Statistical Parameter for the Quantification of Orientation in Two Dimensions: Application to Cells on Grooves of Nanometric Depths. *Acta Biomater.* **2010**, *6* (7), 2590–2598. https://doi.org/10.1016/j.actbio.2010.01.038.

(40) Karlon, W. J.; Hsu, P. P.; Song, L. I.; Chien, S.; McCulloch, A. D.; Omens, J. H. Measurement of Orientation and Distribution of Cellular Alignment and Cytoskeletal Organization. *Ann. Biomed. Eng.* **1999**, *27* (6), 712–720. https://doi.org/10.1114/1.226.

(41) Su, W.-T.; Liao, Y.-F.; Chu, I.-M. Observation of Fibroblast Motility on a Micro-Grooved

Hydrophobic Elastomer Substrate with Different Geometric Characteristics. *Micron* **2007**, *38*, 278–285.

(42) Wang, Y.; Son, S.; Swartz, S. M.; Goulbourne, N. C. A Mixed von Mises Distribution for Modeling Soft Biological Tissues with Two Distributed Fiber Properties. *Int. J. Solids Struct.* **2012**, *49* (21), 2914–2923. https://doi.org/10.1016/j.ijsolstr.2012.04.004.

(43) Grosberg, A.; Kuo, P. L.; Guo, C. L.; Geisse, N. A.; Bray, M. A.; Adams, W. J.; Sheehy, S. P.; Parker, K. K. Self-Organization of Muscle Cell Structure and Function. *PLoS Comput. Biol.* **2011**, *7* (2). https://doi.org/10.1371/journal.pcbi.1001088.

(44) Volfson, D.; Cookson, S.; Hasty, J.; Tsimring, L. S. Biomechanical Ordering of Dense Cell Populations. *Proc. Natl. Acad. Sci. U. S. A.* **2008**, *105* (40), 15346–15351. https://doi.org/10.1073/pnas.0706805105.

(45) Sun, J. G.; Tang, J.; Ding, J. D. Cell Orientation on a Stripe-Micropatterned Surface. *Chinese Sci. Bull.* **2009**, *54* (18), 3154–3159. https://doi.org/10.1007/s11434-009-0240-1.

(46) Grosberg, A.; Alford, P. W.; McCain, M. L.; Parker, K. K. Ensembles of Engineered Cardiac Tissues for Physiological and Pharmacological Study: Heart on a Chip. *Lab Chip* **2011**, *11* (24), 4165–4173. https://doi.org/10.1039/c1lc20557a.

(47) Starck, J. L.; Elad, M.; Donoho, D. L. Image Decomposition via the Combination of Sparse Representations and a Variational Approach. *IEEE Trans. Image Process.* **2005**, *14* (10), 1570–1582. https://doi.org/10.1109/TIP.2005.852206.

(48) Nguyen, U. T. V.; Bhuiyan, A.; Park, L. A. F.; Ramamohanarao, K. An Effective Retinal Blood Vessel Segmentation Method Using Multi-Scale Line Detection. *Pattern Recognit.*

2013, *46* (3), 703–715. https://doi.org/10.1016/j.patcog.2012.08.009.

(49) Wellner, P. D. Adaptive Thresholding for the DigitalDesk. *Xerox, EPC1993-110* **1993**, 1–19.

Chapter 3

Quantitative analysis of actin cytoskeleton's morphological changes during EMT in lung cancer cells

This chapter describes an application of the image quantification technique discussed in Chapter 2 (SPOCC). Using SPOCC, a novel partial EMT phenotype with unique cytoskeletal signature was identified in lung cancer cells. This chapter is about to be submitted/published as a research article titled “New image quantification technique reveals novel cytoskeletal phenotype with partial EMT signature in lung cancer cells” by authors A. Basu, M. K. Paul, M. Alioscha-Perez, A. Grosberg, H. Sahli, S. M. Dubinett and S. Weiss.

New image quantification technique reveals novel cytoskeletal phenotype with partial EMT signature in lung cancer cells

Arkaprabha Basu*, Manash K. Paul*, Mitchel Alioscha-Perez*, Anna Grosberg*, Hichem Sahli*, Steven M. Dubinett*, Shimon Weiss*

Abstract:

Epithelial Mesenchymal Transition (EMT) is a multi-step process that involves cytoskeletal rearrangement. Here, using novel image quantification tools, we have identified an intermediate in EMT with a specific cytoskeletal signature. We have been able to partition EMT into two steps: (1) initial formation of transverse arcs and dorsal stress fibers and (2) their subsequent conversion to ventral stress fibers with a concurrent alignment of fibers. Using Orientational Order Parameter (OOP) as a figure of merit, we have been able to track EMT progression in live cells as well as characterize and quantify drug responses. Our technique, Statistical Parametrization of the Cell Cytoskeleton (SPOCC), has improved throughput and is non-destructive, making it a viable candidate for studying a broad range of biological processes. Further, owing to the decreased stiffness (and hence invasiveness) of the intermediate phenotype compared to mesenchymal cells, our work can be instrumental in aiding the search for new treatment strategies that combat metastasis through specifically targeting the fiber alignment process.

Corresponding author: Shimon Weiss (shiweiss@g.ucla.edu)

Keywords: EMT, actin, cytoskeleton, image analysis, stress fibers, OOP

Introduction:

Cancer is a neoplastic disease that has presented itself as a major health threat to the human society. Though there are more than 200 distinct variations of this disease, certain hallmarks are consistent across different categories. A healthy tissue can develop a primary tumor based on genetic mutations[1] that can sustain proliferative signaling while resisting growth suppressors and apoptosis. With the formation of a new blood circulation system (angiogenesis)[2], the primary tumor starves the neighboring healthy tissue and due to their uninhibited growth, the cancer tissue achieves replicative immortality. Cells from the primary tumor can eventually metastasize and start secondary tumors[3]. Metastasis often creates insurmountable difficulties in developing treatment strategies and contributes to the high mortality rates.

Numerous studies have been carried out to further our understanding of metastasis and its markers[4,5,6], which have shown that metastasis is a complex process involving a myriad of cellular transformation and migration events. One of the key steps in metastasis is Epithelial Mesenchymal Transition (EMT), through which the cells in epithelial tissue are transformed into a highly invasive mesenchymal phenotype[7,8]. Epithelial cells are characterized by cell-cell adhesion and apical to basal polarity both of which are lost upon undergoing EMT[9]. This process involves downregulation of proteins such as E-cadherin and cytokeratin with a concurrent increase in expression levels of N-cadherin, Snail and Slug. Cells are known to demonstrate altered drug response and resistance properties upon undergoing EMT[10,11,12]. The EMT program is also activated during embryo development[13] and wound healing in scarred tissue.

Another phenomenon that accompanies EMT is cytoskeletal rearrangement, in which cortical actin[14] is transformed into highly aligned actin stress fibers[15]. This, in turn, plays an important role

in changing the elasticity and migration capabilities of the tumor cells. This altered elasticity of mesenchymal cells is essential as it enables them to travel through the highly crowded environment of tumors and enter blood vessels through extremely small pores. Thus, the corresponding cytoskeletal rearrangement is conserved across most solid tumor types. Therefore, better understanding of the interrelation between the genetic program for EMT and stress fiber formation is needed.

The cytoskeletal reorganization required for the formation and alignment of stress fibers during EMT is yet to be fully understood. Stress fibers are responsible for maintaining cell shape, aiding in cell migration and intracellular cargo transport. These fibers are a complex moiety consisting of actin filaments held together by actin binding proteins (ABPs) such as myosin, α-actinin and filamin[16,17]. Based on the presence and localization of specific ABPs, the stress fibers can have vastly different structures and functions, such as transverse arcs, dorsal fibers, ventral fibers etc[18,19,20,21,22]. Thus, monitoring the formation of stress fibers in EMT and correlating them with the ABPs to identify their types, could be used to develop a new and reliable reporter for EMT, and to develop screens for inhibitors for different steps along the EMT program.

It is extremely important for cancer research to better understand the sequence of events that transform cells from epithelial to mesenchymal and the intermediate states involved. Over time, there have been multiple approaches to study and track EMT in cells, employing simple biochemical experiments and mass cytometry studies[23,24] to analyze the up and downregulation of EMT marker proteins as well as single cell RNA sequencing techniques[25]. These experiments have confirmed the existence of intermediate states with partial EMT phenotypes based on marker proteins and gene expression levels[23]. However, such techniques can be expensive, low throughput and involve destroying the cells in the process, which poses a problem in cases where the sample

is precious or is needed to be followed in time. Here, we propose an imaging based non-destructive method for quantifying the cytoskeletal change accompanying EMT in live cells which provides a novel tool with improved throughput for tracking EMT progression in real time.

We focused on lung cancer metastasis in our work as lung and bronchial cancer collectively is responsible for the highest percentage of mortality in both male and female patients[26,27]. In this study, we propose that the epithelial cells with cortical actin (C) goes through one or more intermediate states (I) before reaching the final mesenchymal state with aligned stress fibers (A). Since the final aligned state is reported to have enhanced invasiveness, it would be advantageous to intervene at the intermediate states to arrest the increase in invasiveness. We further propose that the formation of stress fibers is a separate event from fiber alignment and as such the intermediate states should have non-aligned stress fibers. We have exploited the sequential formation of different types of stress fibers as a key for identifying a non-binary EMT state that exists as an intermediate between the epithelial and mesenchymal phenotypes. This intermediate phenotype is characterized by disorganized actin cytoskeleton and predominantly different stress fibers compared to normal mesenchymal cells. Actin stress fibers can be treated as a composition of quasi-straight elements, which will have a distinctive geometric pattern from other artefact structures and noise. We have used previously described tools[28,29,30] to extract the geometry of the actin cytoskeleton as a series of straight lines with their corresponding locations, lengths and angles. We used the angular distribution of the cell cytoskeleton to calculate the Orientational Order Parameter (OOP)[31,32,33], which serves as a figure of merit for stress fiber alignment (enabling us to identify the C, I and A states) as well as EMT progression. We confirmed the viability of OOP as an EMT reporter by inhibiting EMT using multiple drugs to arrest the alignment of fibers.

We have also correlated the intermediate phenotype with lower stiffness compared to mesenchymal cells (stiffer than epithelial cells) supporting their partial EMT nature.

Results:

Cells in early phases of EMT demonstrate a novel cytoskeletal architecture distinct from later phases. Since formation of actin stress fibers is a well-established phenomenon when cells undergo EMT (Fig. 1a), we intended to understand the evolution of the cytoskeleton of cells during EMT. There is a growing recognition that EMT is a non-binary process and there have been multiple studies to identify the intermediate states involved using mass cytometry and single cell RNA sequencing[23]. Due to the extensive interconnectedness between the genetic pathways responsible for EMT and actin stress fiber formation, the intermediate partial EMT states are likely to have their own cytoskeletal signatures. We chose A549, H460 and H1299 cell-lines because they are well-established models for lung cancer. To study the sequential evolution of stress fibers, we induced EMT in the cells using Targeted Growth Factor-β1 (TGFβ1) and fixed them at specific time intervals up to 48 hours after the addition of TGFβ1. Initially, there were no stress fibers (Fig. 1b). We observed that cells at the later time-points had well-aligned (semi-parallel) stress fibers consistent with the mesenchymal phenotype (Fig. 1c). In contrast, at earlier time-points, stress fibers were observed, but they were completely disorganized (Fig. 1d). H460 and H1299 cells also demonstrated similar features for early and late phase EMT (Supplementary Information Figs. SI-1a-f). Though the stress fibers in individual cells were aligned in the mesenchymal phenotype, different cells in the same region demonstrated different directions of fiber orientation (Fig. SI-1c). The progress of EMT was also confirmed by tracking the expression levels of E-cadherin and N-cadherin with time in A549 cell. Not only E-cadherin almost completely lost in the cells treated with TGFβ1 for 48 hours confirming their mesenchymal nature, after 14 hours of TGFβ1

treatment, there was still a significant amount of E-cadherin (though it is less than untreated cells), indicating at a partial EMT nature of the earlier cytoskeletal phenotype. Expression of Vimentin, Slug and N-cadherin were upregulated as a function of time with the earlier time-points having an intermediate level of N-cadherin expression (Fig. SI-2).

To quantify the difference in the angular distribution of stress fibers, we extracted the actin filaments as a series of straight lines with their corresponding locations, angles and their lengths using a morphological component analysis and line segmentation algorithm. We then calculated the Orientational Order Parameter (OOP) from the angular distributions (Fig. SI-3). A narrow angular distribution of well-aligned stress fibers corresponds to a high OOP value (Fig. 1e) and a broad distribution in disorganized fibers results in a low OOP value (Fig. 1f). The cell population demonstrated alignment of fibers with time in EMT and the OOP value concurrently increased (Fig. 1g), making the OOP value a good phenotypic marker (or 'figure of merit') for the alignment of stress fibers as well as the progression of EMT. Previous works have used aspect ratio of cells as well as the actin fluorescence intensity as markers for cytoskeletal remodeling[34,35]. But a comparison of simple fluorescence intensity cannot uncover reorganization of the existing cytoskeleton effectively. Also, cells with well-aligned fibers can also have completely different aspect ratios (Fig. 1i,j). Thus, the OOP value is a more relevant cell state marker during the EMT and can extract more information from similar fluorescent images than existing methods.

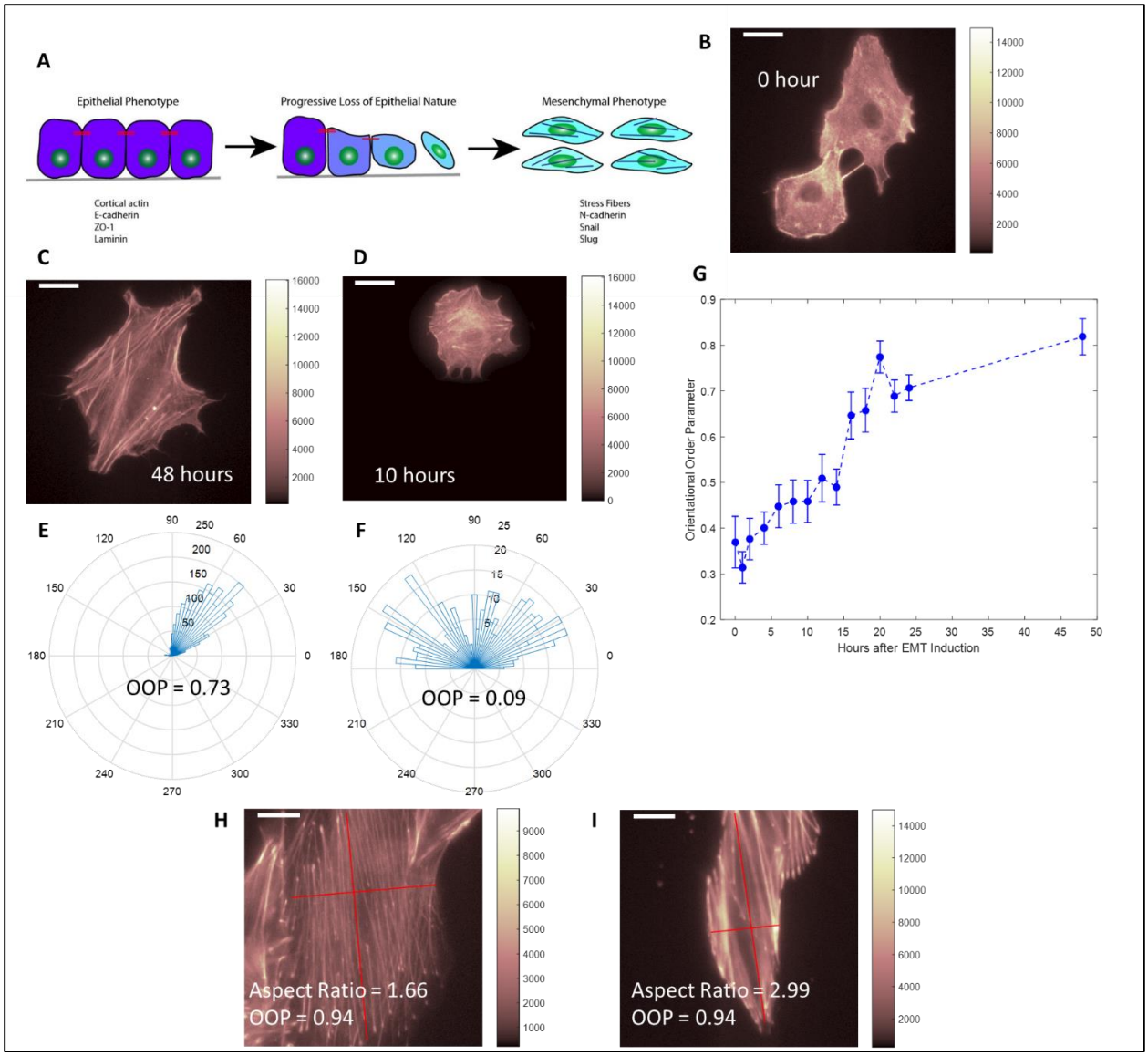


Fig. 1 | Identification and quantification of cytoskeletal phenotypes. a, Cartoon image of cells undergoing EMT with formation of stress fibers and up/downregulation of proteins. **b, c, d,** Fluorescent images of A549 cells stained with phalloidin after 0, 48 and 10 hours of TGFβ1 induced EMT respectively. **e, f,** Angular distribution of stress fibers and corresponding Orientational Order Parameter (OOP) values for cells shown in **c** and **d** respectively. **g,** Plot of OOP values for a cell population against time of TGFβ1 treatment. Error bars correspond to standard error values for every time point. **h, i,** Fluorescent images of two cells stained with phalloidin with highly aligned stress fibers (similar OOP values) but drastically difference aspect ratios. Scale bar: 16μm.

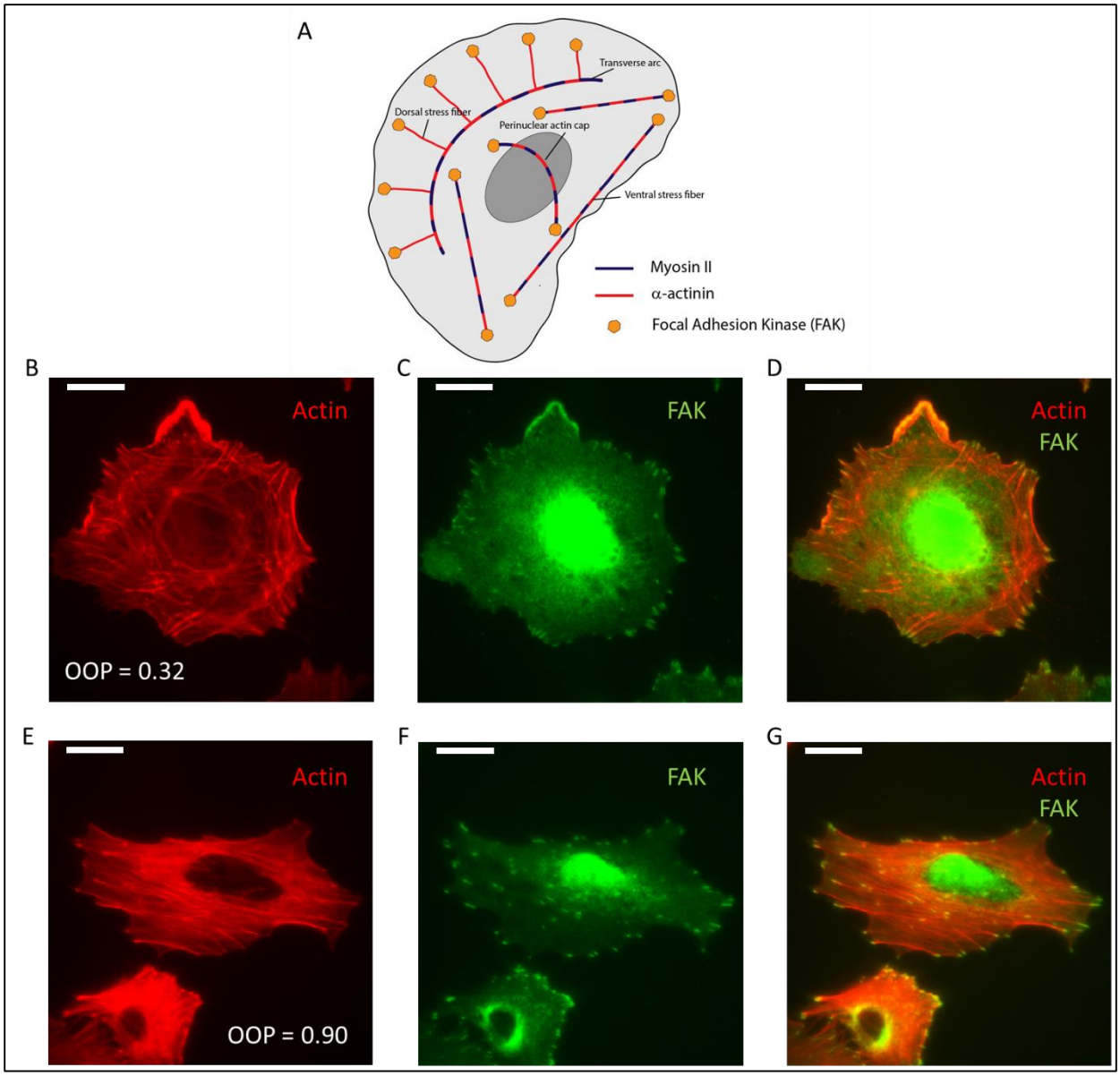


Fig. 2 | Focal Adhesion Kinase (FAK) pattern reveals types of stress fibers. a, Cartoon representation of stress fibers and actin binding proteins. **b, e,** Fluorescent image of actin stress fibers for A549 cells stained with phalloidin with OOP values 0.32 and 0.90 respectively. **c, f,** Fluorescent image of FAK of the same cells shown in **b** and **e** using antibody staining. **d, g,** Overlay of actin (red) and FAK (green) for the same cells showing FAK spots at the end of stress fibers. Scale bar: 16μm.

Early and late stage EMT cells have predominantly different types of stress fibers. It can be inferred from the alignment of stress fibers that EMT is a continuous process where first the stress

fibers are formed throughout the cell in different orientations and then simply align to produce the final phenotype. In such a case, the cells with nest-like architecture would be a simple snapshot of an undefined point along the transition pathway. In order to verify whether or not the two architectures were distinct phenotypes, we investigated the nature of the stress fibers in them. Based on the presence and localization of Actin Binding Proteins (ABPs), the stress fibers can have completely different morphology and function (Fig. 2a). Focal Adhesion Kinase demonstrates the most distinct localization patterns across different stress fiber types[18,19]. We stained cells for both actin (Figs. 2b,e) and FAK (Figs. 2c,f) and compared the patterns in the two phenotypes. Cells in early EMT had fewer FAK spots mostly around the cell edge compared to cells in late EMT which had FAK spots throughout the cell. From the overlay images (Figs. 2d,g) we observed that the stress fibers in the late EMT stage cells were capped on both ends with FAK. Comparatively, the early EMT cells had stress fibers with only one or neither of their ends FAK-capped.

Identifying and quantifying a phenotypic transition in single cell EMT trajectories. Two possible models could explain the existence of the two phenotypes in early and later stage EMT. In the first model, the two phenotypes represent two separate cell populations resulting from different genetic pathways that were activated at different time points. A second model describes the disorganized phenotype transitioning into a higher degree of alignment with the progression of EMT. To find out which of the two proposed models is correct, we tracked single cells (stained with SiR-Actin) (Figs. 3a,d and Fig. SI-4) undergoing EMT over time. The gradual increase in the OOP value (Fig. 3g, SI-4) suggests a phenotypic transition rather than two independent and distinct populations.

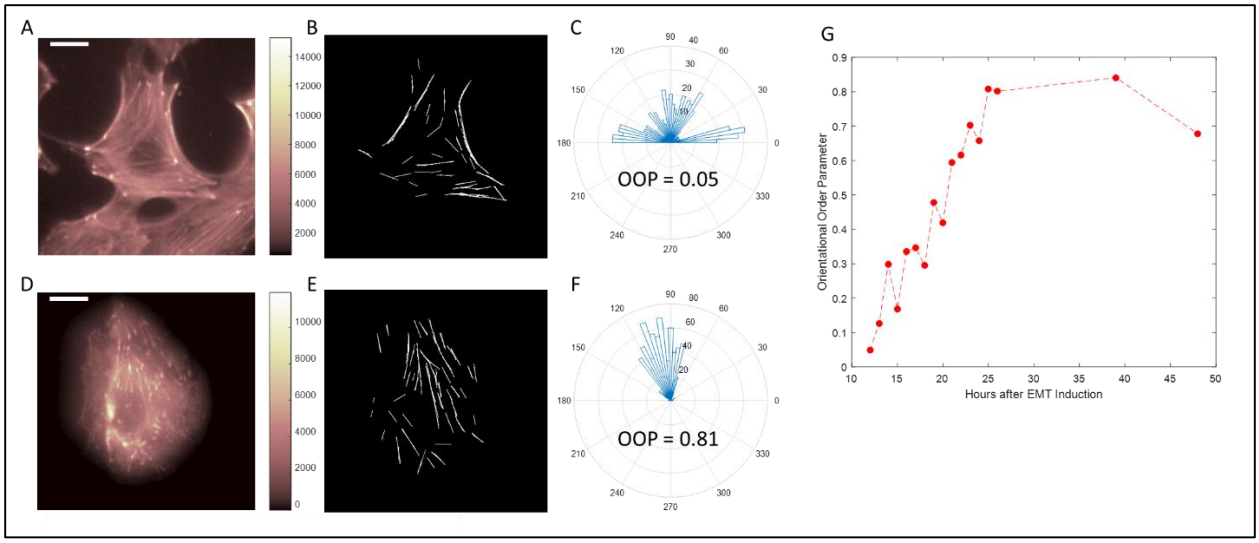


Fig. 3 | Tracking phenotypic transition in single cell stained with SiR-actin. a, d, A single A549 cell stained with SiR-actin after 12 hours and 25 hours of TGFβ1 addition respectively. **b, f,** Extracted stress fiber image from **a** and **d** respectively. **c, f,** Angular distribution and OOP values of the cell at 12 and 25 hours respectively. **g,** Plot of OOP values of a single cell against time of TGF⍰1 treatment. Scale bar: 16μm.

Phenotypic transition responds to EMT pathway inhibition. Multiple genetic pathways are involved in EMT. These pathways can operate consecutively or in parallel and each of these pathways have different levels of crosstalk with the formation of stress fibers. As the stress fiber alignment is a distinct process from the formation of stress fibers, we can expect each step to be controlled by a different part of the EMT signaling cascade. We sought out to verify the two-step nature of EMT by differentially affecting the two steps using known pathway inhibitors for EMT. First, we inhibited the Rho-ROCK pathway, which is one of the most well-known EMT pathways[36,37,38.39,40,41]. When we inhibited this pathway with Rhosin[42], it resulted in a complete suspension of stress fiber formation in the drug treated cells (Fig.4b). To quantify the suspension of stress fiber formation, we compared the number of extracted fibers as well as the total length of fiber extracted in untreated cells vs inhibitor treated cells (Fig.4e, Fig. SI-5). We observed that inhibitor treated cells had demonstrably fewer extracted fibers. The next pathway we chose to

inhibit was the Wnt pathway[43,44,45,46] in two different ways. We used XAV 939 to inhibit Tankyrase1/2[47,48] and JNK-I-8 to inhibit c-Jun N-terminal kinase 1/2 (JNK 1/2)[49] both of which are involved in the Wnt pathway. For both these cases the cells demonstrated a disorganized stress fiber arrangement. (Figs. 4c,d,f). Next, we asked how accurately could the OOP value characterize the drug response of cells. We calculated the OOP values for a series of cell populations (Fig. 4g) as well as single cell trajectories (Fig. 4h) undergoing EMT with and without pathway inhibitors. We found OOP for inhibitor treated cells did not increase with time which corroborated the arrest of phenotypic transition.

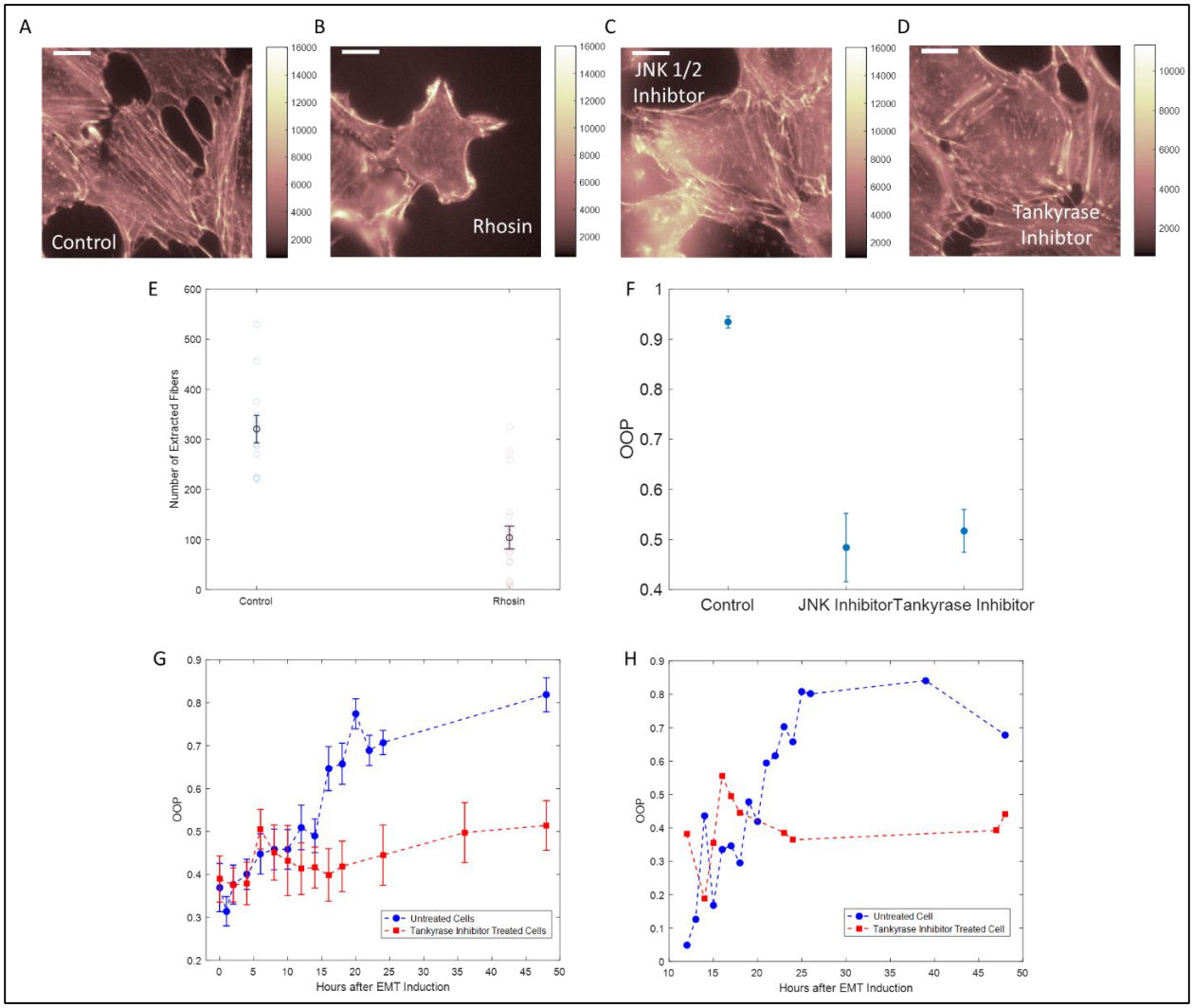


Fig. 4 | Quantification of drug response of EMT over 48 hours. a-d, A549 cells stained with phalloidin after 48 hours of EMT induction in the presence of no drug (**a**), Rhosin (**b**), JNK 1/2 Inhibitor (**c**) and TankyraseInhibitor (**d**). **e,** Comparison of the number of stress fibers extracted from control (no drug) cells vs Rhosin treated cells. **f,** Comparison of average OOP values for control cells and cells treated with JNK 1/2 and Tankyrase Inhibitors. **g,** Plots of OOP values against time of a cell population undergoing EMT with (blue) and without (red) the presence of Tankyrase Inhibitor. Error bars correspond to standard errors at each time point. **h,** Plots of OOP values against time of a single cell undergoing EMT with (blue) and without (red) the presence of Tankyrase Inhibitor. Scale bar 16μm.

The early EMT phenotype demonstrates a partial EMT nature and has different elastic properties compared to mesenchymal cells. Lung cancer mesenchymal cells are known to be stiffer compared to epithelial cells[50]. Due to the extensive interrelation between the actin cytoskeleton and elastic properties of cells, the nest-like phenotype can also be expected to demonstrate partial epithelial nature and be softer compared to the mesenchymal phenotype. To investigate this, we conducted atomic force microscopy to perform force curve measurement experiments to calculate the elastic modulus (Young's Modulus) of the three phenotypes. The epithelial cells had the lowest Young's modulus and the late EMT mesenchymal phenotype had the highest Young's modulus. The Young's modulus of the nest-like phenotype was in between the two (Fig.5). It is worth mentioning here that the over-all trend in cell stiffness we observed is not in agreement with most of the reported data in the field.

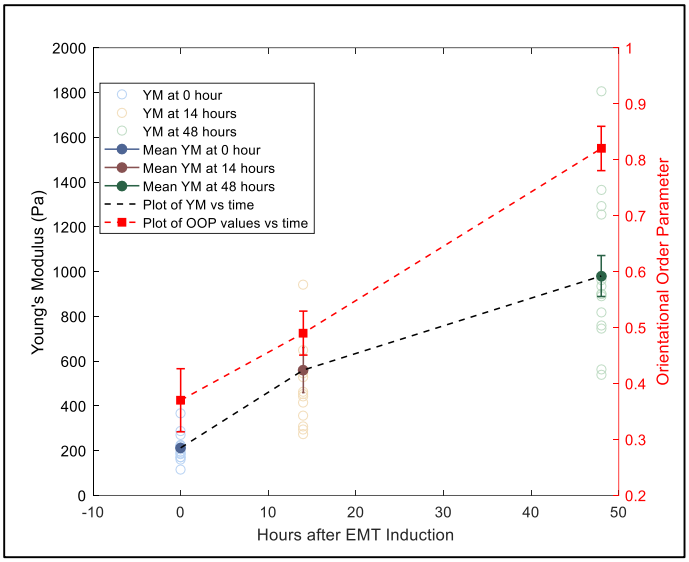


Fig. 5 | Measurement of elastic properties of cells. Young's Modulus values at 0 (blue), 14 (brown) and 48 (green) hours after EMT induction using TGFβ1 showing their mean and standard errors along with a plot of the mean values (black). Young's modulus values were extracted from AFM force curve measurements. Plot of mean OOP values for cell populations against hours after EMT (red) showing mean values and standard errors at 0, 14 and 48 hour time points.

Discussion:

In trying to better understand the cytoskeletal rearrangements involved in EMT we tracked EMT progression in lung cancer cells. We discovered a novel phenotype where the stress fibers were not aligned in any particular direction. This alignment process was also identified in single cells by tracking them through EMT. Thus, we identified the alignment process as a phenotypic transition. These results indicate that EMT is at least a two-step process, the first step being the formation of stress fibers followed by their alignment. The nest-like phenotype is an intermediate along the pathway. The lack of a common direction of alignment of stress fibers from cell to cell is indicative that alignment process is likely not influenced by availability of space is a particular direction. Cells respond to matrix stiffness by altering their own mechanical properties[51,52]. This disoriented stress fiber architecture without any particular direction of alignment was previously

reported for cells grown on soft surfaces[34]. So, the difference in their fiber alignment is indicative of a difference between the stiffness of the two phenotypes. Our AFM experiments corroborate the hypothesis that difference in cytoskeletal architecture results in altered mechanical properties. We demonstrated that the nest-like phenotype occupies an intermediate elastic niche between epithelial and mesenchymal cells. Most papers have reported a decrease in cell stiffness as cells undergo EMT[53,54,55,56]. But recently, it has been demonstrated that in the case of pre-invasive breast cancer cells and non-small cell there is a concurrent increase in cell stiffness/rigidity with EMT progression resulting from regulation of motor proteins[50,57]. A possible explanation is that EMT induced by growth factors have different physiological effects resulting in cell stiffening. Growth factor concentration is usually highest at the tumor margins from where the cells start migrating, so in a way our experiments better mimic the in vivo conditions the cells face at tumor margins. It is also possible that this phenomenon is unique to certain types of cancer cells. Cells in the lung and airways responsible for constant expansion and compression which might require very low stiffness in the lung epithelium. Upon EMT induction, the remodeling of the cytoskeleton helps the cells gain elevated rigidity. But irrespective of the trend, what our work demonstrates is that the stiffness of the intermediate phenotype is actually in between epithelial and mesenchymal phenotypes. This observation supports the claim that the intermediate phenotype bears partial epithelial nature.

To quantify this cytoskeletal phenomenon, we developed an image analysis and quantification technique that can identify and differentiate between the phenotypes from simple fluorescent images of the cell cytoskeleton. Though recently reported techniques can extract similar information about the stress fibers[58,59], our technique assigns a figure of merit for the relative

alignment of fibers to individual cells. Beyond EMT, our technique is also capable of quantifying any biological process that involves a cytoskeletal remodeling and as such has broad applications.

Transverse arcs don't have any FAK-capping whereas dorsal and ventral stress fibers have one and both ends FAK-capped respectively[18,19]. Based on the FAK patterns on the two phenotypes we identified the stress fiber types in each phenotype. We demonstrated that the mesenchymal phenotype has ventral stress fibers whereas the intermediate phenotype predominantly has dorsal fibers and transverse arcs. The enhancement of ventral stress fibers results in better anchoring on the substrate. This in turn is likely to increase the motility of the cells considerably. Also, as the stress fiber mesh moves to the ventral side of the cells with progression of EMT, the elastic properties of the cells are likely to change as well.

Our results expectedly demonstrate that either the first step or both the steps discussed in the previous sections are dependent on the Rho-GTPase (Rho-ROCK) pathway. The Wnt pathway is recently emerging as another important pathway and based on our results it is involved in stress fiber alignment process but not their formation. JNK is also involved in the p38-MAPK pathway[60,61], which is known to have comprehensive cross-talk with the Wnt pathway[46]. But inhibition of just the Wnt pathway with tankyrase resulted in similar outcomes which brings into question the involvement of p38_MAPK pathway in the fiber alignment process. So, we expect that the stress fiber alignment is carried out with the help of a kinase controlled by the Wnt (or Wnt/p38-MAPK) pathway and this is a previously unknown function of the said kinase. The identification and silencing of this kinase can be a valuable tool for controlling similar biological processes.

As stress fibers are involved in multiple functions of healthy cells it is unlikely that the complete termination of stress fiber formation is a viable clinical approach to counter metastasis. On the

other hand, arresting just the second step (alignment process) is expected to not hinder the proper functioning of cells. Furthermore, the intermediate phenotype has lower stiffness and lower invasiveness as a result. So, by inhibiting the second step, it might be possible to prevent (or drastically impede) cell migration which could possibly prevent metastasis.

Conclusions:

In this work we discovered a new partial EMT phenotype in lung cancer cells with its unique cytoskeletal signature which are likely to demonstrate decreased invasiveness. We have partitioned the cytoskeletal component of EMT into two separate steps: (1) formation of stress fibers and (2) alignment of stress fibers. Here, we have also demonstrated that it is possible to arrest the alignment process selectively by inhibiting the Wnt pathway. We have also developed an image quantification technique that can identify and differentiate between different cytoskeletal morphologies from simple fluorescent images.

In future, we intend to study EMT in a broader pool of cell lines (lung cancer as well as other types) to further our understanding of partial epithelial phenotypes. Expanding our work into 3D cultures will also help up mimic tissue environments more accurately. A key unanswered question that our work raises is identifying the kinase responsible for the stress fiber alignment process. Correlating the time-evolution of the transcriptome with the increase in OOP, followed by subsequent silencing of key genes can shed light in that regard.

Identification of this partial epithelial phenotype along with our ability to prevent it from going to full mesenchymal nature begs the following question: can arresting the second step prohibit cell migration to any extent and what are the possible clinical ramifications of it? If there is indeed a clinical advantage in freezing EMT at the intermediate state, then it is essential to develop a library

of specific drugs that can essentially stop migration of tumor cells but not inhibit the normal functions of the cell that are carried out but the stress fibers.

In conclusion we have demonstrated that an extensive amount of information can be extracted from cytoskeletal dynamics (than previously thought possible) that can have molecular biological as well as clinical applications.

Materials and Methods:

Cell Culture: A549 cells were cultured in DMEM (Gibco, catalog no. 11995-065) supplemented with 10% FBS (Gibco, catalog no. A31604-01) and 1% penicillin streptomycin (10000U/ml, Gibco, catalog no. 15140-122). H460 and H1299 cells were cultured in RPMI (Gibco, catalog no. A10491-01) supplemented with 10%FBS (Gibco, catalog no. A31604-01) and 1% penicillin streptomycin (10000U/ml, Gibco, catalog no.15140-122). EMT in all cell lines were induced by addition of 5ng/ml Targeted Growth Factor-β1 (TGFβ1) (Peprotech, catalog no. 100-21-10UG) for 48 hours.

Cell Staining (End Point Study): Cells were grown on 8 well culture slides (Sarstedt, Catalog no. 94.6170.802) for 24 hours and treated with 5ng/ml TGFβ1 (and drugs) for 48 hours. After 48 hours, cells were rinsed with PBS (Gibco, catalog no. 14190-136) and fixed with 4% paraformaldehyde (diluted from 10%) (Electron Microscopy Sciences, catalog no. 15712-S) for 20 minutes.

Time-point Study: Cells were grown on fibronectin coated cover-slides (neuVitro, catalog no. GG-12-fibronectin) for 24 hours and treated with 5ng/ml TGFβ (and drugs). At specific time intervals after TGFβ1 treatment, the cover-slides were rinsed with PBS (Gibco, catalog no. 14190-

136) and fixed with 4% paraformaldehyde (diluted from 10%, Electron Microscopy Sciences, catalog no. 15712-S) for 20 minutes.

Western Blot Analysis: Western blots were performed according to standard procedures. Cells grown in culture dishes for 24 hours and treated with 5ng/ml TGFβ1. After specified time of TGFβ1 treatment, the cells were washed with ice-cold PBS and lysed with RIPA buffer using standard methods. 20μg of each cell lysate was loaded per lane, and proteins were resolved by SDS-PAGE and transferred to an Immobilon-P Transfer Membrane (Millipore, Billerica, MA). The membranes were blocked with 5% nonfat milk and then incubated with primary antibodies diluted in blocking solution according to the manufacturer's recommendations. Horseradish peroxidase-conjugated secondary antibodies (Bio-Rad, Hercules, CA) and enhanced chemiluminescence (ECL) reagent (Amersham Biosciences, Piscataway, NJ) were used for protein detection. BCA method was used for estimation of protein concentrations using manufacturer's guidance. An equal volume of 2xSDS sample buffer was added and the samples were denatured by boiling for 5 minutes. Samples were applied to a SDS-PAGE and transferred to an Immobilon PVDF membrane (Millipore, USA). The membranes were blocked with 5% skimmed milk prepared using Tris-buffered saline with 0.05% Tween 20, and then treated with primary antibodies. The membranes were incubated with primary antibodies overnight at 4^{o}C. The membranes were then rinsed three times with Tris-buffered saline containing 0.1 percent Tween 20 (TBST) after incubation with primary antibodies. The membranes were then incubated in TBST containing 5% BSA for 1 hour with horseradish peroxidase-conjugated goat anti-mouse IgG and horseradish peroxidase-conjugated goat anti-rabbit IgG secondary antibodies (LI-COR Biosciences, Lincoln, NE). After that, the blots were washed three times in TBST and the immune-complexes were visualized with the ECL kit (GEHealthcare, USA). Proteins were observed and

scanned using an Odyssey Infrared Imaging System (LI-COR Biosciences, Lincoln, NE) with 700- and 800-nm channels to scan the membrane. As internal loading controls, the blots were re-probed with anti-GAPDH or anti-actin antibodies.

Image J software was used to compute the relative densitometric values. Band intensity was also quantified by ImageJ software (Rasband,1997–2014). The obtained images were converted to 8-bit format and then subjected to background subtraction through the rolling ball radius method. Quantification of peak area of obtained histograms were performed for each individually selected band. All Western blots were performed independently in triplicates and the data are represented as the standard error of the mean (SEM) for all performed repetitions. Internal loading controls were used to normalize the data. The results from the untreated groups were used to calculate relative values.

Antibody name	**Company**	**Catalogue No.**	**Primary dilution**	**Incubation time**	**Incubation temperature (ºC)**
GAPDH	Advanced Immuno Chemical Inc	2-RGM2	1:10,000	Overnight	4
β-Actin	Cell Signaling Technology	12262	1:10,000	Overnight	4
E-Cadherin	BD Transduction Laboratories	610182	1: 400	Overnight	4
N-Cadherin	BD Transduction Laboratories	610920	1:400	Overnight	4
Slug	Cell Signaling Technology	9585	1: 300	Overnight	4
Vimentin	BD Pharmingen	550513	1: 400	Overnight	4

Drug Treatment: Cells were grown for 24 hours before being treated with 5ng/ml TGFβ1 and specific drugs.

Target Protein	Drug Name	Catalog No. (Selleckchem.com)	Concentration
Rho-GTPase	Rhosin Hydrochloride	S8988	0.4 μM
JNK ½	JNK-IN-8	S4901	20 nM
Tankyrase ½	XAV-939	S1180	11 nM

Cell Staining: Fixed cells permeabilized with 0.1% Triton X-100 (Research Products International Corp., catalog no. 11036) for 5 minutes, blocked with freshly prepared 5% BSA (Fisher BioReagents, catalog no. BP 1600-100, CAS no. 9048-46-8) for 25 minutes, treated with 1:100 solution of primary antibody in blocking medium at 4^{o}C overnight. Next, the cells were rinsed thoroughly and stained with 1:200 solution of secondary antibody in PBS for 2 hours followed by staining with Acti-Stain^{TM} 670 Fluorescent Phalloidin (Cytoskeleton.Inc, catalog no. PHDN1). Then the cover-slides were mounted on glass slides using ProLong Diamond Antifade Mountant (Invitrogen, catalog no. P36961) and sealed with clear nail-polish. Primary antibodies: Anti-FAK (D1) mouse monoclonal IgG_1 antibody (Santa Cruz Biotechnology, catalog no. sc-271126). Secondary antibody: Alexa Fluor® 488 AffiniPure $F(ab')_2$ Fragment Donkey Anti-Mouse IgG (H+L) (Jackson ImmunoResearch Laboratories Inc., code no. 715-546-151).

Live Cell Staining: A549 cells were grown on glass bottomed dishes (Cellvis, catalog no. D35-20-1.5-N) for 24 hours and treated with 5ng/ml TGFβ1 and 100nM SiR-actin kit (Cytoskeleton.Inc, CY-SC001).

Fluorescence Imaging: Fluorescent cells were imaged on a Nikon Ti-Eclipse microscope equipped with an AURA light engine (Lumencor) light source and 60X oil immersion objectives lens (Nikon, Plan Apo VC 60X/1.4). The images were captured using an iXon+ camera (Andor Technologies, model no. DU-897E-CSO-#BV). For live cell imaging, a microscope mounted incubator (Warner Instruments, Inc., model no. DH-40iL) coupled with an automatic temperature controller (Warner Instruments, Inc., model no. TC-324C) was used, which kept the cells at 37^{o}C, 5% CO_2 and 90% relative humidity.

Image Analysis and OOP Calculation: Fluorescent images were processed using Matlab (version 2016a) and analyzed using previously described protocol[30]. The raw fluorescent images were decomposed into filament image, artefact image and noise. The filament image was enhanced to improve the contrast. Next, a multi-scale line segmentation approach was used to extract the fibers as straight lines. Then fibers that had similar orientation and were close to one another were stitched together. The filament angles were extracted from the output and Orientational Order Parameter (OOP) was calculated from the angular distribution[31,32]. OOP is calculated by generating a tensor from every angle (vector) and evaluating the maximum eigen value of the mean order tensor. A more detailed description of this technique is provided in chapter 2.

Atomic Force Microscopy: Cells were grown on glass bottomed dishes (FluoroDish, World Precision Instruments Inc.) for 24 hours before addition of 5ng/ml TGFβ1. AFM force curves were obtained using a Bruker Nanowizard 4A instrument coupled with a Zeiss Observer.Z1 Microscope

with LSM5 Exciter laser scanning confocal module and 40X oil immersion objective lens (Zeiss, EC Plan-NeoFluar 40X/1.3). A nitride tip (Bruker, SAA_SPH-5UM) with a nitride lever was used. All the force curves were analyzed using the JPKSPM Data Processing Software.

Acknowledgements:

We acknowledge NSF-Strobe grant for partial support of our work. We acknowledge Dr. Michael Lake and the use of the Nano and Pico Characterization Lab at California NanoSystems Institute for the AFM experiments. We also acknowledge Ms. Maya Segal for her help in organization and writing of this manuscript.

Authors' contributions:

A.B. and S.W. designed the research in consultation with M.P. and S.D. A.B. carried out the experiments, data analysis and interpretation. M.P. performed the western blot analyses. S.D. provided the cell lines and drugs used. M.A. and H.S. developed the basic stress fiber extraction algorithm. A.G. developed the code for OOP calculations. A.B. and S.W. wrote the manuscript.

References:

(1) Martínez-Jiménez, F.; Muiños, F.; Sentís, I.; Deu-Pons, J.; Reyes-Salazar, I.; Arnedo-Pac, C.; Mularoni, L.; Pich, O.; Bonet, J.; Kranas, H.; Gonzalez-Perez, A.; Lopez-Bigas, N. A Compendium of Mutational Cancer Driver Genes. *Nat. Rev. Cancer* **2020**, *20* (10), 555–572. https://doi.org/10.1038/s41568-020-0290-x.

(2) Lugano, R.; Ramachandran, M.; Dimberg, A. Tumor Angiogenesis: Causes, Consequences, Challenges and Opportunities. *Cell. Mol. Life Sci.* **2020**, *77* (9), 1745–1770. https://doi.org/10.1007/s00018-019-03351-7.

(3) Hanahan, D.; Weinberg, R. A. Hallmarks of Cancer: The next Generation. *Cell* **2011**, *144* (5), 646–674. https://doi.org/10.1016/j.cell.2011.02.013.

(4) Hart, I. a N. R. SCIENCE & PRACTICE Biology of Tumour Metastasis. *Cell* 1453–1457.

(5) Ko, J.; Winslow, M. M.; Sage, J. Mechanisms of Small Cell Lung Cancer Metastasis. *EMBO Mol. Med.* **2021**, *13* (1). https://doi.org/10.15252/emmm.202013122.

(6) Weigelt, B.; Peterse, J. L.; Van't Veer, L. J. Breast Cancer Metastasis: Markers and Models. *Nat. Rev. Cancer* **2005**, *5* (8), 591–602. https://doi.org/10.1038/nrc1670.

(7) Lamouille, S.; Xu, J.; Derynck, R. Molecular Mechanisms of Epithelial-Mesenchymal Transition. *Nat. Rev. Mol. Cell Biol.* **2014**, *15* (3), 178–196. https://doi.org/10.1038/nrm3758.

(8) Xiao, D.; He, J. Epithelial Mesenchymal Transition and Lung Cancer. *J. Thorac. Dis.* **2010**, *2* (3), 154–159. https://doi.org/10.3978/j.issn.2072-1439.2010.02.03.7.

(9) Wodarz, A.; Näthke, I. Cell Polarity in Development and Cancer. *Nat. Cell Biol.* **2007**, *9* (9), 1016–1024. https://doi.org/10.1038/ncb433.

(10) Nurwidya, F.; Takahashi, F.; Murakami, A.; Takahashi, K. Epithelial Mesenchymal Transition in Drug Resistance and Metastasis of Lung Cancer. *Cancer Res. Treat.* **2012**, *44* (3), 151–156. https://doi.org/10.4143/crt.2012.44.3.151.

(11) Tan, T. Z.; Miow, Q. H.; Miki, Y.; Noda, T.; Mori, S.; Huang, R. Y.; Thiery, J. P. Epithelial-mesenchymal Transition Spectrum Quantification and Its Efficacy in Deciphering Survival and Drug Responses of Cancer Patients. *EMBO Mol. Med.* **2014**, *6* (10), 1279–1293. https://doi.org/10.15252/emmm.201404208.

(12) Byers, L. A.; Diao, L.; Wang, J.; Saintigny, P.; Girard, L.; Peyton, M.; Shen, L.; Fan, Y.; Giri, U.; Tumula, P. K.; Nilsson, M. B.; Gudikote, J.; Tran, H.; Cardnell, R. J. G.; Bearss, D. J.; Warner, S. L.; Foulks, J. M.; Kanner, S. B.; Gandhi, V.; Krett, N.; Rosen, S. T.; Kim, E. S.; Herbst, R. S.; Blumenschein, G. R.; Lee, J. J.; Lippman, S. M.; Ang, K. K.; Mills, G. B.; Hong, W. K.; Weinstein, J. N.; Wistuba, I. I.; Coombes, K. R.; Minna, J. D.; Heymach, J. V. An Epithelial-Mesenchymal Transition Gene Signature Predicts Resistance to EGFR and PI3K Inhibitors and Identifies Axl as a Therapeutic Target for Overcoming EGFR Inhibitor Resistance. *Clin. Cancer Res.* **2013**, *19* (1), 279–290. https://doi.org/10.1158/1078-0432.CCR-12-1558.

(13) Nieto, M. A. Epithelial Plasticity: A Common Theme in Embryonic and Cancer Cells. *Science (80-.).* **2013**, *342* (6159). https://doi.org/10.1126/science.1234850.

(14) Svitkina, T. M. Actin Cell Cortex: Structure and Molecular Organization. *Trends Cell Biol.* **2020**, *30* (7), 556–565. https://doi.org/10.1016/j.tcb.2020.03.005.

(15) Haynes, J.; Srivastava, J.; Madson, N.; Wittmann, T.; Barber, D. L. Dynamic Actin Remodeling during Epithelial-Mesenchymal Transition Depends on Increased Moesin Expression. *Mol. Biol. Cell* **2011**, *22* (24), 4750–4764. https://doi.org/10.1091/mbc.E11-02-0119.

(16) Tojkander, S.; Gateva, G.; Lappalainen, P. Actin Stress Fibers - Assembly, Dynamics and Biological Roles. *J. Cell Sci.* **2012**, *125* (8), 1855–1864. https://doi.org/10.1242/jcs.098087.

(17) Pollard, T. D.; Cooper, J. A. Actin, a Central Player in Cell Shape and Movement. *Science (80-.).* **2009**, *326* (5957), 1208–1212. https://doi.org/10.1126/science.1175862.

(18) Burridge, K.; Guilluy, C. Focal Adhesions, Stress Fibers and Mechanical Tension. *Exp. Cell Res.* **2016**, *343* (1), 14–20. https://doi.org/10.1016/j.yexcr.2015.10.029.

(19) Livne, A.; Geiger, B. The Inner Workings of Stress Fibers - From Contractile Machinery to Focal Adhesions and Back. *J. Cell Sci.* **2016**, *129* (7), 1293–1304. https://doi.org/10.1242/jcs.180927.

(20) Pollard, T. D. Actin and Actin-Binding Proteins. *Cold Spring Harb Perspect Biol* **2016**, *8*, 1–18.

(21) Gross, S. R. Actin Binding Proteins: Their Ups and Downs in Metastatic Life. *Cell Adhes. Migr.* **2013**, *7* (2), 199–213. https://doi.org/10.4161/cam.23176.

(22) Pollard, T. D. Actin and Actin-Binf=ding Protein. A Critical Evaluation of Mechanisms and Functions. *Ann. Rev. Biochem.* **1986**, *55*, 987–1035.

(23) Karacosta, L. G.; Anchang, B.; Ignatiadis, N.; Kimmey, S. C.; Benson, J. A.; Shrager, J. B.; Tibshirani, R.; Bendall, S. C.; Plevritis, S. K. Mapping Lung Cancer Epithelial-Mesenchymal Transition States and Trajectories with Single-Cell Resolution. *Nat. Commun.* **2019**, *10* (1), 1–15. https://doi.org/10.1038/s41467-019-13441-6.

(24) Krishnaswamy, S.; Zivanovic, N.; Sharma, R.; Pe'Er, D.; Bodenmiller, B. *Learning Time-Varying Information Flow from Single-Cell Epithelial to Mesenchymal Transition Data*; 2018; Vol. 13. https://doi.org/10.1371/journal.pone.0203389.

(25) van Dijk, D.; Sharma, R.; Nainys, J.; Yim, K.; Kathail, P.; Carr, A. J.; Burdziak, C.; Moon, K. R.; Chaffer, C. L.; Pattabiraman, D.; Bierie, B.; Mazutis, L.; Wolf, G.; Krishnaswamy, S.; Pe'er, D. Recovering Gene Interactions from Single-Cell Data Using

Data Diffusion. *Cell* **2018**, *174* (3), 716-729.e27. https://doi.org/10.1016/j.cell.2018.05.061.

(26) Siegel, R. L.; Miller, K. D.; Jemal, A. Cancer Statistics, 2020. *CA. Cancer J. Clin.* **2020**, *70* (1), 7–30. https://doi.org/10.3322/caac.21590.

(27) Jemal, A.; Siegel, R.; Ward, E.; Hao, Y.; Xu, J.; Murray, T.; Thun, M. J. Cancer Statistics, 2008. *CA. Cancer J. Clin.* **2008**, *58* (2), 71–96. https://doi.org/10.3322/ca.2007.0010.

(28) Starck, J. L.; Elad, M.; Donoho, D. L. Image Decomposition via the Combination of Sparse Representations and a Variational Approach. *IEEE Trans. Image Process.* **2005**, *14* (10), 1570–1582. https://doi.org/10.1109/TIP.2005.852206.

(29) Candès, E.; Demanet, L.; Donoho, D.; Ying, L. Fast Discrete Curvelet Transforms. *Multiscale Model. Simul.* **2006**, *5* (3), 861–899. https://doi.org/10.1137/05064182X.

(30) Alioscha-Perez, M.; Benadiba, C.; Goossens, K.; Kasas, S.; Dietler, G.; Willaert, R.; Sahli, H. A Robust Actin Filaments Image Analysis Framework. *PLoS Comput. Biol.* **2016**, *12* (8), 1–23. https://doi.org/10.1371/journal.pcbi.1005063.

(31) Volfson, D.; Cookson, S.; Hasty, J.; Tsimring, L. S. Biomechanical Ordering of Dense Cell Populations. *Proc. Natl. Acad. Sci. U. S. A.* **2008**, *105* (40), 15346–15351. https://doi.org/10.1073/pnas.0706805105.

(32) Grosberg, A.; Kuo, P. L.; Guo, C. L.; Geisse, N. A.; Bray, M. A.; Adams, W. J.; Sheehy, S. P.; Parker, K. K. Self-Organization of Muscle Cell Structure and Function. *PLoS Comput. Biol.* **2011**, *7* (2). https://doi.org/10.1371/journal.pcbi.1001088.

(33) Drew, N. K.; Eagleson, M. A.; Baldo Jr, D. B.; Parker, K. K.; Grosberg, A. Metrics for

Assessing Cytoskeletal Orientational Correlations and Consistency. **2015**, 1–22. https://doi.org/10.7280/D1X59T.

(34) Prager-Khoutorsky, M.; Lichtenstein, A.; Krishnan, R.; Rajendran, K.; Mayo, A.; Kam, Z.; Geiger, B.; Bershadsky, A. D. Fibroblast Polarization Is a Matrix-Rigidity-Dependent Process Controlled by Focal Adhesion Mechanosensing. *Nat. Cell Biol.* **2011**, *13* (12), 1457–1465. https://doi.org/10.1038/ncb2370.

(35) Gupta, S. K.; Li, Y.; Guo, M. Anisotropic Mechanics and Dynamics of a Living Mammalian Cytoplasm. *Soft Matter* **2019**, *15* (2), 190–199. https://doi.org/10.1039/c8sm01708e.

(36) Korol, A.; Taiyab, A.; West-Mays, J. A. RhoA/ROCK Signaling Regulated TGFB-Induced Epithelial-Mesenchymal Transition of Lens Epithelial Cells through MRTF-A. *Mol. Med.* **2016**, *22*, 713–723.

(37) Bendris, N.; Arsic, N.; Lemmers, B.; Blanchard, J. M. Cyclin A2, Rho GTPases and EMT. *Small GTPases* **2012**, *3* (4). https://doi.org/10.4161/sgtp.20791.

(38) Ungefroren, H.; Witte, D.; Lehnert, H. The Role of Small GTPases of the Rho/Rac Family in TGF-β-Induced EMT and Cell Motility in Cancer. *Dev. Dyn.* **2018**, *247* (3), 451–461. https://doi.org/10.1002/dvdy.24505.

(39) Du, W.; Tang, H.; Lei, Z.; Zhu, J.; Zeng, Y.; Liu, Z.; Huang, J. A. MiR-335-5p Inhibits TGF-B1-Induced Epithelial-Mesenchymal Transition in Non-Small Cell Lung Cancer via ROCK1. *Respir. Res.* **2019**, *20* (1), 1–11. https://doi.org/10.1186/s12931-019-1184-x.

(40) Matsuoka, T.; Yashiro, M. Rho/ROCK Signaling in Motility and Metastasis of Gastric

Cancer. *World J. Gastroenterol.* **2014**, *20* (38), 13756–13766. https://doi.org/10.3748/wjg.v20.i38.13756.

(41) Li, B.; Zhao, W. D.; Tan, Z. M.; Fang, W. G.; Zhu, L.; Chen, Y. H. Involvement of Rho/ROCK Signalling in Small Cell Lung Cancer Migration through Human Brain Microvascular Endothelial Cells. *FEBS Lett.* **2006**, *580* (17), 4252–4260. https://doi.org/10.1016/j.febslet.2006.06.056.

(42) Tsubaki, M.; Genno, S.; Takeda, T.; Matsuda, T.; Kimura, N.; Yamashita, Y.; Morii, Y.; Shimomura, K.; Nishida, S. Rhosin Supressed Tumor Cell Metastasis through Inhibitionof Rho/YAP Pathway and Expression of RHAMM AndCXCR4 in Melanoma and Breast Cancer Cells. *Biomedicines* **2021**, *9* (35).

(43) Esposito, M.; Fang, C.; Cook, K. C.; Park, N.; Wei, Y.; Spadazzi, C.; Bracha, D.; Gunaratna, R. T.; Laevsky, G.; DeCoste, C. J.; Slabodkin, H.; Brangwynne, C. P.; Cristea, I. M.; Kang, Y. TGF-β-Induced DACT1 Biomolecular Condensates Repress Wnt Signalling to Promote Bone Metastasis. *Nat. Cell Biol.* **2021**, *23* (3), 257–267. https://doi.org/10.1038/s41556-021-00641-w.

(44) Zhang, J.; Tian, X.-J.; Xing, J. Signal Transduction Pathways of EMT Induced by TGF-B, SHH and WNT and Their Crosstalks. *J. Clin. Med.* **2016**, *5* (41).

(45) Steinway, S. N.; Zanudo, J. G. T.; Rountree, C. B.; Feith, D. J.; Loughran, T. P.; Albert, R. Network Modeling of TGFB Signaling in Hepatocellular Carcinoma Epithelial-to-Mesenchymal Transition Reveals Joint Sonic Hedgehog and Wnt Pathway Activation. *Cancer Res.* **2014**, *74* (21), 5963–5977.

(46) Wu, Y.; Ginther, C.; Kim, J.; Mosher, N.; Chung, S.; Salmon, D.; Vadgama, J. V.

Expression of Wnt3 Activates Wnt/B-Catenin Pathway and Promotes EMT-like Phenotype in Trastuzumab-Resistant HER2-Overexpressing Breast Cancer Cells. *Mol. Cancer Res.* **2012**, *10* (12), 1597–1606.

(47) Huang, S. M. A.; Mishina, Y. M.; Liu, S.; Cheung, A.; Stegmeier, F.; Michaud, G. A.; Charlat, O.; Wiellette, E.; Zhang, Y.; Wiessner, S.; Hild, M.; Shi, X.; Wilson, C. J.; Mickanin, C.; Myer, V.; Fazal, A.; Tomlinson, R.; Serluca, F.; Shao, W.; Cheng, H.; Shultz, M.; Rau, C.; Schirle, M.; Schlegl, J.; Ghidelli, S.; Fawell, S.; Lu, C.; Curtis, D.; Kirschner, M. W.; Lengauer, C.; Finan, P. M.; Tallarico, J. A.; Bouwmeester, T.; Porter, J. A.; Bauer, A.; Cong, F. Tankyrase Inhibition Stabilizes Axin and Antagonizes Wnt Signalling. *Nature* **2009**, *461* (7264), 614–620. https://doi.org/10.1038/nature08356.

(48) Casás-Selves, M.; Kim, J.; Zhang, Z.; Helfrich, B. A.; Gao, D.; Porter, C. C.; Scarborough, H. A.; Bunn, P. A.; Chan, D. C.; Tan, A. C.; DeGregori, J. Tankyrase and the Canonical Wnt Pathway Protect Lung Cancer Cells from EGFR Inhibition. *Cancer Res.* **2012**, *72* (16), 4154–4164. https://doi.org/10.1158/0008-5472.CAN-11-2848.

(49) Yamanaka, H.; Moriguchi, T.; Masuyama, N.; Kusakabe, M.; Hanafusa, H.; Takada, R.; Takada, S.; Nishida, E. JNK Functions in the Non-Canonical Wnt Pathway to Regulate Convergent Extension Movements in Vertebrates. *EMBO Rep.* **2002**, *3* (1), 69–75. https://doi.org/10.1093/embo-reports/kvf008.

(50) Gladilin, E.; Ohse, S.; Boerries, M.; Busch, H.; Xu, C.; Schneider, M.; Meister, M.; Eils, R. TGFβ-Induced Cytoskeletal Remodeling Mediates Elevation of Cell Stiffness and Invasiveness in NSCLC. *Sci. Rep.* **2019**, *9* (1), 1–12. https://doi.org/10.1038/s41598-019-43409-x.

(51) Discher, D. E.; Janmey, P.; Wang, Y. L. Tissue Cells Feel and Respond to the Stiffness of Their Substrate. *Science (80-.).* **2005**, *310* (5751), 1139–1143. https://doi.org/10.1126/science.1116995.

(52) Engler, A. J.; Sen, S.; Sweeney, H. L.; Discher, D. E. Matrix Elasticity Directs Stem Cell Lineage Specification. *Cell* **2006**, *126*, 677–689.

(53) Osborne, L. D.; Li, G. Z.; How, T.; O'Brien, E. T.; Blobe, G. C.; Superfine, R.; Mythreye, K. TGF-β Regulates LARG and GEF-H1 during EMT to Affect Stiffening Response to Force and Cell Invasion. *Mol. Biol. Cell* **2014**, *25* (22), 3528–3540. https://doi.org/10.1091/mbc.E14-05-1015.

(54) Guck, J.; Schinkinger, S.; Lincoln, B.; Wottawah, F.; Ebert, S.; Romeyke, M.; Lenz, D.; M., E. H.; Ananthakrishnan, R.; Mitchell, D.; Kas, J.; Ulvick, S.; Bilby, C. Optical Deformability as an Inherent Cell Marker for Testing Malignant Transformation and Metastatic Competence. *Biophys. J.* **2005**, *88*, 3689–3698.

(55) Fritsch, A.; Höckel, M.; Kiessling, T.; Nnetu, K. D.; Wetzel, F.; Zink, M.; Käs, J. A. Are Biomechanical Changes Necessary for Tumour Progression? *Nat. Phys.* **2010**, *6* (10), 730–732. https://doi.org/10.1038/nphys1800.

(56) Lin, H. H.; Lin, H. K.; Lin, I. H.; Chiou, Y. W.; Chen, H. W.; Liu, C. Y.; Harn, H. I. C.; Chiu, W. T.; Wang, Y. K.; Shen, M. R.; Tang, M. J. Mechanical Phenotype of Cancer Cells: Cell Softening and Loss of Stiffness Sensing. *Oncotarget* **2015**, *6* (25), 20946–20958. https://doi.org/10.18632/oncotarget.4173.

(57) Tavares, S.; Vieira, A. F.; Taubenberger, A. V.; Araújo, M.; Martins, N. P.; Brás-Pereira, C.; Polónia, A.; Herbig, M.; Barreto, C.; Otto, O.; Cardoso, J.; Pereira-Leal, J. B.; Guck,

J.; Paredes, J.; Janody, F. Actin Stress Fiber Organization Promotes Cell Stiffening and Proliferation of Pre-Invasive Breast Cancer Cells. *Nat. Commun.* **2017**, *8* (May). https://doi.org/10.1038/ncomms15237.

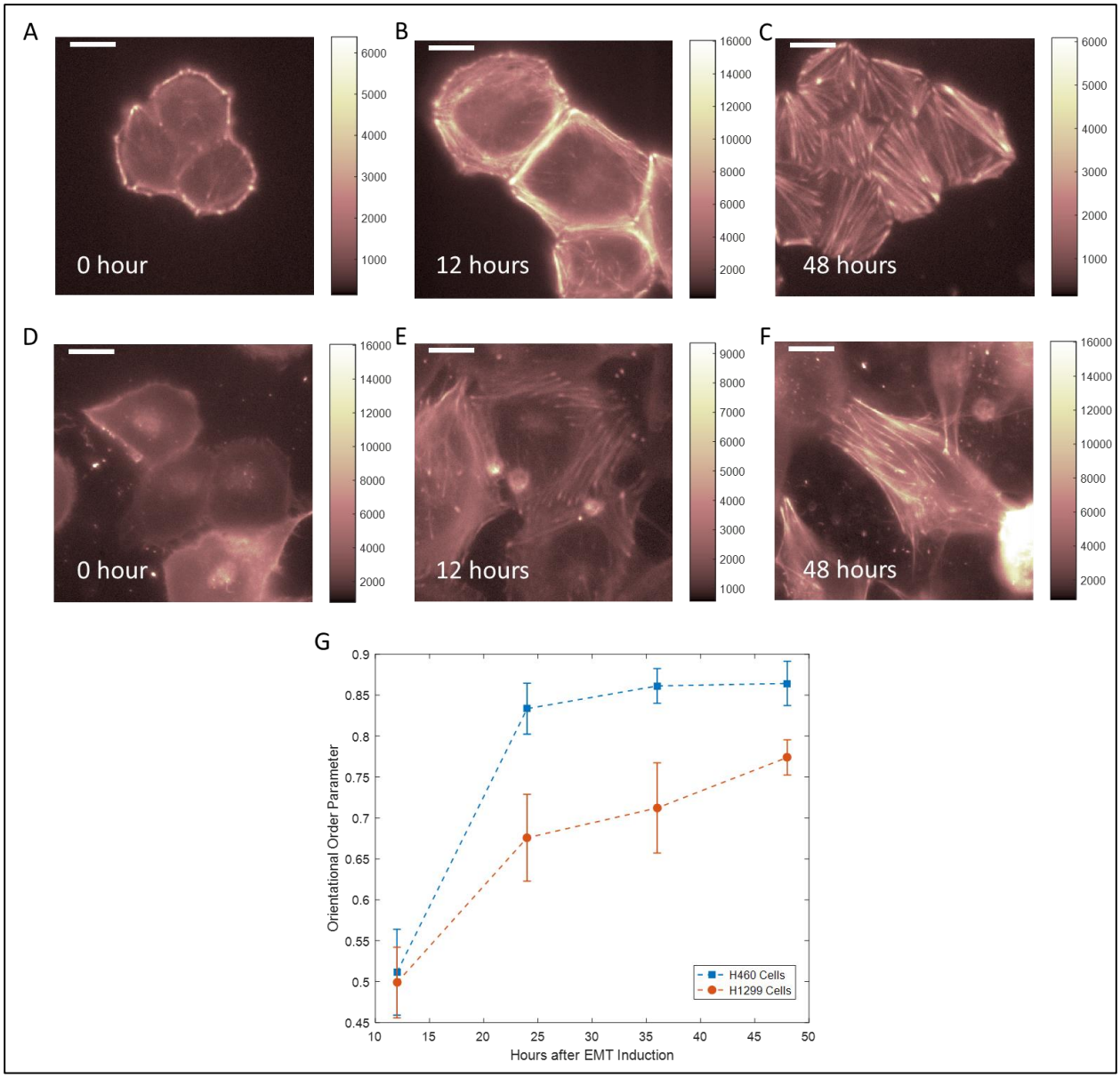
(58) Hauke, L.; Narasimhan, S.; Primeßnig, A.; Kaverina, I. A Focal Adhesion Filament Cross-Correlation Kit for Fast , Automated Segmentation and Correlation of Focal Adhesions and Actin Stress Fibers in Cells . Author Summary. **2021**.

(59) Rimoli, C. V.; Augusto, C.; Cruz, V.; Curcio, V.; Mavrakis, M.; Brasselet, S. 4polar-STORM Polarized Super-Resolution Imaging of Actin Filament Organization in Cells. *bioRxiv* **2021**, 2021.03.17.435879.

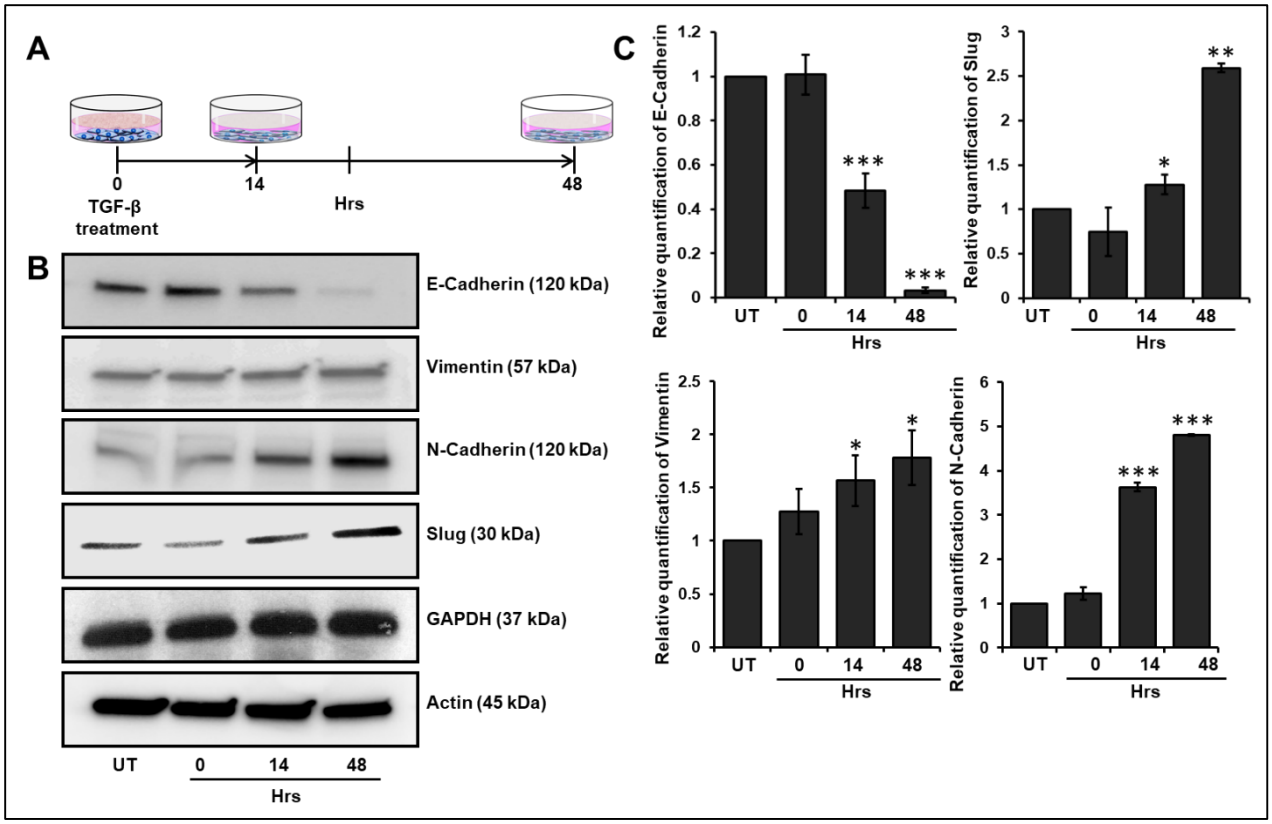
(60) Xiang, Y.; Ye, W.; Huang, C.; Lou, B.; Zhang, J.; Yu, D.; Huang, X.; Chen, B.; Zhou, M. Brusatol Inhibits Growth and Induces Apoptosis in Pancreatic Cancer Cells via JNK/P38 MAPK/NF-Kb/Stat3/Bcl-2 Signaling Pathway. *Biochem. Biophys. Res. Commun.* **2017**, *487* (4), 820–826. https://doi.org/10.1016/j.bbrc.2017.04.133.

(61) Wang, B.; Zhang, L.; Zhao, L.; Zhou, R.; Ding, Y.; Li, G.; Zhao, L. LASP2 Suppresses Colorectal Cancer Progression through JNK/P38 MAPK Pathway Meditated Epithelial-Mesenchymal Transition. *Cell Commun. Signal.* **2017**, *15* (1), 1–8. https://doi.org/10.1186/s12964-017-0179-9.

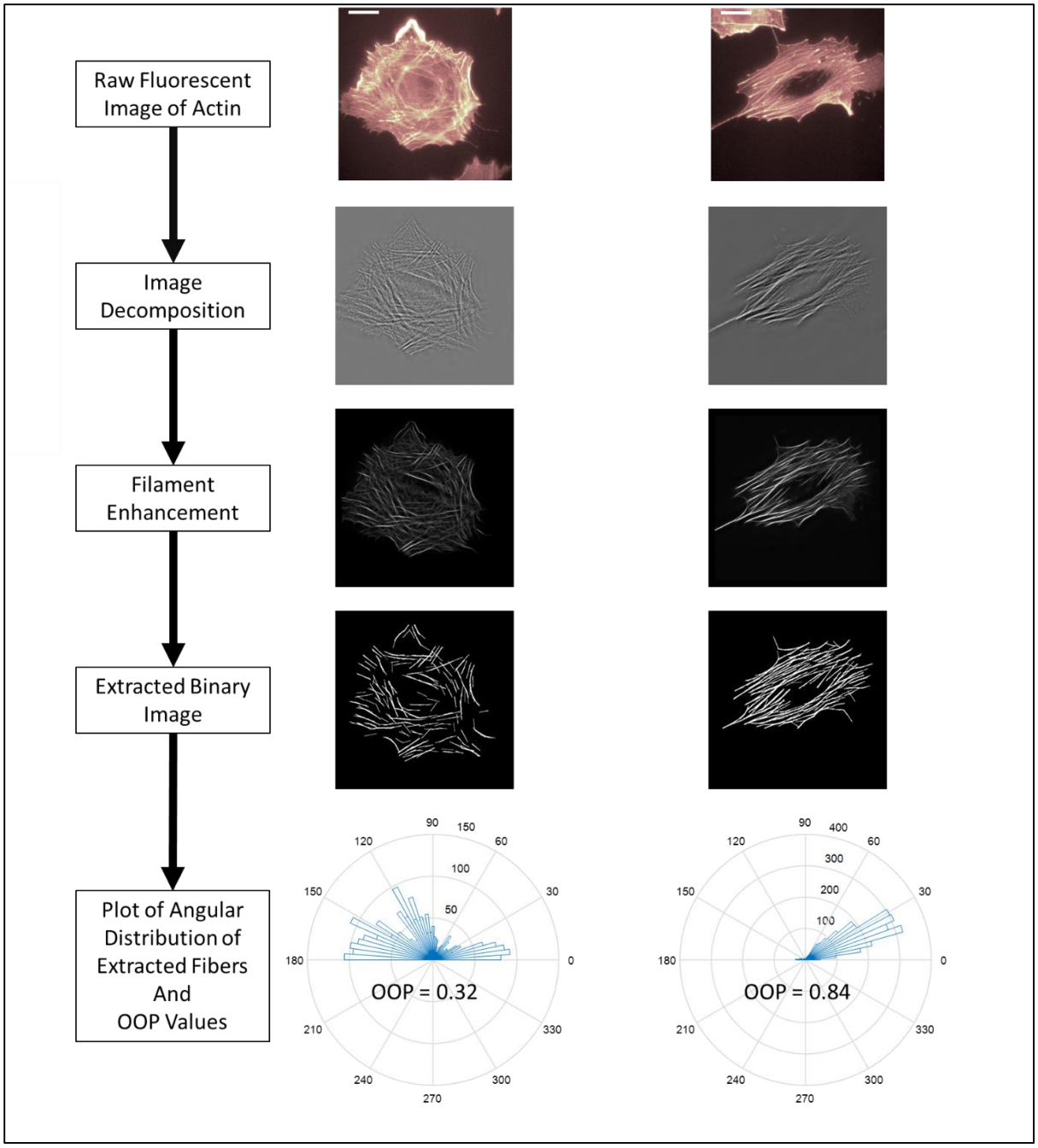
Supplementary Information



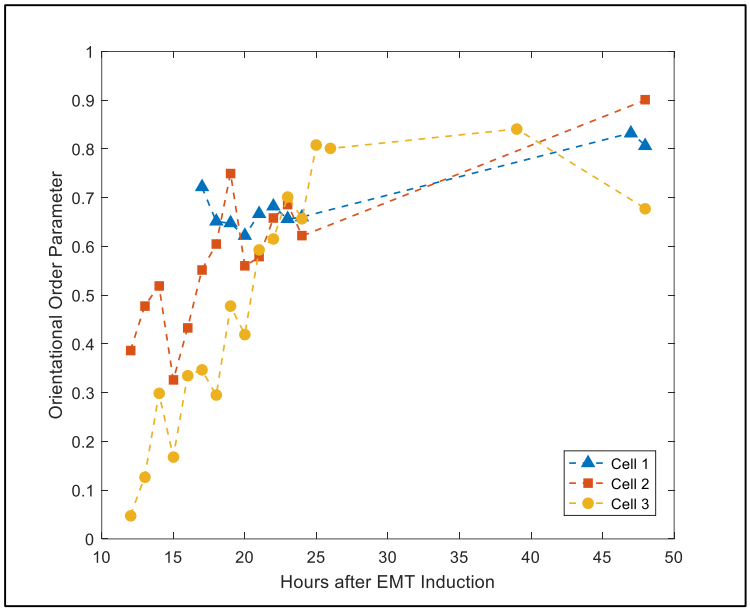
Supplementary Fig. 1 | H460 and H1299 cell lines undergoing EMT stained with SiR-actin. **a-c,** H460 cells at 0, 12 and 48 hours after addition of TGFβ1 respectively. **d-f,** H1299 cells at 0, 12 and 48 hours after addition of TGFβ1 respectively. **g,** Plots of average OOP values vs time of TGFβ1 treatment for H460 (blue) and H1299 (red) respectively. Error bars correspond to standard error at respective time-points. Scale bar: 16μm.



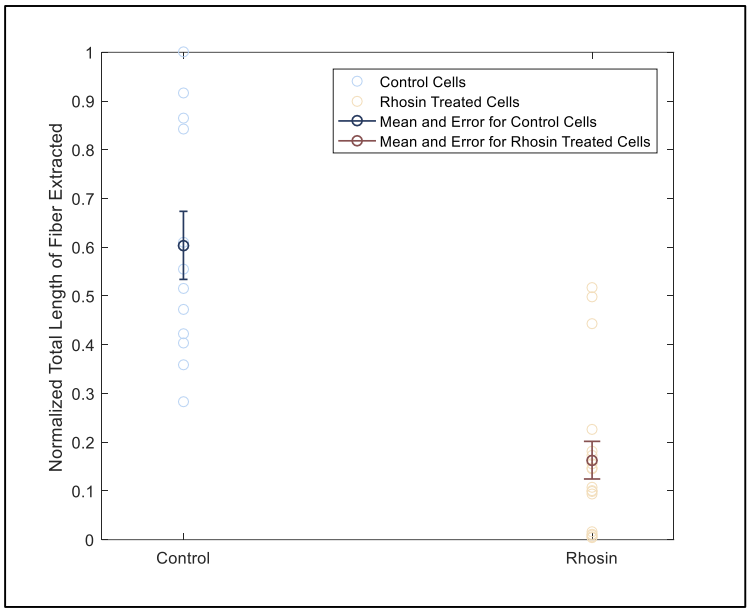
Supplementary Fig. 2 | Expression of E-Cadherin, N-Cadherin, Vimentin and Slug in A549 cells undergoing EMT. A, Schematic of experimental design. **B,** Gel segments with four lanes corresponding to untreated cells and cells treated with TGFβ1 for 0, 14, 48 hours respectively (from left to right) and the corresponding protein expressions. **C,** Densitometric analysis of the western blot showing the relative expression levels of the proteins with respect to time of TGFβ1 treatment.



Supplementary Fig. 3 | Flowchart for Image Analysis and Quantification. Scale bar: 16μm.



Supplementary Fig. 4 | Plot of multiple single cell OOP trajectories with time of EMT induction.



Supplementary Fig. 5 | Comparison of length of actin fibers extracted from fluorescent images. Every length is normalized with respect to the length of the longest extracted fiber.

Chapter 4

Pre-malignancy and Cytoskeleton

This chapter is a study of the actin cytoskeleton of pre-malignant cells. Using techniques described in chapter 2 (SPOCC), the difference between the cytoskeleton of high migratory and low migratory cells have been quantified. Changes in the stress fiber patterns (SPOOC in some cases) was used to quantify the drug response of these cells to obtain in-depth knowledge regarding their differences. This work was done in collaboration with the group of Prof. Steven Dubinett, UCLA.

Regulation and role of actin dynamics in promoting pre-malignant cell migration

Abstract:

Migration of pre-malignant cells often cause insurmountable difficulty in clinical diagnostics and therapy. To better understand the cause of such pre-malignant cell migration, a highly migratory sub-population of Human Bronchial Epithelial Cell (HBEC) was used as a model. This subpopulation showed drastically faster movements in scratch wound assays and isolated culture conditions compared to the rest of the cells. We demonstrated a clear relation between the enhanced motility of these cells with the existence of actin stress fibers in this subpopulation. Differences in the expression and localization of actin binding proteins have been used to validate the stress fibers models. Further investigation into the multiple signaling networks in these cells have been carried out by observing their cytoskeletal response to drug treatments. Using Statistical Parametrization of the Cell Cytoskeleton (SPOCC) to quantify their cytoskeletal response, we have demonstrated that the ERK/MAPK pathway is likely responsible for the enhance motility of this subpopulation.

Keywords: Pre-malignancy, actin, cytoskeleton, image analysis, drug response, SPOCC

Introduction:

The existing theory of cancer progression follows a certain pattern with a sequence of event for most types of cancer[1] (Figure. 1A). First a tumor is formed in a healthy tissue. In normal tissues, growth suppressors[2,3,4] as well contact inhibition control[5,6] and maintain the tissue architecture. Programmed cell death or apoptosis also functions as a barrier to tumor formation[7,8]. Cancer cells in the tumor are characterized by their ability to resist growth suppression[9,10,11] as well as apoptosis[7,8,12]. They can achieve this by either simple suppression of the retinoblastoma-associated proteins or the TP53 proteins. This can also be achieved by recruited neighboring tissues to supply growth factors. Loss of contact inhibition[13,14] can also aid in unrestricted growth of the tumor. Eventually, the tumor develops its own blood circulation system (angiogenesis) thereby starving the tissue around[15]. This tumor can be benign for a prolonged period of time. A tumor can also be metastatic which means cells from the tumor can migrate to other locations and form secondary tumors. This is a complex multistep process termed as the invasion-metastasis cascade[16,17]. One of the most important steps of metastasis is Epithelial Mesenchymal Transition (EMT)[18,19,20,21]. One of the key aspects of EMT, and in turn metastasis, is the loss of cell-cell adhesion that is characteristic of epithelial cells. E-cadherin protein is essential in maintaining the layer like structure of epithelial tissue and it is lost/ down-regulated as a result of EMT[22]. Transforming Growth Factor (TGFβ) is known to be an anti-proliferative agent, but cancer cells repurpose their signaling pathways to initiate EMT in the presence of TGFβ[23,24,25]. EMT in itself can be a multistep protocol with a network of genetic pathways inter-connecting among themselves[26].

Based on the current cancer progression model, metastasis is considered a late-stage event. In other words, only a well-developed tumor can metastasize. But around 30% of patients report a reappearance of metastatic cancer even after surgical resection of early-stage lung cancer[27,28].

There have also been evidences of metastases with no identifiable primary tumor[29]. Circulating tumor cells have been observed in patients with stage-I non-small cell lung cancer (NSLC)[30,31,32]. Combined, these findings indicate that there might be metastasis or metastasis-like event going on in early phases of cancer. The level of this micro-metastasis is likely below the detection capacity of current clinical techniques and as such goes undetected. An early activation of EMT in cells have been reported for pancreatic[33] and breast[34,35] cancer already. Cells derived from pre-malignant lesions have a broad spectrum of physical and morphological properties which correspond to varied levels of stemness. There have been attempts to identify and separate the cells based on their stiffness[36] and motility[37,38], both of which are markers of stemness. In premalignant human airway epithelial cells, a highly migratory subpopulation has been identified and separated based on their ability to successfully pass through sub-nuclear sized pores[39]. This high migratory property in these cells is controlled by Rac1 activation and is heritable upon multiple cell-division cycles. These cells demonstrate some mesenchymal properties such as expression of Snail, but are not entirely mesenchymal in nature (Fig. 2A,B). Though a theoretical description of such early stage EMT in premalignant lesions is reported[40], a better understanding of this phenomenon at the cellular level is required. In this model, termed 'Field Cancerization', cells from premalignant lesions can undergo EMT, migrate to a different section of the body even before a tumor is formed in the primary location. As such, metastatic tumors are formed without there being a primary tumor (Figure. 1B).

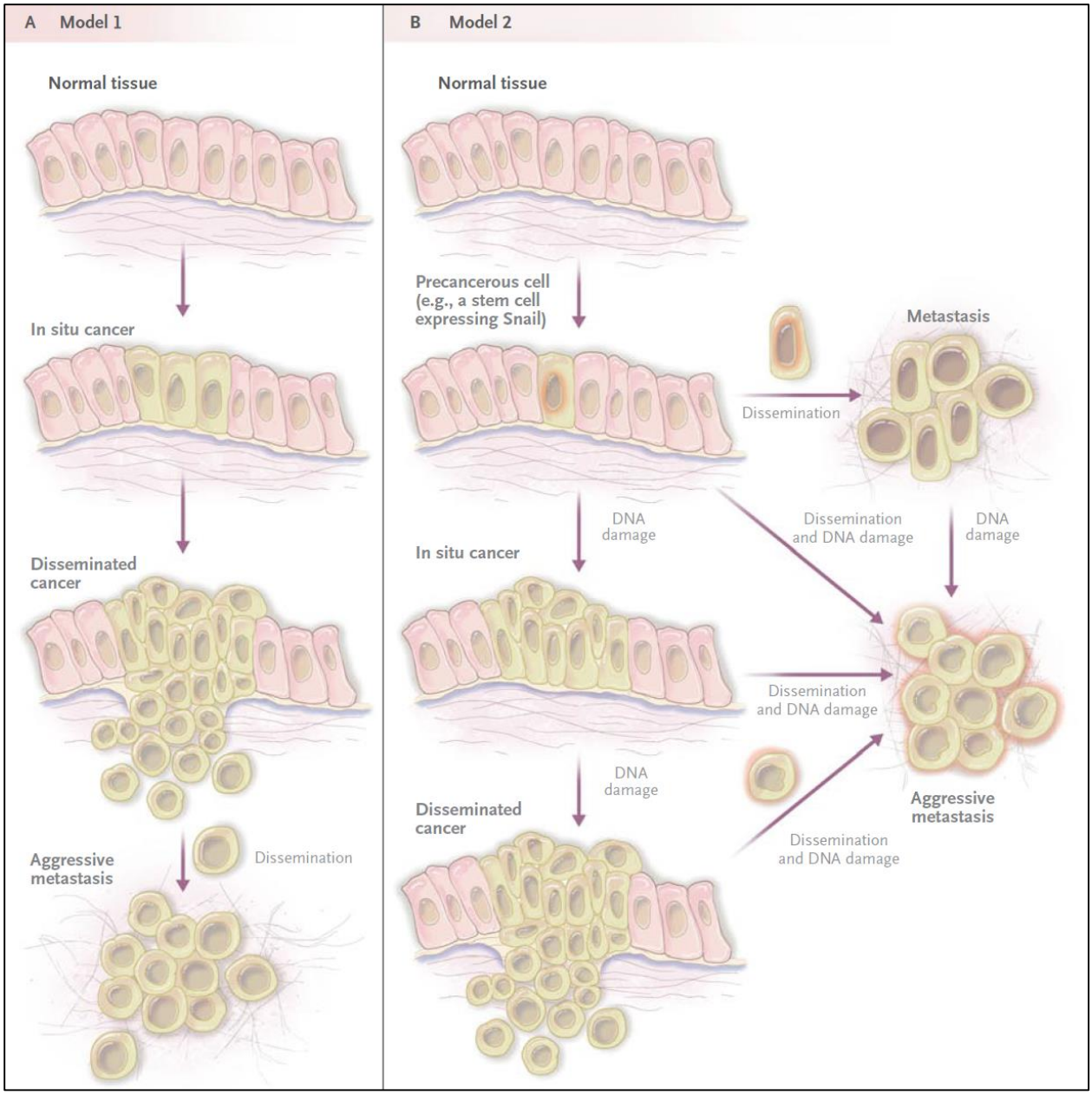


Fig. 1 | Two models for cancer progression[40]**. A,** Classical model for cancer progression showing metastasis of the primary tumor. **B,** Field-cancerization model for cancer progression showing metastasis occurring in premalignant cells before tumor formation. Image courtesy Sanchez-Garcia et. al. (ref. 40).

The deep inter-relation between EMT, cellular morphology and the actin cytoskeleton has already been discussed in previous chapters. The actin cytoskeleton is the main structure responsible for cellular stiffness[41,42]. It is also evidenced by the cytoskeletal response to the matrix rigidity[43,44]. The interplay between the cytoskeleton and biological processes is demonstrated in stem cells

showing lineage specification based on matrix elasticity and the cytoskeletal organization[45]. The relationship between motility and cytoskeleton is less defined as cells have multiple ways of migration each of which is dependent on different signaling pathways as well as biological conditions. Some highly motile cells show very little or no stress fibers but the motility of fibroblasts have also been linked with the existence of ventral stress fibers[46]. Formation of stress fibers has been established as a very important aspect of EMT (and hence metastasis) and are often ascribed as the reason for the high motility of mesenchymal cells[25]. It is worth noting here that the highly migratory subpopulation of the airway epithelial cells also demonstrated a different cytoskeletal architecture compared to the rest of the cell population[39].

Our hypothesis going into this work is that these highly migratory cells are partially mesenchymal due to activation of the EMT protocol. But the activation mechanism is likely different from malignant cell lines and that is why these cells do not undergo the complete EMT. It is important to understand why EMT is activated in these cells and why exactly does it arrest before completion. Also given the multi-step nature of EMT[26], we intend to determine whether these highly migratory cells correspond to a partial EMT phenotype in lung cancer. To understand the genetic protocol inherently active in these high migratory cells, their response to a series of drugs (demonstrated to be relevant in the EMT protocol) is likely to provide key insights into their genetic network. Given the high degree of correlation between the actin cytoskeleton and EMT (discussed in chapter 3), we chose the cytoskeletal structure of these cells as our observable/ quantifier. We used SPOCC to evaluate the drug response of these cells.

Results:

Isolated HBEC sub-population demonstrates better migration as isolated cells and in wound healing assays. Given the difference in the ability of these cells to migrate in transwell migration assays, we intended to investigate whether this difference was an inherent property of the sub-population or whether they developed this property while passing through pores. We tracked isolated cells for 15 hours and observed a clear difference in migration abilities between the subpopulation and the unselected cells (Fig. 2C,D). The subpopulation demonstrated much higher rates of migration for most of the cells than the unselected cells; and henceforth they shall be mentioned as HBEC-HM (High Migratory) and HBEC-UN (Unselected). In addition, HBEC cells were also observed in scratch wound assays which demonstrated a clear heterogeneity in their migration patterns (Fig. 2E).

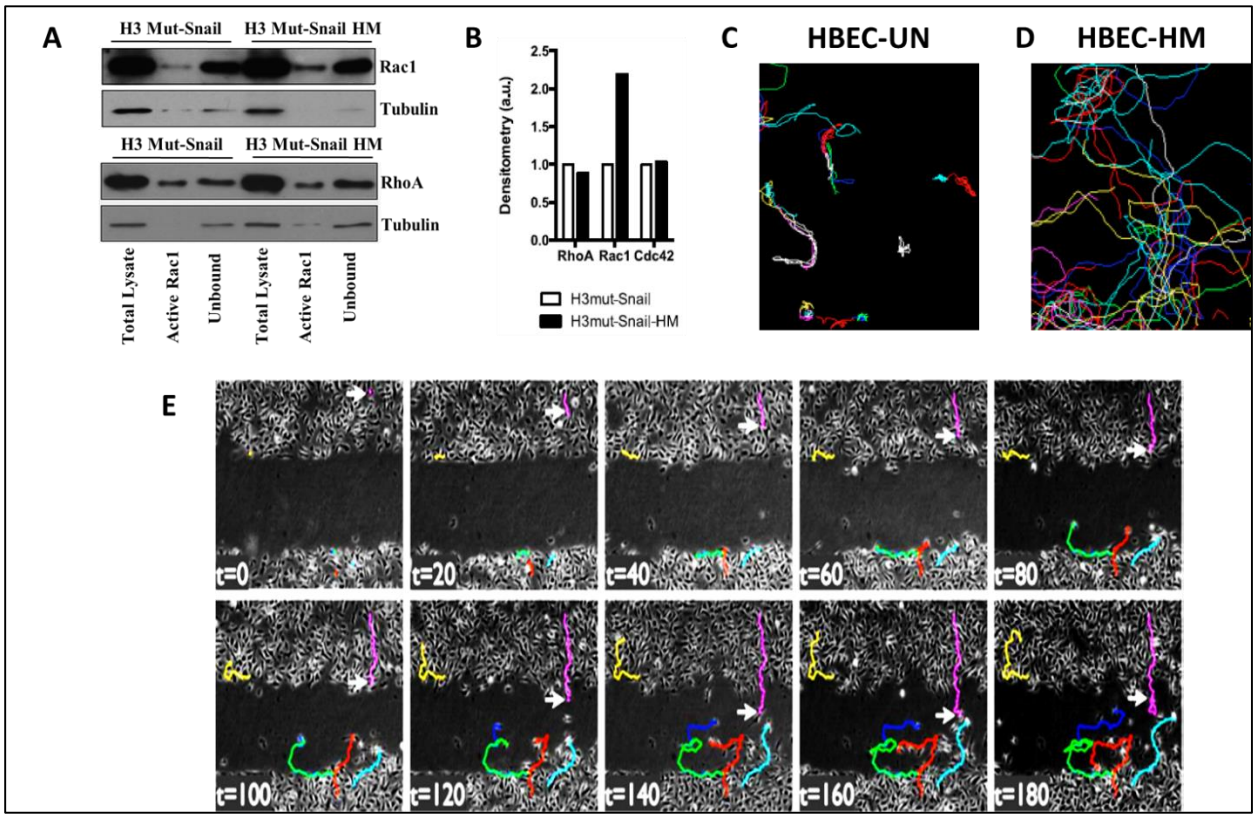


Fig. 2 | Differential behavior of HBEC-HM compared to HBEC-UN cells. A, Western blot analysis of HBEC cells overexpressing Snail demonstrating HM cells have higher Rac1 expression compared to UN cells[39]. **B,**

Densitometry analysis confirming that there is an upregulation of Rac1 in the HM population compared to the UN population while expression levels of RhoA and Cdc42 remain quite similar. **C, D,** Single cell tracking of HBEC-UN and HBEC-HM respectively showing the clear difference between their migratory abilities. **E,** Time-lapse microscopy of a scratch-wound assay with a series of time-points (mentioned in white) and the corresponding single cell tracks (performed with IncuCyte live cell analysis system) showing the heterogeneity in migration abilities in HBECs, where few cells clearly have much higher motility than the rest of the population. Image (A and B) courtesy Pagano et. al. (ref. 39).

High-migratory and unselected cells have completely different actin patterns irrespective of overexpression of Snail. The difference between HM and UN populations is magnified by the programmed overexpression of Snail. So, it was important to establish whether there is any quantifiable difference in the actin cytoskeleton of HM and UN populations. For that we stained both HBEC-Snail-HM and HBEC-HM lines to fluorescently label their actin cytoskeleton. For both HBEC-Snail-HM and HBEC-HM, the cells showed clear existence of stress fibers (Fig. 3A,B, Supplementary Fig. 1A). On the other hand, HBEC-UN demonstrated a positive lack of stress fibers (Fig. 3D). The data for HBEC-Snail-UN was highly heterogeneous with some cells showing stress fibers (Fig. 3C while others lacking them (Supplementary Fig. 1B-E). The cytoskeletal difference between HBEC-HM and HBEC-UN demonstrate that the overexpression of Snail is not the source of this difference. Also, filopodia like structures were characteristic of UN cell populations.

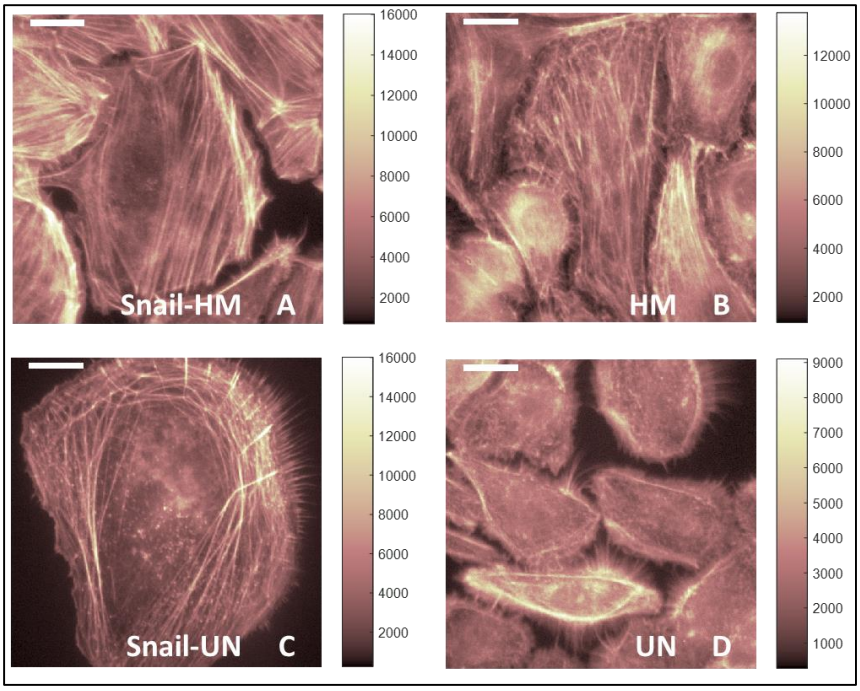


Fig. 3 | HBECs demonstrating cytoskeletal heterogeneity. A-D, HBEC-Snail-HM, HBEC-HM, HBEC-Snail-UN and HBEC-UN cells respectively stained with Phalloidin 670. Scale bar: 16μm.

Pattern of actin binding proteins were different in HBEC-HM vs HBEC-UN cell. Having established the difference in actin stress fiber structures in HM vs UN populations, we sought to determine whether any differences existed in the expression and localization of actin binding proteins. Fascin is an actin binding protein found in stress fibers. So, cells with stress fibers are likely to show fascin expression throughout the cell while cells without stress fibers should have localized fascin around the nucleus. We stained HBEC-HM and HBEC-UN cells with both actin and fascin and compared their patterns. In HBEC-HM cells, fascin showed co-localization with actin throughout the cell indicating the existence of stress fibers. On the other hand, in HBEC-UN fascin was almost entirely localized around the nucleus and shows a completely opposite pattern to actin. This means there is very low to no interaction between actin and fascin in UN cells which is indicative of a lack of stress fibers. α-actinin is a known cross-linker of actin filaments found and is another ABP that is found in stress fibers. So, α-actinin staining should generate a similar

pattern to fascin. We stained HBEC-HM and HBEC-UN cells for α-actinin to compare their localization. As expected, in the HM cells, α-actinin was present throughout the cell whereas in UN cells it was localized exclusively around the nucleus, once again supporting the lack of stress fibers in UN cells. For better comparison, both the images were taken at the plane of the nucleus. Focal Adhesion Kinase (FAK) caps the actin stress fibers are characteristic of focal adhesion spots and in turn indicate the existence of stress fibers. Comparison of FAK patterns in HBEC-Snail-HM and HM-Snail-UN cells showed that HM cells which are supposed to contain stress fibers had clear FAK spots near the cell edge whereas HBEC-Snail-UN cells showed no identifiable FAK spotting.

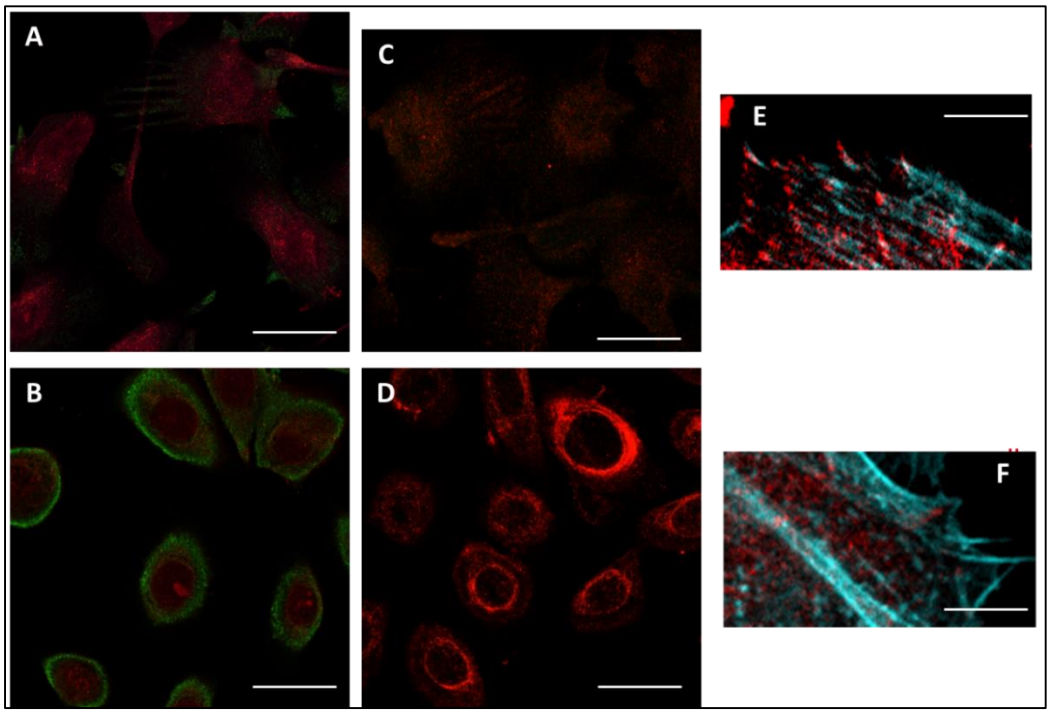


Fig. 4 | Actin binding protein patterns in HBEC-HM and HBEC-UN cells. A, B, Actin (green) and Fascin (red) staining of HBEC-HM and HBEC-UN cells respectively. **C, D,** α-actinin staining (red) of HBEC-HM and HBEC-UN cells respectively showing different localization patterns. **E, F,** HBEC-Snail-HM and HBEC-Snail-UN cells respectively showing completely different FAK patterns. Scale bar (A-D): 20μm. Scale bar (E, F): 5 μm.

Different drugs show different levels of effect on the cell cytoskeleton. To better understand the genetic protocols active in the HBEC-HM cells, they were subjected to a series of drugs. Choosing a specific set of drugs that are known to inhibit different stages of EMT, we looked at the cytoskeletal response to the drugs. Genistein is a naturally occurring compound that is known to prevent the proliferation of melanoma by altering actin polymerization through FAK and paxillin[47]. We treated HBEC-Snail-HM, HBEC-HM, HBEC-Snail-UN and HBEC-UN with genistein for 48 hours and stained their actin fibers with Phalloidin. HBEC-Snail-HM, HBEC-HM and HBEC-Snail-UN showed a marked decrease is stress fibers (Fig. 5A-C). HBEC-UN cells had no fiber structures to begin with but even their distribution was altered (Fig. 5D). We observed an unexpected spotting pattern in the actin structure. Counter-staining with FAK antibodies demonstrated that the cells had uniform distribution of FAK owing to the lack of stress fibers with some dark spots. These dark spots correlated perfectly with the bright spots in the actin image (Supplementary Fig. 2).

We also chose to inhibit Tankyrase using XAV-939 as it had shown some interesting results in the EMT of A549 cells. We treated HBEC-Snail-HM, HBEC-HM, HBEC-Snail-UN and HBEC-UN with XAV939 for 48 hours and their actin fibers were stained with Phalloidin 670 (Fig. 5E-H). Neither of the cell lines showed any identifiable difference from the untreated cell.

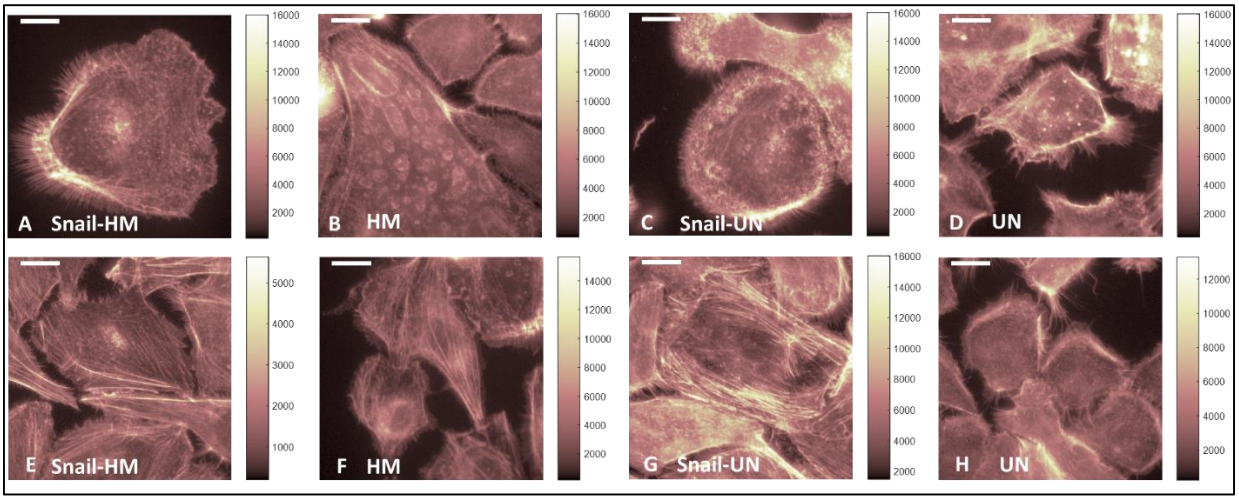


Fig. 5 | Cytoskeletal response of HBEC cells to Genistein and Tankyrase inhibitor. A-D, HBEC-Snail-HM, HBEC-HM, HBEC-Snail-UN and HBEC-UN cells respectively treated with Genistein for 48hours and stained with Phalloidin 670. **E-H,** HBEC-Snail-HM, HBEC-HM, HBEC-Snail-UN and HBEC-UN cells respectively treated with XAV-939 for 48hours and stained with Phalloidin 670. Scale bar: 16 μm.

HBEC-Snail-HM had the most homogeneous cytoskeletal structure (Fig. 6A,B) and hence showed the highest degree of cytoskeletal response on being treated with drugs. We intended to quantify this response using SPOCC to produce a screening platform for future experiments. Ribosomal S6 Kinase (RSK) is an effector of the Ras/ERK pathway which is highly relevant for metastasis as well as actin polymerization[48]. Inhibition of RSK using LJI308[49] resulted in a clear disintegration of the stress fibers (Fig. 6C,D). Based on the nuclear blebbing reported in transwell migration of HBEC-HM cells, an interaction between the nuclear structure and actin cytoskeleton is expected. KPT276 is a nuclear export inhibitor, selectively inhibiting the Chromosomal Region Maintenance 1 (CRM1) protein[50]. Upon inhibition of CRM1, the cells demonstrated a completely different stress fiber patter (Fig. 6E,F). SL327 is a MEK1/2 inhibitor in the MAPK pathway[51] and its treatment caused stress fiber disintegration in the cells as well (Fig. 6G,H). The OOP values for the untreated and treated cells strongly validate the cytoskeletal difference (Fig. 6G). Real-time cytoskeletal response of HBEC-Snail-HM cells upon treatment of U0126 (a MEK 1/2 inhibitor) can also be quantified using SPOCC (Supplementary Fig. 3).

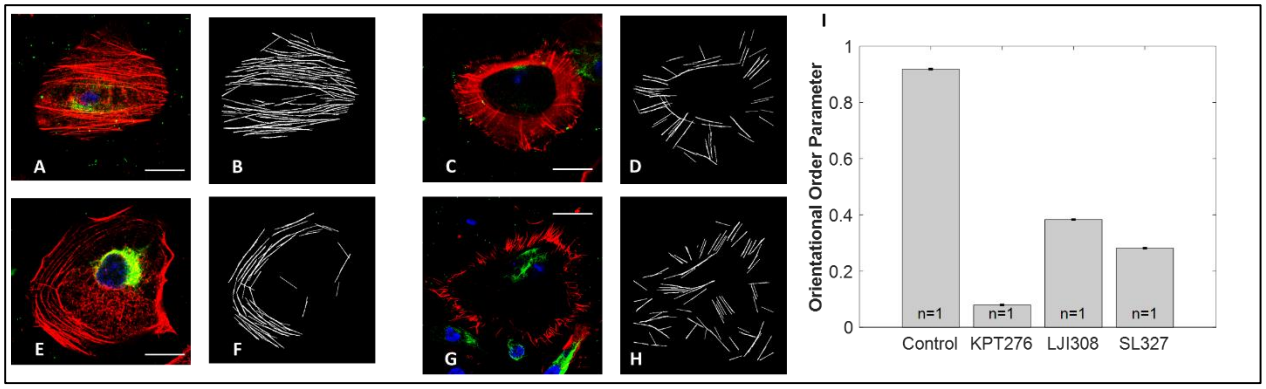


Fig. 6 | SPOCC quantification of cytoskeletal response of HBEC-Snail-HM cells under different drug treatments. Images of HBEC-Snail-HM cells treated with different drugs and their nucleus (blue), vimentin (green) and F-actin (red) were stained. **A, B,** Untreated HBEC-Snail-HM cell and its extracted fiber image respectively. **C, D,** LJI308 treated HBEC-Snail-HM cell and its extracted fiber image respectively. **E, F,** KPT276 treated HBEC-Snail-HM cell and its extracted fiber image respectively. **G, H,** SL327 treated HBEC-Snail-HM cell and its extracted fiber image respectively. **I,** OOP values of the four cells. Scale bar: 10μm.

Actin Binding proteins validate the cytoskeletal response of Snail-HM cells to drugs. FilaminA cross-links the stress fibers to the cortical actin mesh and the cell membrane[52], so its existence and co-localization with stress fibers is essential for stress fibers (Fig. 7A). Upon inhibiting the stress fiber formation through MEK1/2 inhibition by U0126, we observed a complete collapse of filaminA structure (Fig. 7B) as well resulting from the loss of stress fibers. Vasodilator-stimulated phosphoprotein (VASP) serves as the nucleation site for actin filament formation near the cell membrane[53] and localizes as puncta that mark the end of a stress fiber (Fig. 7C). On treating Snail-HM cells with U0126, the VASP spots disappeared (Fig. 7D) indicating a cessation of actin polymerization in the drug treated cells.

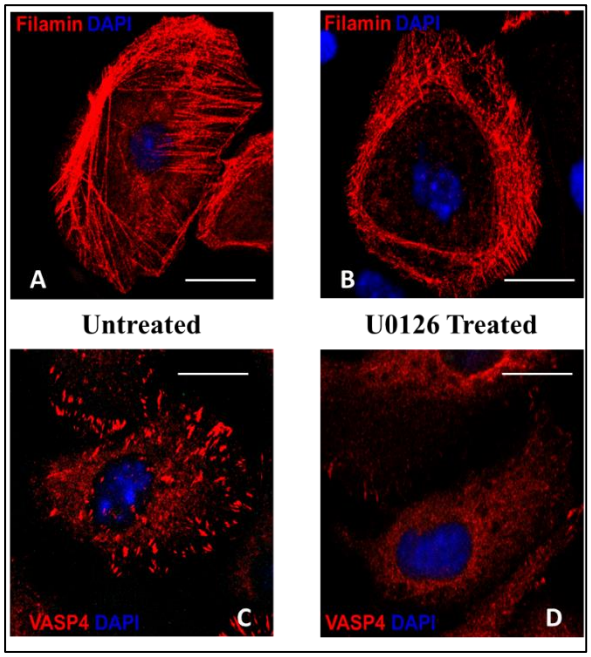


Fig. 7 | Response of Actin Binding Proteins (ABPs) in drug treated Snail-HM cells. A, B, Untreated and U0124 treated cells respectively stained for the nucleus (blue) using DAPI and filaminA (red). **C, D,** Untreated and U0126 treated cells respectively stained for the nucleus (blue) using DAPI and VASP (red). Scale bar: 10μm.

Discussion:

The main goal for this work was to improve our understanding of the root cause of the enhanced motility in the high migratory sub-population of HBEC. Given the amount of inter-dependence of the cell cytoskeleton and their migration capabilities, we focused on the cell cytoskeleton as our quantifiable reporter for the morphological properties of the cell. We demonstrated that the high migratory (HM) sub-population had a completely different cytoskeletal model from the unselected (UN) cell. The HM sub-population had clear, long stress fibers throughout the cell. On the other hand, the UN cells mostly had cortical actin and filopodia-like protrusions; any actin fiber structure they had was mostly localized near the edge of the cells. HBEC cells that overexpressed Snail were also compared in a similar fashion. Although the Snail-HM sub-population expectedly had stress fibers, the Snail-UN population had a high degree of heterogeneity in their cytoskeletal structures.

A non-negligible percentage of the Snail-UN cells showed clear and long stress fibers similar to the HM sub-population, making any statistical analysis of them non-viable. The HM sub-population has been reported to have an upregulation of Snail inherently, so it is possible that by overexpressing Snail in the UN cells, we are artificially transforming some of them to the HM phenotype, thereby making the percentage of HM cells much higher. Thus, it might be more judicious to carry out future experiments on cells without Snail overexpression or at least have them as a control. But it is worth noting that the similarity between HM and Snail-HM cytoskeletal patterns mean that the difference in the cytoskeleton of these cells is inherent and not induced by Snail overexpression.

A difference in cytoskeletal organization has to correspond to a difference in expression and localization of actin binding proteins (ABPs) as well. The FAK spotting revealed that for Snail-HM cells, the stress fibers were capped with FAK near the edges, but for Snail-UN, even the cells that had stress fibers, didn't have FAK-capping. This indicates that the type of stress fibers is likely different in the Snail-HM phenotype. Both fascin and α-actinin were almost entirely localized around the nucleus in the UN cells. A possible explanation of this pattern can be that UN cells do not have stress fibers to recruit cross-linking proteins such as fascin and α-actinin and so these proteins are mostly localized where they were expressed. In case of HM cells, both fascin and α-actinin were expressed all over the cell indicating their recruitment in stress fibers throughout the cell. The signal intensity for actin and both the ABPs were very low in HM cells. This is likely because in the HM cells the stress fiber structure is in a different plane than the nucleus (where the images were taken).

A very interesting observation was the lack of effect upon inhibition of Tankyrase. As discussed in Chapter 3, lung cancer cells undergoing EMT respond strongly to tankyrase inhibition. This

indicates that the signaling mechanism active in these HM cells are likely to be distinct from simple EMT mechanism. Genistein is a tyrosine kinase inhibitor that can inhibit metastasis[54] through interactions with EGFR-FAK-paxillin path[47,55], ultimately affecting actin polymerization. Genistein has also been reported to affect the expression level of proteins that are involved in the MAPK pathway. So, it is expected that both actin and FAK patterns would be altered upon addition of Genistein. The coincidence of bright actin and dark FAK spots is less intuitive. It is possible that due to the inhibition of stress fiber formation, actin and FAK proteins are undergoing a liquid-liquid phase separation[56] and localizing in distinct regions. The interplay between the nucleus and actin for the HM cells could be conjectured from their ability to form nuclear blebs while migrating through pores and healing the nucleus afterwards. The cytoskeletal response to inhibition of CRM1 using KPT276 validates that conjecture. We have also investigated the cytoskeletal response for JNK 1/2 Inhibition, JAK2 Inhibition, NF-κB inhibition and p38 MAPK inhibition on all the cell lines. Small levels of response were observed, such as an increase in filopodia like structures in HBEC-Snail-HM and HBEC-HM for NF-κB inhibition, but due to heterogeneity in the response, no statistical conclusion could be drawn.

Genistein, SL327, LJI308 and U0126 all affect the MAPK/ERK pathway in some way and their inhibition has resulted in very drastic cytoskeletal reorganization in HBEC cells demonstrated directly in the stress fiber architecture as well as actin binding proteins. So, we can convincingly claim that the MAPK/ERK pathway is likely responsible for the high motility of the HM sub-population of HBEC cells. It is true that some other inhibitors of the MAPK/ERK pathway did not generate statistically significant cytoskeletal change. But not every protein of the MAPK/ERK pathway affects the cytoskeleton to the same extent. It is quite likely that inhibition of some of those proteins will be less influential and thus result in a high degree of heterogeneity in the

cytoskeletal structure, which is what was observed in those cases. It might also be possible that the concentrations of the inhibitors used were not enough to induce any change in the actin dynamics.

Future Direction:

In future, we need to identify exactly how the MAPK/ERK pathway affects the cytoskeleton and hence the motility of these cells and how that mechanism is different from normal cells. Using si-RNAs might be more specific than using inhibitor molecules. Correlating the cytoskeletal structure with transcriptomics and proteomics analyses will help in developing further insight into these cells. We also need to answer what kind of stress/mutation resulted in these cells obtaining their distinct genetic signaling. To achieve that, we can simulate a series of stress/mutation in parental cells and observe whether they are transformed into the HM phenotype. Understanding the inner workings of this phenomenon and being able to control it has a multitude of clinical applications starting from better identification of primary sites of metastasis to designing drugs to prevent it.

Materials and Methods:

Cell Culture: All Human Bronchial Epithelial Cells (HBECs) were cultured as previously described[57]. Cells were cultured in Keratinocyte Serum Free Medium (KSFM) supplemented with 30μg/ml Bovine Pituitary Extract and 0.2ng/ml recombinant human Epidermal Growth Factor (rh-EGF).

Drug Treatment and Cell Staining: Cells were grown on 8 well culture slides (Sarstedt, Catalog no. 94.6170.802) for 24 hours before being treated with specific drugs. After 48 hours of drug treatment the cells were rinsed with PBS (Gibco, catalog no. 14190-136) and fixed with 4% paraformaldehyde (diluted from 10%) (Electron Microscopy Sciences, catalog no. 15712-S) for 20 minutes. Fixed cells permeabilized with 0.1% Triton X-100 (Research Products International

Corp., catalog no. 11036) for 5 minutes, blocked with freshly prepared 5% BSA (Fisher BioReagents, catalog no. BP 1600-100, CAS no. 9048-46-8) for 25 minutes, treated with 1:100 solution of primary antibody in blocking medium at 4^{o}C overnight. Next, the cells were rinsed thoroughly and stained with 1:200 solution of secondary antibody in PBS for 2 hours followed by staining with Acti-Stain^{TM} 670 Fluorescent Phalloidin (Cytoskeleton.Inc, catalog no. PHDN1). Cells were stained with DAPI (Vector Laboratories, Burlingame, CA) for 5 mins. Then the cover-slides were mounted on glass slides using ProLong Diamond Antifade Mountant (Invitrogen, catalog no. P36961) and sealed with clear nail-polish. Primary antibodies: (1) Anti-Fascin 1 (D-10) mouse monoclonal IgG_1 antibody (Santa Cruz Biotechnology, catalog no. sc-46675), (2) Anti-FAK (D1) mouse monoclonal IgG_1 antibody (Santa Cruz Biotechnology, catalog no. sc-271126), (3) Anti-VASP (A-11) mouse monoclonal IgG_{2a} antibody (Santa Cruz Biotechnology, catalog no. sc-46668), (4) Anti-Filamin 1 (E-3) mouse monoclonal IgG_{2a} antibody (Santa Cruz Biotechnology, catalog no. sc-17749), (5) Anti-α-actinin (G-4) mouse monoclonal IgG_{2a} antibody (Santa Cruz Biotechnology, catalog no. sc-390205) and (6) Anti-Vimentin (D21H3) XP® rabbit mAb antibody (Cell Signaling Technology, catalog no. 5741). Secondary antibodies: (1) Alexa Fluor® 488 AffiniPure $F(ab')_2$ Fragment Donkey Anti-Mouse IgG (H+L) (Jackson ImmunoResearch Laboratories Inc., code no. 715-546-151), (2) AlexaFluor® 594 AffiniPure $F(ab')_2$ Fragment Donkey Anti-Mouse IgG (H+L) (Jackson ImmunoResearch Laboratories Inc., code no. 715-586-151) and (3) Anti-Vimentin rabbit antibody. Secondary antibodies: (1) Alexa Fluor® 488 AffiniPure $F(ab')_2$ Fragment Donkey Anti-Rabbit IgG (H+L) (Jackson ImmunoResearch Laboratories Inc., code no. 711-546-152).

Target Protein	Drug	Company/ Catalog No.	Concentration
MEK 1/2	U0126-EtOH	MedChemExpress	72nM

		HY-12031	
MEK 1/2	SL327	MedChemExpress HY-15437	220nM
Ribosomal S-6 Kinase	LJI308	MedChemExpress HY-19713	13nM
Tyrosine Kinase (EGFR)	Genistein	MedChemExpress HY-14596	0.6μM
CRM1	KPT-276	Selleck Chemicals S7251	50nM
Tankyrase	XAV-939	Selleck Chemicals S1180	11nM

Migration Assay: Cell migration is a multistep process and was measured using the Sartorius, IncuCyte live imaging system and the IncuCyte scratch wound assay. To ensure homogenous cell scratching and preventing a Woundmaker pin damage, no wells were left empty (dry). Precaution was taken to avoid the formation of bubbles inside wells. A cell density at or very near to 100% confluence is used for scratch wound generation. Cells were plated on tissue culture plastic approximately 10 hours before making the scratch wound. An Imagelock 96-well plate (Sartorius Cat. No. 4379) was used to plate the cells and at a density of 10,000-40,000 cells/well (100 μL/well) into each well. The cells were allowed to settle at ambient temperature for 15 minutes, then place the plate into a 37°C incubator, 5% CO_2 overnight or as pre-determined in assay optimization. After carefully removing the Imagelock plate from the incubator, the IncuCyte 96-Well Woundmaker tool (Sartorius, catalog no. 4563) was used to simultaneously create wounds in all the 96 wells. After wounding, the media was immediately aspirated from each well and the cells were carefully washed twice with culture media (100 μL/well; without serum). After the was experiment was started by the addition of small molecule inhibitors to each well. The plate was placed into the IncuCyte Live-Cell Analysis System and allowed to warm to 37° C for 30 minutes prior to scanning. An objective: 10X, with phase contrast channel, Scan type: Scratch Wound

(Wide Mode) for 10X, with scan intervals of 3hrs was selected for imaging over time. Data generated using the migration assay was analyzed using a Software Module (Sartorius, cat. no. 9600-0012).

Motility Assay: Cells were plated at a density of 25 cells/mm^2 in 12-well plates. Prior to imaging cells were stained with 1 g/mL Hoechst-33342, washed, and incubated for 8 hours after overnight attachment. Three random fields in duplicate wells were scanned for 12 hours at 100x total magnification using a Nikon Eclipse Ti inverted microscope with a temperature and CO_2 controlled stage (Nikon 10x PlanFluor, 0.30 NA). Nikon Elements AR software was used to operate a Cascade II EM-CCD (Photometrics, Tucson, AZ) at a 30 ms exposure with maximum gain. Neutral density filters were used to reduce UV exposure. The image sequence was imported into ImageJ, thresholded, and binary objects were then tracked using MtrackJ plugin. MTrackJ is an ImageJ plugin to facilitate tracking of moving objects in image sequences and the measurement of track statistics. Data shown represent the average cell speed across the entire experiment. Experiments were repeated at least three times.

Live Cell Transfection: Cells were grown for 24 hours and allowed to achieve 50-70% confluency and transfected with Dronpa-C-12-β-actin plasmid using Lipofectamine 3000 as transfection agent in reduced serum medium OPTI-MEM and imaged after 36 hours. The cells were also stained with Hoechst 33342 solution for nuclear staining before imaging.

Fluorescence Imaging: Wide-field fluorescence imaging was done on a Nikon Ti-Eclipse microscope equipped with an AURA light engine (Lumencor) light source and 63X oil immersion objectives lens (Nikon, Plan Apo VC 60X/1.4). The images were captured using an iXon+ camera (Andor Technologies, model no. DU-897E-CSO-#BV). For live cell imaging, a microscope mounted incubator (Warner Instruments, Inc., model no. DH-40iL) coupled with an automatic

temperature controller (Warner Instruments, Inc., model no. TC-324C) was used, which kept the cells at 37^{o}C, 5% CO_2 and 90% relative humidity. Confocal images were taken using a LSM 780 Zeiss confocal microscope (Carl Zeiss, Jena, Germany) with a 63X oil immersion objective.

Image Analysis and OOP Calculation: Fluorescent images were processed using Matlab (version 2016a) and analyzed using previously described protocol[58]. The raw fluorescent images were decomposed into filament image, artefact image and noise. The filament image was enhanced to improve the contrast. Next, a multi-scale line segmentation approach was used to extract the fibers as straight lines. Then fibers that had similar orientation and were close to one another were stitched together. The filament angles were extracted from the output and Orientational Order Parameter (OOP) was calculated from the angular distribution[59,60]. OOP is calculated by generating a tensor from every angle (vector) and evaluating the maximum eigen value of the mean order tensor. A more detailed description of this technique is provided in chapter 2.

References:

(1) Hanahan, D.; Weinberg, R. A. Hallmarks of Cancer: The Next Generation. *Cell* **2011**, *144* (5), 646–674. https://doi.org/10.1016/j.cell.2011.02.013.

(2) Lemmon, M. A.; Schlessinger, J. Cell Signaling by Receptor Tyrosine Kinases. *Cell* **2010**, *141* (7), 1117–1134. https://doi.org/10.1016/j.cell.2010.06.011.

(3) Burkhart, D. L.; Sage, J. Cellular Mechanisms of Tumour Suppression by the Retinoblastoma Gene. *Nat. Rev. Cancer* **2008**, *8* (9), 671–682. https://doi.org/10.1038/nrc2399.

(4) Deshpande, A.; Sicinski, P.; Hinds, P. W. Cyclins and Cdks in Development and Cancer: A Perspective. *Oncogene* **2005**, *24* (17), 2909–2915.

https://doi.org/10.1038/sj.onc.1208618.

(5) Curto, M.; Cole, B. K.; Lallemand, D.; Liu, C. H.; McClatchey, A. I. Contact-Dependent Inhibition of EGFR Signaling by Nf2/Merlin. *J. Cell Biol.* **2007**, *177* (5), 893–903. https://doi.org/10.1083/jcb.200703010.

(6) Okada, T.; Lopez-Lago, M.; Giancotti, F. G. Merlin/NF-2 Mediates Contact Inhibition of Growth by Suppressing Recruitment of Rac to the Plasma Membrane. *J. Cell Biol.* **2005**, *171* (2), 361–371. https://doi.org/10.1083/jcb.200503165.

(7) Adams, J. M.; Cory, S. The Bcl-2 Apoptotic Switch in Cancer Development and Therapy. *Oncogene* **2007**, *26* (9), 1324–1337. https://doi.org/10.1038/sj.onc.1210220.

(8) Evan, G.; Lowe, S.; Cepero, E. Intrinsic Tumour Suppression. *Nature* **2004**, *432* (NOVEMBER), 1–9.

(9) Cheng, N.; Chytil, A.; Shyr, Y.; Joly, A.; Moses, H. L. Transforming Growth Factor-β Signaling-Deficient Fibroblasts Enhance Hepatocyte Growth Factor Signaling in Mammary Carcinoma Cells to Promote Scattering and Invasion. *Mol. Cancer Res.* **2008**, *6* (10), 1521–1533. https://doi.org/10.1158/1541-7786.MCR-07-2203.

(10) Lipinski, M. M.; Jacks, T. The Retinoblastoma Gene Family in Differentiation and Development. *Oncogene* **1999**, *18* (55), 7873–7882. https://doi.org/10.1038/sj.onc.1203244.

(11) Ghebranious, N.; Donehower, L. A. Mouse Models in Tumor Suppression. *Oncogene* **1998**, *17* (25), 3385–3400. https://doi.org/10.1038/sj.onc.1202573.

(12) Junttila, M. R.; Evan, G. I. P53 a Jack of All Trades but Master of None. *Nat. Rev. Cancer*

2009, *9* (11), 821–829. https://doi.org/10.1038/nrc2728.

(13) Partanen, J. I.; Nieminen, A. I.; Klefstrom, J. 3D View to Tumor Suppression: Lkb1, Polarity and the Arrest of Oncogenic c-Myc. *Cell Cycle* **2009**, *8* (5), 716–724. https://doi.org/10.4161/cc.8.5.7786.

(14) Shaw, R. J. Tumor Suppression by LKB1: SIK-Ness Prevents Metastasis. *Sci. Signal.* **2009**, *2* (86), 53–56. https://doi.org/10.1126/scisignal.286pe55.

(15) Lugano, R.; Ramachandran, M.; Dimberg, A. Tumor Angiogenesis: Causes, Consequences, Challenges and Opportunities. *Cell. Mol. Life Sci.* **2020**, *77* (9), 1745–1770. https://doi.org/10.1007/s00018-019-03351-7.

(16) Talmadge, J. E.; Fidler, I. J. AACR Centennial Series: The Biology of Cancer Metastasis: Historical Perspective. *Cancer Res.* **2010**, *70* (14), 5649–5669. https://doi.org/10.1158/0008-5472.CAN-10-1040.

(17) Fidler, I. J. The Pathogenesis of Cancer Metastasis: The "seed and Soil" Hypothesis Revisited. *Nat. Rev. Cancer* **2003**, *3*, 453–458. https://doi.org/10.1097/00006454-199103000-00027.

(18) Kalluri, R.; Weinberg, R. A. The Basics of Epithelial-Mesenchymal Transition. *J. Clin. Invest.* **2009**, *119* (6), 1420–1428. https://doi.org/10.1172/JCI39104.1420.

(19) Lamouille, S.; Xu, J.; Derynck, R. Molecular Mechanisms of Epithelial-Mesenchymal Transition. *Nat. Rev. Mol. Cell Biol.* **2014**, *15* (3), 178–196. https://doi.org/10.1038/nrm3758.

(20) Nurwidya, F.; Takahashi, F.; Murakami, A.; Takahashi, K. Epithelial Mesenchymal

Transition in Drug Resistance and Metastasis of Lung Cancer. *Cancer Res. Treat.* **2012**, *44* (3), 151–156. https://doi.org/10.4143/crt.2012.44.3.151.

(21) Xiao, D.; He, J. Epithelial Mesenchymal Transition and Lung Cancer. *J. Thorac. Dis.* **2010**, *2* (3), 154–159. https://doi.org/10.3978/j.issn.2072-1439.2010.02.03.7.

(22) Berx, G.; van Roy, F. Involvement of Members of the Cadherin Superfamily in Cancer. *Cold Spring Harb. Perspect. Biol.* **2009**, *1* (6). https://doi.org/10.1101/cshperspect.a003129.

(23) Ikushima, H.; Miyazono, K. TGFB 2 Signalling: A Complex Web in Cancer Progression. *Nat. Rev. Cancer* **2010**, *10* (6), 415–424. https://doi.org/10.1038/nrc2853.

(24) Bierie, B.; Moses, H. L. Tumour Microenvironment - TGFB: The Molecular Jekyll and Hyde of Cancer. *Nat. Rev. Cancer* **2006**, *6* (7), 506–520. https://doi.org/10.1038/nrc1926.

(25) Ju, H. K.; Young, S. J.; Eom, K. S.; Young, I. H.; Hae, R. K.; Seung, H. J.; Cheol, H. K.; Young, B. P.; Myung, G. L.; In, G. H.; Jung, K. S.; Kim, D. G. Transtorming Growth Factor B1 Induces Epithelial-to-Mesenchymal Transition of A549 Cells. *J. Korean Med. Sci.* **2007**, *22* (5), 898–904. https://doi.org/10.3346/jkms.2007.22.5.898.

(26) Karacosta, L. G.; Anchang, B.; Ignatiadis, N.; Kimmey, S. C.; Benson, J. A.; Shrager, J. B.; Tibshirani, R.; Bendall, S. C.; Plevritis, S. K. Mapping Lung Cancer Epithelial-Mesenchymal Transition States and Trajectories with Single-Cell Resolution. *Nat. Commun.* **2019**, *10* (1), 1–15. https://doi.org/10.1038/s41467-019-13441-6.

(27) Endo, C.; Sakurada, A.; Notsuda, H.; Noda, M.; Hoshikawa, Y.; Okada, Y.; Kondo, T. Results of Long-Term Follow-up of Patients with Completely Resected Non-Small Cell

Lung Cancer. *Ann. Thorac. Surg.* **2012**, *93* (4), 1061–1068. https://doi.org/10.1016/j.athoracsur.2012.01.004.

(28) Pantel, K.; Brakenhoff, R. H.; Brandt, B. Detection, Clinical Relevance and Specific Biological Properties of Disseminating Tumour Cells. *Nat. Rev. Cancer* **2008**, *8* (5), 329–340. https://doi.org/10.1038/nrc2375.

(29) Greco, F. A.; Hainsworth, J. D. Introduction: Unknown Primary Cancer. *Semin. Oncol.* **2009**, *36* (1), 6–7. https://doi.org/10.1053/j.seminoncol.2008.10.007.

(30) Tanaka, F.; Yoneda, K.; Kondo, N.; Hashimoto, M.; Takuwa, T.; Matsumoto, S.; Okumura, Y.; Rahman, S.; Tsubota, N.; Tsujimura, T.; Kuribayashi, K.; Fukuoka, K.; Nakano, T.; Hasegawa, S. Circulating Tumor Cell as a Diagnostic Marker in Primary Lung Cancer. *Clin. Cancer Res.* **2009**, *15* (22), 6980–6986. https://doi.org/10.1158/1078-0432.CCR-09-1095.

(31) Okumura, Y.; Tanaka, F.; Yoneda, K.; Hashimoto, M.; Takuwa, T.; Kondo, N.; Hasegawa, S. Circulating Tumor Cells in Pulmonary Venous Blood of Primary Lung Cancer Patients. *Ann. Thorac. Surg.* **2009**, *87* (6), 1669–1675. https://doi.org/10.1016/j.athoracsur.2009.03.073.

(32) Ignatiadis, M.; Rothé, F.; Chaboteaux, C.; Durbecq, V.; Rouas, G.; Criscitiello, C.; Metallo, J.; Kheddoumi, N.; Singhal, S. K.; Michiels, S.; Veys, I.; Rossari, J.; Larsimont, D.; Carly, B.; Pestrin, M.; Bessi, S.; Buxant, F.; Liebens, F.; Piccart, M.; Sotiriou, C. HER2-Positive Circulating Tumor Cells in Breast Cancer. *PLoS One* **2011**, *6* (1), 6–11. https://doi.org/10.1371/journal.pone.0015624.

(33) Rhim, A. D.; Mirek, E. T.; Aiello, N. M.; Maitra, A.; Bailey, J. M.; McAllister, F.;

Reichert, M.; Beatty, G. L.; Rustgi, A. K.; Vonderheide, R. H.; Leach, S. D.; Stanger, B. Z. EMT and Dissemination Precede Pancreatic Tumor Formation. *Cell* **2012**, *148* (1–2), 349–361. https://doi.org/10.1016/j.cell.2011.11.025.

(34) Hüsemann, Y.; Geigl, J. B.; Schubert, F.; Musiani, P.; Meyer, M.; Burghart, E.; Forni, G.; Eils, R.; Fehm, T.; Riethmüller, G.; Klein, C. A. Systemic Spread Is an Early Step in Breast Cancer. *Cancer Cell* **2008**, *13* (1), 58–68. https://doi.org/10.1016/j.ccr.2007.12.003.

(35) Podsypanina, K.; Du, Y.-C. N.; Jechlinger, M.; Beverly, L. J.; Hambardzumyan, D.; Varmus, H. Seeding and Propagation of Untransformed Mouse Mammary Cells in the Lung. *Science (80-.).* **2008**, *321* (September), 1841–1845.

(36) Zhang, W.; Kai, K.; Choi, D. S.; Iwamoto, T.; Nguyen, Y. H.; Wong, H.; Landis, M. D.; Ueno, N. T.; Chang, J.; Qin, L. Microfluidics Separation Reveals the Stem-Cell-like Deformability of Tumor-Initiating Cells. *Proc. Natl. Acad. Sci. U. S. A.* **2012**, *109* (46), 18707–18712. https://doi.org/10.1073/pnas.1209893109.

(37) Seo, M.; Lee, W.; Suk, K. Identification of Novel Cell Migration-promoting Genes by a Functional Genetic Screen. *FASEB J.* **2010**, *24* (2), 464–478. https://doi.org/10.1096/fj.09-137562.

(38) Patsialou, A.; Wang, Y.; Lin, J.; Whitney, K.; Goswami, S.; Kenny, P. A.; Condeelis, J. S. Selective Gene-Expression Profiling of Migratory Tumor Cells in Vivo Predicts Clinical Outcome in Breast Cancer Patients. *Breast Cancer Res.* **2012**, *14* (5). https://doi.org/10.1186/bcr3344.

(39) Pagano, P. C.; Tran, L. M.; Bendris, N.; O'Byrne, S.; Tse, H. T.; Sharma, S.; Hoech, J.

W.; Park, S. J.; Liclican, E. L.; Jing, Z.; Li, R.; Krysan, K.; Paul, M. K.; Fontebasso, Y.; Larsen, J. E.; Hakimi, S.; Seki, A.; Fishbein, M. C.; Gimzewski, J. K.; Di Carlo, D.; Minna, J. D.; Walser, T. C.; Dubinett, S. M. Identification of a Human Airway Epithelial Cell Subpopulation with Altered Biophysical, Molecular, and Metastatic Properties. *Cancer Prev. Res.* **2017**, *10* (9), 514–524. https://doi.org/10.1158/1940-6207.CAPR-16-0335.

(40) Sanchez-Garcia, I. The Crossroads of Oncogenesis and Metastasis. *N. Engl. J. Med.* **2009**, 297–299.

(41) Pegoraro, A. F.; Janmey, P.; Weitz, D. A. Mechanical Properties of the Cytoskeleton and Cells. *Cold Spring Harb. Perspect. Biol.* **2017**, *9* (11). https://doi.org/10.1101/cshperspect.a022038.

(42) Zhou, Z. L.; Sun, X. X.; Ma, J.; Tong, M. H.; To, S. K. Y.; Wong, A. S. T.; Ngan, A. H. W. Actin Cytoskeleton Stiffness Grades Metastatic Potential of Ovarian Carcinoma Hey A8 Cells via Nanoindentation Mapping. *J. Biomech.* **2017**, *60*, 219–226. https://doi.org/10.1016/j.jbiomech.2017.06.040.

(43) Discher, D. E.; Janmey, P.; Wang, Y. L. Tissue Cells Feel and Respond to the Stiffness of Their Substrate. *Science (80-.).* **2005**, *310* (5751), 1139–1143. https://doi.org/10.1126/science.1116995.

(44) Prager-Khoutorsky, M.; Lichtenstein, A.; Krishnan, R.; Rajendran, K.; Mayo, A.; Kam, Z.; Geiger, B.; Bershadsky, A. D. Fibroblast Polarization Is a Matrix-Rigidity-Dependent Process Controlled by Focal Adhesion Mechanosensing. *Nat. Cell Biol.* **2011**, *13* (12), 1457–1465. https://doi.org/10.1038/ncb2370.

(45) Engler, A. J.; Sen, S.; Sweeney, H. L.; Discher, D. E. Matrix Elasticity Directs Stem Cell Lineage Specification. *Cell* **2006**, *126*, 677–689.

(46) Pellegrin, S.; Mellor, H. Actin Stress Fibers. *J. Cell Sci.* **2007**, *120* (20), 3491–3499. https://doi.org/10.1242/jcs.018473.

(47) Cui, S.; Wang, J.; Wu, Q.; Qian, J.; Yang, C.; Bo, P. Genistein Inhibits the Growth and Regulates the Migration and Invasion Abilities of Melanoma Cells via the FAK/Paxillin and MAPK Pathways. *Oncotarget* **2017**, *8* (13), 21674–21691. https://doi.org/10.18632/oncotarget.15535.

(48) Doehn, U.; Hauge, C.; Frank, S. R.; Jensen, C. J.; Duda, K.; Nielsen, J. V.; Cohen, M. S.; Johansen, J. V.; Winther, B. R.; Lund, L. R.; Winther, O.; Taunton, J.; Hansen, S. H.; Frödin, M. RSK Is a Principal Effector of the RAS-ERK Pathway for Eliciting a Coordinate Promotile/Invasive Gene Program and Phenotype in Epithelial Cells. *Mol. Cell* **2009**, *35* (4), 511–522. https://doi.org/10.1016/j.molcel.2009.08.002.

(49) Davies, A. H.; Reipas, K.; Hu, K.; Berns, R.; Firmino, N.; Stratford, A. L.; Dunn, S. E. Inhibition of RSK with the Novel Small-Molecule Inhibitor LJI308 Overcomes Chemoresistance by Eliminating Cancer Stem Cells. *Oncotarget* **2015**, *6* (24), 20570–20577. https://doi.org/10.18632/oncotarget.4135.

(50) Schmidt, J.; Braggio, E.; Kortuem, K. M.; Egan, J. B.; Zhu, Y. X.; Xin, C. S.; Tiedemann, R. E.; Palmer, S. E.; Garbitt, V. M.; McCauley, D.; Kauffman, M.; Shacham, S.; Chesi, M.; Bergsagel, P. L.; Stewart, A. K. Genome-Wide Studies in Multiple Myeloma Identify XPO1/CRM1 as a Critical Target Validated Using the Selective Nuclear Export Inhibitor KPT-276. *Leukemia* **2013**, *27* (12), 2357–2365. https://doi.org/10.1038/leu.2013.172.

(51) Wang, W.; Zhou, J.; Zhao, L.; Chen, S. Combination of SL327 and Sunitinib Malate Leads to an Additive Anti-Cancer Effect in Doxorubicin Resistant Thyroid Carcinoma Cells. *Biomed. Pharmacother.* **2017**, *88*, 985–990. https://doi.org/10.1016/j.biopha.2017.01.135.

(52) Donada, A.; Balayn, N.; Sliwa, D.; Lordier, L.; Ceglia, V.; Baschieri, F.; Goizet, C.; Favier, R.; Tosca, L.; Tachdjian, G.; Denis, C. V.; Plo, I.; Vainchenker, W.; Debili, N.; Rosa, J. P.; Bryckaert, M.; Raslova, H. Disrupted Filamin A/AIIbb3 Interaction Induces Macrothrombocytopenia by Increasing RhoA Activity. *Blood* **2019**, *133* (16), 1778–1788. https://doi.org/10.1182/blood-2018-07-861427.

(53) Krause, M.; Dent, E. W.; Bear, J. E.; Loureiro, J. J.; Gertler, F. B. Ena/VASP Proteins: Regulators of the Actin Cytoskeleton and Cell Migration. *Annu. Rev. Cell Dev. Biol.* **2003**, *19*, 541–564. https://doi.org/10.1146/annurev.cellbio.19.050103.103356.

(54) Pavese, J. M.; Farmer, R. L.; Bergan, R. C. Inhibition of Cancer Cell Invasion and Metastasis by Genistein. *Cancer Metastasis Rev.* **2010**, *29* (3), 465–482. https://doi.org/10.1007/s10555-010-9238-z.

(55) Akiyama, T.; Ishida, J.; Nakagawa, S.; Ogawara, H.; Watanabe, S.; Itoh, N.; Shibuya, M.; Fukami, Y. Genistein, a Specific Inhibitor of Tyrosine-Specific Protein Kinases. *J. Biol. Chem.* **1987**, *262* (12), 5592–5595. https://doi.org/10.1016/s0021-9258(18)45614-1.

(56) Chong, P. A.; Forman-Kay, J. D. Liquid–Liquid Phase Separation in Cellular Signaling Systems. *Curr. Opin. Struct. Biol.* **2016**, *41* (Dvl), 180–186. https://doi.org/10.1016/j.sbi.2016.08.001.

(57) Grant, J. L.; Fishbein, M. C.; Hong, L. S.; Krysan, K.; Minna, J. D.; Shay, J. W.; Walser,

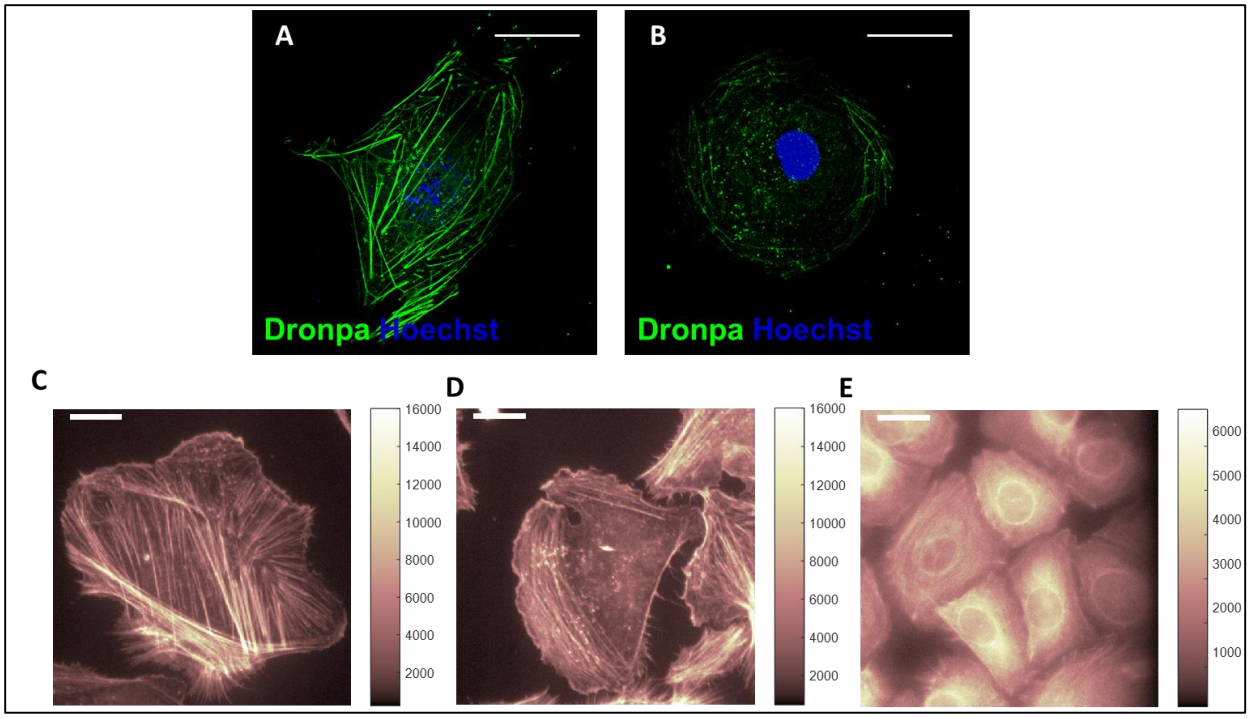
T. C.; Dubinett, S. M. A Novel Molecular Pathway for Snail-Dependent, SPARC-Mediated Invasion in Non-Small Cell Lung Cancer Pathogenesis. *Cancer Prev. Res.* **2014**, *7* (1), 150–160. https://doi.org/10.1158/1940-6207.CAPR-13-0263.

(58) Alioscha-Perez, M.; Benadiba, C.; Goossens, K.; Kasas, S.; Dietler, G.; Willaert, R.; Sahli, H. A Robust Actin Filaments Image Analysis Framework. *PLoS Comput. Biol.* **2016**, *12* (8), 1–23. https://doi.org/10.1371/journal.pcbi.1005063.

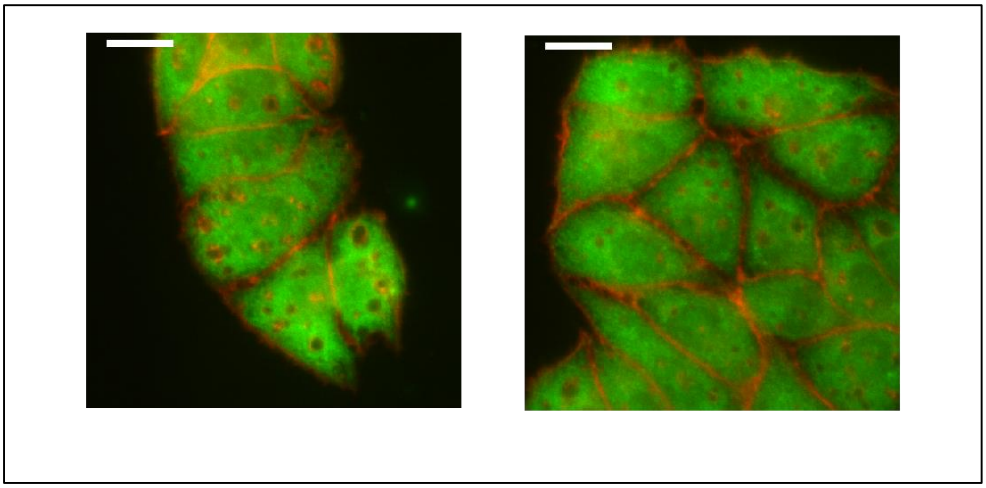
(59) Volfson, D.; Cookson, S.; Hasty, J.; Tsimring, L. S. Biomechanical Ordering of Dense Cell Populations. *Proc. Natl. Acad. Sci. U. S. A.* **2008**, *105* (40), 15346–15351. https://doi.org/10.1073/pnas.0706805105.

(60) Grosberg, A.; Kuo, P. L.; Guo, C. L.; Geisse, N. A.; Bray, M. A.; Adams, W. J.; Sheehy, S. P.; Parker, K. K. Self-Organization of Muscle Cell Structure and Function. *PLoS Comput. Biol.* **2011**, *7* (2). https://doi.org/10.1371/journal.pcbi.1001088.

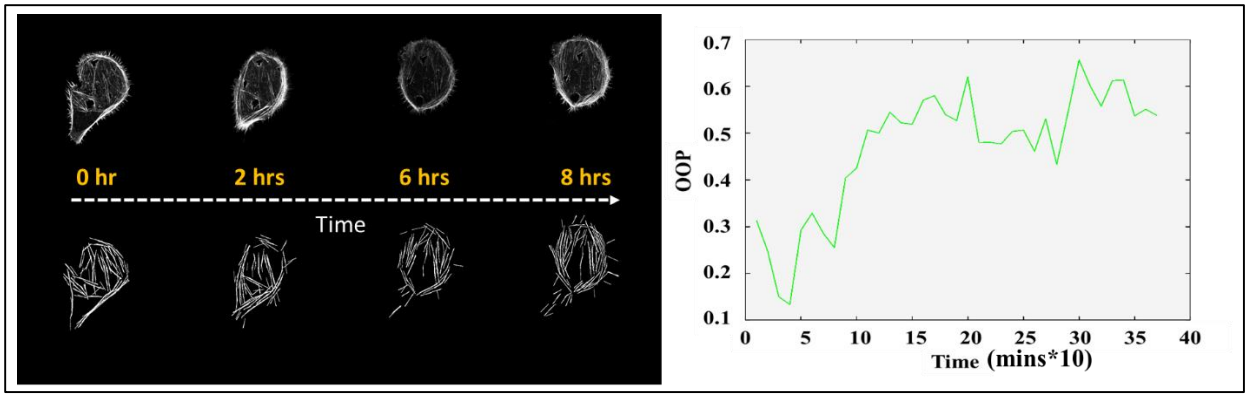
Supplementary Information



Supplementary Fig. 1 | HBEC cells demonstrating cytoskeletal heterogeneity. A, B, HBEC-Snail-HM and HBEC-Snail-UN cells respectively transfected with Dronpa-C-12-β-actin (green) and stained with Hoechst (blue) demonstrating different cytoskeletal structure. For HBEC-Snail-HM, the actin stress fibers are predominantly in a different plane from the nucleus. **C-D,** HBEC-Snail-UN cells demonstrating a high degree of heterogeneity in their cytoskeleton. Scale bar (A,B): 10μm. Scale bar (C-E): 16μm.



Supplementary Fig. 2 | Complementary expression of FAK and actin in Genistein treated HBEC-Snail-HM cells. HBEC-Snail-HM cells were treated with genistein for 48 hours and their actin (red) and FAK (green) were stained. Bright actin spots coincide with the dark spots in FAK staining. Scale bar: 16μm.



Supplementary Fig. 3 | HBEC-Snail-HM cell undergoing U0126 treatment and the concomitant change in the OOP values.